DISSERTATION

FILM CHARACTERIZATION AND MECHANISTIC STUDIES OF FLUOROSILANE PLASMAS: FROM FILM CHEMISTRY TO RADICAL SURFACE REACTIONS

Submitted by

Keri L. Williams

Department of Chemistry

In partial fulfillment of the requirements

for the degree of Doctor of Philosophy

Colorado State University

Fort Collins, Colorado

Spring 2003

Reproduced with permission of the copyright owner. Further reproduction prohibited without permission.

UMI Number: 3092701

UMI®

UMI Microform 3092701

Copyright 2003 by ProQuest Information and Learning Company.

All rights reserved. This microform edition is protected against

unauthorized copying under Title 17, United States Code.

ProQuest Information and Learning Company
300 North Zeeb Road
P.O. Box 1346
Ann Arbor, MI 48106-1346

Reproduced with permission of the copyright owner. Further reproduction prohibited without permission.

COLORADO STATE UNIVERSITY

February 17, 2003

WE HEREBY RECOMMEND THAT THE DISSERTATION PREPARED UNDER OUR SUPERVISION BY KERI L. WILLIAMS ENTITLED **FILM CHARACTERIZATION AND MECHANISTIC STUDIES OF FLUOROSILANE PLASMAS: FROM FILM CHEMISTRY TO RADICAL SURFACE REACTIONS** BE ACCEPTED AS FULFILLING IN PART THE REQUIREMENTS FOR THE DEGREE OF DOCTOR OF PHILOSOPHY.

Committee on Graduate Work

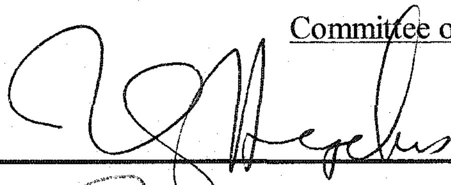

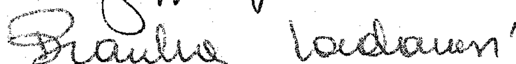

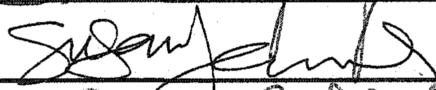

Advisor

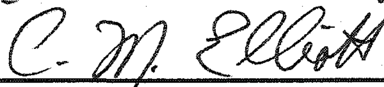

Department Head

Reproduced with permission of the copyright owner. Further reproduction prohibited without permission.

ABSTRACT OF DISSERTATION

FILM CHARACTERIZATION AND MECHANISTIC STUDIES OF FLUOROSILANE PLASMAS: FROM FILM CHEMISTRY TO RADICAL-SURFACE REACTIONS

An inductively coupled rf plasma was used to study the effects of plasma parameters on fluorosilane plasmas. A variety of gas phase, gas-surface, and surface analysis techniques were used to provide a complete study of the SiF_4 plasma system resulting in elucidation of gas and gas-surface interface reactions responsible for etching and film deposition. The effect of plasma power (*P*) and source gas ratios on film, plasma-surface, and gas-phase composition were studied for SiF_4/H_2 plasmas. Film characterization was performed using FTIR, X-ray photoelectron spectroscopy (XPS), and ellipsometry. The imaging of radicals interacting with surfaces (IRIS) technique was used to collect spatially-resolved laser-induced fluorescence (LIF) images of SiF_x radicals. LIF was used to characterize both the plasma-surface interface and the gas phase. From these data, three plasma types were defined. Type 1 plasmas result in silicon etching. These systems include 100% SiF_4 plasmas at $P > 20$ W. Type 2 systems neither etch nor deposit, rather F implantation is observed. XPS analysis of substrates exposed to a 100% SiF_4 plasma with $P = 20$ W, showed only F incorporation at the

Reproduced with permission of the copyright owner. Further reproduction prohibited without permission.

substrate surface. Similar results were observed for the 50% H_2 plasma system at $P > 40$ W. These systems are thus categorized as Type 2 plasmas. The third plasma type is defined as those plasmas resulting in net deposition. Most SiF_4/H_2 systems, all 10% and 50% H_2 at $P \leq 40$ W, resulted in net deposition of a-Si:H,F films, defining these systems as Type 3 plasmas. Gas phase and surface reactions to describe these three plasma types are proposed. Additional gas phase measurements of the SiF radical in SiF_4 plasmas as a function of H_2 and O_2 dilution and applied rf power were performed using [2+1] resonance enhanced multiphoton ionization (REMPI) time of flight mass spectrometry (TOFMS). The absorption band from the (1,0) $C''^2\Sigma^+$ -- $X^2\Pi_{1/2}$ SiF transition was monitored as a function of H_2 and O_2 dilution and applied rf power. These additional studies compare well with the imaging of radicals interacting with surfaces (IRIS) technique and quadrupole mass spectrometry (MS) measurements.

Using the Imaging of Radicals Interacting with Surfaces (IRIS) technique, the effect of substrate temperature, T_S, on SiF and SiF_2 surface reactivity in SiF_4 and SiF_4:H_2 plasmas under a variety of plasma conditions was measured. At $T_S = 300$ K, there is significantly more SiF_2 than SiF emanating from the surface. This is expected as SiF_2 is a known etch product. Interestingly, higher substrate temperatures result in significant increases in surface scatter for both molecules. These results are discussed with respect to the role that each molecule plays in etching and deposition mechanisms, as well as in comparison to results for plasma species in other plasma systems. In addition to surface interaction measurements, rotational temperatures (Θ_R) for SiF and SiF_2 were measured in a 170 W plasma as 450 ± 50 K and 752 ± 100 K, respectively.

Reproduced with permission of the copyright owner. Further reproduction prohibited without permission.

Films of fluorine and carbon-doped silicon dioxide (SiO:F,C) were prepared by plasma-enhanced chemical vapor deposition using an inductively coupled rf plasma reactor. Hexamethyldisiloxane (HMDSO) and tetraethoxysilane (TEOS) were used as the silicon precursors with O_2 as the oxidant. With both silicon sources, three different fluorocarbon (FC) gases were studied: CF_4, C_2F_6, and hexafluoropropylene oxide (HFPO). FTIR, XPS, and ellipsometry are used to characterize films as a function of O_2 and FC source concentrations. In general, all six systems behaved similarly with respect to overall film deposition parameters. Increasing oxidant in the feed resulted in decreased carbon incorporation in the deposited material and more stoichiometric SiO_2 films, albeit at lower deposition rates for all six systems. Varying the silicon source gas significantly affected the F bonding environment, whereas the FC affected this to a lesser extent. Increasing fluorocarbon concentration in the feed generally resulted in a broadening of the Si-O IR absorption peak, indicating decreased order in the SiO_2 material.

Keri L. Williams
Department of Chemistry
Colorado State University
Fort Collins, Colorado 80523-1872
Spring 2003

Reproduced with permission of the copyright owner. Further reproduction prohibited without permission.

ACKNOWLEDGMENTS

First and foremost I give thanks to my family. They are the ones who have helped make me the person I am today and have shared in the failures and successes in my life. Mom, thanks for always believing in me and offering words of encouragement when things were tough. Carolyn, you are the best sister a girl could have. I will always treasure our annual trips canoeing on the Niabrara. Doug and Chris, thanks for opening up your home and family to share with me so often over the years. Thanks also for your "care packages". They were so greatly appreciated. To my friends who have become like family, thanks you for all the good times and the friendships that will last a lifetime.

Reproduced with permission of the copyright owner. Further reproduction prohibited without permission.

DEDICATION

This dissertation is written in memory of my grandparents, Harry and Omadeen Dillon. They taught me truths about what is really important in life, and demonstrated those truths in their own lives. I am deeply indebted.

Reproduced with permission of the copyright owner. Further reproduction prohibited without permission.

TABLE OF CONTENTS

ABSTRACT OF DISSERTATION iii

ACKNOWLEDGMENTS vi

DEDICATION vii

TABLE OF CONTENTS viii

TABLE OF ABBREVIATIONS xiii

CHAPTER 1. Introduction to Fluorosilane Plasmas 1

1.1 Plasma Fundamentals 2

1.1.1 Igniting and sustaining plasmas 2

1.1.2 RF plasmas 3

1.2 Fluorinated Plasma Systems 5

1.2.1 Plasma deposition 5

1.2.1.1 Fluorinated silicon dioxide films 6

1.2.1.2 Hydrogenated fluorinated amorphous silicon films 6

1.2.2 Fluorine atom etching of silicon 7

1.3 Overview of Research—Fluorosilane Plasmas 9

Reproduced with permission of the copyright owner. Further reproduction prohibited without permission.

References 10

CHAPTER 2. Experimental Methods 17

2.1 Gas Phase Analytical Techniques 17

2.1.1 REMPI-MS technique 17

2.1.2 IRIS data collection 20

2.1.3 Mass spectrometry experiments 27

2.1.4 Optical emission spectroscopy 27

2.2 Surface Characterization Methods 29

2.2.1 Amorphous Si:H,F deposition 29

2.2.2 SiO_2:F,C deposition 31

2.2.3 Fourier transform infrared spectroscopy 34

2.2.4 Scanning electron microscopy 34

2.2.5 X-ray photoelectron spectroscopy 34

2.2.6 Variable angle spectroscopic ellipsometry 35

References 36

CHAPTER 3. Multiphoton Ionization Detection of SiF Radicals 38

3.1 Introduction 39

3.2 Results and Discussion 41

3.2.1 Mass and excitation spectra 41

3.2.2 Power dependence 41

3.2.3 Constant total gas flow 45

Reproduced with permission of the copyright owner. Further reproduction prohibited without permission.

3.2.4 Constant SiF_4 gas flow 49

3.3 Conclusion 49

References 51

CHAPTER 4. Substrate Temperature Effects on Surface Reactivity of SiF_x (x = 1, 2) Radicals in Fluorosilane Plasmas 54

4.1 Introduction 55

4.2 Results 58

4.2.1 Spectroscopy 58

4.2.2 Temperature dependence for surface reactivity of SiF and SiF_2 61

4.2.3 Determination of Θ_R 68

4.3 Discussion 73

4.4 Conclusion 76

References 78

CHAPTER 5. Mechanisms for Deposition and Etching in Fluorosilane Plasma Processing of Silicon 82

5.1 Introduction 83

5.2 Results 86

5.2.1 Plasma regime determined by film characterization 86

5.2.2 Gas-phase production of plasma species 91

5.2.3 Gas-surface interactions of SiF_x radicals in SiF_4 plasmas 104

Reproduced with permission of the copyright owner. Further reproduction prohibited without permission.

5.2.4 Effect of plasma ions on SiF_x reactivity 107

5.3 Discussion 112

5.3.1 Type 1 systems 113

5.3.2 Type 2 systems 114

5.3.3 Type 3 systems 116

5.3.3.1 Role of SiF in film deposition 116

5.3.3.2 SiF as a deposition precursor 118

5.3.3.3 Role of $HSiF_x$ during film deposition 121

5.3.4 Predicting plasma chemistry from SiF_2 and SiF 123

5.4 Summary 124

References 126

CHAPTER 6. Comparison of Silicon and Fluorine Sources in SiO:F,C Thin Film Deposition 131

6.1. Introduction 132

6.2. Results 134

6.2.1. Film composition 135

6.2.2. Deposition rates 142

6.2.3. Refractive index 147

6.2.4. Detailed film chemistry 149

6.3. Discussion 155

6.4. Summary 163

References 164

Reproduced with permission of the copyright owner. Further reproduction prohibited without permission.

CHAPTER 7. Research Summary 168

References 173

Reproduced with permission of the copyright owner. Further reproduction prohibited without permission.

TABLE OF ABBREVIATIONS

DC	direct current
E_0	initial kinetic energy
E_{trans}	transferred energy
FCP	fluorocarbon plasma
FTIR	Fourier transform infrared
HFPO	hexafluoropropyleneoxide

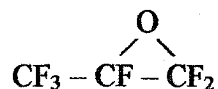

HMDSO	hexamethyldisiloxane

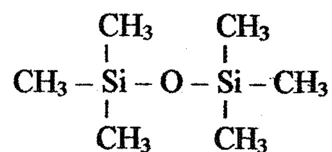

IRIS	imaging of radicals interacting with surfaces
LIF	laser induced fluorescence
M_c	charged species mass
MEM	microelectromechanical
M_n	neutral species mass
MS	mass spectrometry

Reproduced with permission of the copyright owner. Further reproduction prohibited without permission.

OES	optical emission spectroscopy
PECVD	plasma enhanced chemical vapor deposition
rf	radio frequency
REMPI	resonance enhanced multi-photon ionization
Θ_R	rotational temperature
S	Scatter coefficient
S_{corr}	corrected scatter coefficient
T_e	electron temperature
TEOS	tetraethoxysilane

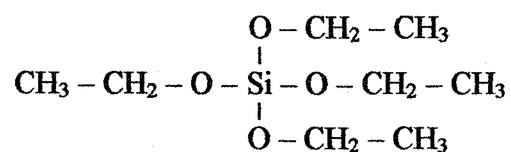

T_g	gas temperature
T_i	ion temperature
TOF	time of flight
T_S	substrate temperature

Reproduced with permission of the copyright owner. Further reproduction prohibited without permission.

CHAPTER 1

INTRODUCTION TO FLUOROSILANE PLASMAS

This dissertation chapter provides an introduction to the fundamentals of plasmas and gives general information about fluorine-based plasmas with special emphasis on the SiF_4 plasma system. This chapter also contains an overview of the research discussed in Chapters 2-6.

Reproduced with permission of the copyright owner. Further reproduction prohibited without permission.

1.1. Plasma Fundamentals

1.1.1. Igniting and Sustaining Plasmas. Plasmas have often been called the fourth state of matter because they are partially ionized gases consisting of ions, electrons, radicals, metastables, photons, and the parent species.[1] The presence of such reactive components makes these systems extremely useful, but also very complex and difficult to fully understand. To characterize these systems, plasma discharges are categorized by the temperatures of the different species in the system as well as by the form of energy used for ionization. The two main categories based upon temperature are thermal plasmas and cold plasmas.[2] Thermal plasmas, such as the sun, are characterized by equivalent gas and charged particle temperatures, whereas cold plasmas, which are in non-local thermodynamic equilibrium, show electron temperatures (T_e) much greater than the gas temperature (T_g).[1] It is these "cold plasmas" that are of particular use to industry because of their capacity to produce new materials and modify bulk properties at relatively low gas temperatures (<1000 K).[1] These are the only type of plasma discussed in this document.

Cold plasmas are generated and sustained by driving current through a low pressure gas (1 mtorr to 1 torr) between two electrodes or an rf coil and have the following features: a) charged particle collisions with neutral gas molecules are important, b) the electrons are not in thermal equilibrium with the ions ($T_e >> T_i$), c) ionization of neutrals sustains the plasma in a steady state, and d) there are boundaries at which surface losses are important.[1,3]

As stated above, different species in cold plasmas are not in thermodynamic equilibrium. Specifically, the electron temperature, T_e, is much greater than the ion

Reproduced with permission of the copyright owner. Further reproduction prohibited without permission.

temperature, T_i, and neutral gas temperature, T_g. This can be explained by considering the cooling effect of elastic collisions, in which both kinetic energy and momentum are conserved, equation 1.1.[2]

$$E_{trans} = \frac{4m_c m_n}{(m_c + m_n)^2} E_o \tag{1.1}$$

In this equation, m_c is the electron or ion mass and m_n is the neutral mass. E_{trans} is the energy transferred, and E_o is the initial kinetic energy of the electron or ion. Although the external applied field supplies energy to both ions and electrons, elastic collisions with the neutral gas species transfer energy from ions and electrons differently because of the mass differences. Ions and neutrals have relatively equal masses allowing significant kinetic energy transfer and, thus, thermal equilibration of ion and gas species. Since the initial kinetic energy for neutrals is assumed to be zero, ions quickly lose energy in these collisions and equilibrate to the gas temperature, $T_i \sim T_g$. In contrast, little kinetic energy is transferred between electrons and neutrals because $m_n >> m_e$. Thus, electrons gain energy from the external field and equilibrate mostly with other electrons. High-energy electrons ($T_e >> T_i$ and T_g) are, therefore, capable of sustaining the plasma through ionization of neutral species.

1.1.2. RF Plasmas. Cold plasmas are ignited and maintained electrically using direct current, radio frequency (rf), or microwave power across the source gas. Radio frequency was used for all studies presented in the following chapters. Although rf plasmas may be operated using a range of frequencies, only 13.56 MHz plasmas are used here. DC plasmas will only be discussed in comparison to rf glow discharges.

Reproduced with permission of the copyright owner. Further reproduction prohibited without permission.

The most notable difference between rf and dc plasmas is the energy and directionality of charged species in the plasma. In dc plasmas, charged particles acquire the maximum energy from the electric field. However, critical ion frequencies can be overcome using alternating electric (AC) fields such that the maximum field energy is not gained by the plasmas ions. When an AC field is applied across a gas, the anode and cathode switch polarity at a frequency, ω, equal to that of the AC current. Differences in electron and ion masses produce differences in their ability to respond to the changing electric field. Hence, if ω exceeds a critical ion frequency, defined in equation 1.2, the time required by an ion to travel the distance between the two electrodes is greater than half the period of the electric field.[4]

$$f_{ci} = \frac{\langle v \rangle_{di}}{2L} \quad (1.2)$$

f_{ci} is the critical ion frequency; $\langle v \rangle_{di}$ is the average drift velocity of the ion; and L is the distance between the electrodes. Since ion properties such as mass and charge directly affect ion velocity, the f_{ci} value can range from 500 kHZ to several MHz.[4] Rf plasmas used in our laboratories (13.56 MHz) are well above the f_{ci}. This results in plasma conditions with relatively low energy ions, unable to reach the maximum energy permitted by the field.

In contrast to ions, electrons have much higher mobility because of their small mass. Thus, the critical electron frequency, f_{ce}, is much greater than f_{ci}. Radio frequency plasmas operating at 13.56 MHz oscillate below f_{ce}. Consequently, electrons in the plasmas described in chapters 2 – 7 collect most of their energy from

Reproduced with permission of the copyright owner. Further reproduction prohibited without permission.

the external electric field, and thus can have temperatures ranging from 1 – 10 eV.[1,2] This is much larger than those of ions in the same systems, which usually have temperatures < 5 eV.[1,2]

Plasma characteristics, such as critical ion and electron frequencies, hold true for the bulk plasma where no perturbations to the microscopic environment exist. However, interactions at surfaces introduce significant perturbation. Due to higher electron mobility, more electrons are initially lost at surfaces exposed to the plasma than are ions. This results in an electron depletion region called the plasma sheath. Thus, the steady state condition of the bulk plasma is a positive potential with respect to the surface, resulting in electrons being turned back into the bulk plasma while positively charged ions are accelerated towards the surface. Typical energies for ions accelerated across the sheath are 10 - 1000 eV.[1] General plasma characteristics such as molecule fragmentation, plasma species energy distributions, and ion bombardment are important to determining overall plasma processes. Furthermore, process parameters, which control general plasma characteristics, are critical in halogenated systems because these plasmas exhibit a dual nature capable of both etching and deposition.

1.2. Fluorinated Plasma Systems

1.2.1. Plasma Deposition. Plasma-enhanced chemical vapor deposition (PECVD) has proven to be critical in the microelectronics industry for deposition of a variety of thin films, including amorphous silicon, oxides, nitrides, metal alloys, and doped materials.[5-10] Because of the complex nature of plasmas, a wide range of material structure and composition can be achieved by varying plasma parameters

Reproduced with permission of the copyright owner. Further reproduction prohibited without permission.

such as rf power, chamber pressure, and feed gas composition. Sensitivity to plasma parameters is useful for tailoring film properties to specific needs. Understanding how the films are created, however, is not a simple task. Currently, radicals are considered to be the largest contributor to material growth.[11,12] Thus, it is desirable to characterize radical reactivities and gas phase densities while producing materials with desirable properties.

1.2.1.1. Fluorinated Silicon Dioxide Films. Silicon dioxide is currently used as the industry standard for low k dielectric materials.[7-9,13-18] Plasma-deposited SiO_2 is commonly used in complimentary metal organic semiconductor (CMOS) fabrication as the intermetal dielectric.[7,13] With continually decreasing circuitry, however, there is an increasing need to develop new materials with lower dielectric constant, ε, than is currently afforded by pure SiO_2. The introduction of fluorine into SiO_2 to create F-SiO_2 significantly lowers ε.[8,17] In spite of this improvement, F-SiO_2 has significant drawbacks for industrial use because of increased moisture sensitivity upon addition of fluorine. Carbon incorporation has shown promise in stabilizing these materials without sacrificing the lowered dielectric constant.[19-24] Consequently, much research has been performed to characterize these materials and understand the effects of F and C atom concentrations as well as plasma parameters (power, gas ratios, and pressure) on electrical and optical constants for these materials.[19-21,23-27]

1.2.1.2. Hydrogenated Fluorinated Amorphous Silicon Films. Deposition processes for amorphous silicon (a-Si) and its alloys (a-Si:H,F; a-Si_3N_4:H,F; and a-$Si_{1-x}C_x$:H,F) are of great importance to the microelectronics industry and F doped materials show significantly improved properties over that of traditional a-Si

Reproduced with permission of the copyright owner. Further reproduction prohibited without permission.

films.[5,6,8,10,11,14,28-32] Specifically, a-Si:H,F films are used in the fabrication of solar cells,[33-35] photoreceptors,[36] and thin film transistors.[29] Because of this, much work has been done to characterize film deposition as a function of various plasma parameters including rf power, flow ratios, and total pressure.[6,33,37-39] Moreover, several deposition mechanisms have been proposed based upon suggested deposition precursors.[6,29,34,37,40-42] Historically, these have depended primarily on the most abundant silicon radical species present in the plasma rather than surface reactivity of the species. The importance of a radical to film growth, however, is directly related to both the abundance of that radical and its reactivity at the surface.[43] Consequently, there is still controversy as to the true deposition mechanism for a-Si:H,F films. Experiments measuring gas-phase density and radical-surface reactivity are necessary for a full understanding of the role of species in the plasma.

1.2.2. Fluorine Atom Etching of Silicon. Dry etch processing of Si is used quite extensively in the fabrication of semiconductor integrated circuits because it offers the fabrication of high aspect ratio trenches without undercutting while maintaining high etch selectivity.[1,3,44-46] For example, a 0.2 μm wide, 4 μm deep trench, easily fabricated using dry plasma processing, is not attainable by any other commercial method.[1] Knowledge of both physical sputter etching by bombarding ions and chemical etching as well as side wall passivation by plasma species impinging upon the surface, however, is necessary for total etch control.[47-50] Moreover, the movement toward reducing feature dimensions increases the need for improving process control and a complete fundamental knowledge of plasma etch processes occurring in the gas phase and at the gas-surface interface.

Reproduced with permission of the copyright owner. Further reproduction prohibited without permission.

Many of the etch processes used in the semiconductor industry employ halogenated plasmas to etch silicon-containing materials.[3,51] A variety of feedgases and feedgas mixtures are used because of the range of requirements, including etch rate, selectivity, and anisotropy. Common silicon etch feedgases include fluorocarbons (CF_4, CHF_3, C_2F_6, etc),[52] chlorocarbons (CCl_4),[53] chlorofluorocarbons (CF_3Cl), halogenated inorganic molecules (SF_6, SiF_4),[54,55] pure etchants (F_2, Cl_2, Br_2),[3] as well as general etch compounds, including oxidants (O_2), reductants (H_2), and nonreactive gases (N_2, Ar, He).[1]

Fluorocarbon plasmas (FCPs) have been widely used in industry because of their intrinsic dual nature as both depositing and etching plasmas. Polymeric films deposited from FCPs promote etch anisotropy as a result of sidewall passivation amidst F atom etching. This versatility of FCPs comes from the formation of two types of long lived neutral species in the plasma. CF_x ($x = 1 - 3$) radicals promote film formation while F atoms promote silicon etching.[56] The presence of these two types of species is responsible for the competing processes.

Similar to FCPs, fluorosilane plasmas also have a dual nature. Addition of diluents such as O_2 and H_2 to fluorosilane plasmas can shift the overall process from etching to deposition.[6,54] Also analogous to FCPs, two types of neutral species are primarily responsible for competing processes. In these systems, SiF_x species are thought to promote film growth while F atoms are primarily responsible for silicon etching.[6,54] Many materials produced from fluorosilane plasmas have been investigated because of their desirable properties, yet no definitive mechanisms have been determined. Thus, further investigations into fluorosilane plasma processing

Reproduced with permission of the copyright owner. Further reproduction prohibited without permission.

may offer insight that will improve control over silicon etching and film formation in these systems.

1.3. Overview of Research-Fluorosilane Plasmas

Plasma processing, including deposition of thin films, surface modification of bulk materials, and selective etching, has found uses in a wide variety of applications. PECVD is useful for the generation of new and promising materials, like fluorine-doped materials, that can further technology in industries ranging from biomedicine to semiconductor fabrication.[1] Much research has been performed to characterize many of these materials, yet most of these studies are empirical in nature. Although such research is invaluable and demonstrates the versatility of plasma processing, it does not provide a solid understanding of plasma-surface modification mechanisms, which often remain unknown due to the complex nature of the plasma system. Thus, a more in-depth examination of the overall plasma system, including bulk material properties and radical-surface chemistry, is important to gain a better understanding and to obtain greater control of the resulting surface modification processes.

There are two main motivations for studying the film properties and radical surface interactions of fluorosilane systems. First, fluorosilane plasmas are technologically relevant for both Si etching and deposition of fluorinated silicon alloys. Although not currently used on a large scale, fluorosilane plasmas offer versatility in the types of materials and processes that can be achieved. In spite of this, definitive mechanisms still have not been elucidated. Characterization of plasma-surface interactions for key species in the plasma complements the existing research. Second, SiF_4 offers a good model system for fluorine-containing

Reproduced with permission of the copyright owner. Further reproduction prohibited without permission.

plasmas. It allows the examination of multiple radicals in a single system by a variety of analytical techniques. Of these techniques, laser-induced fluorescence (LIF) is capable of characterizing SiF, SiF_2 and HSiF, which allows a more complete mechanistic study of the system.[33,34,54] This research not only offers insight into the fluorosilane systems studied, but provides preliminary studies for characterization of SiF_x species in fluorocarbon etching systems. This is particularly important for studies of SiF_2, which is a known etch product during F atom etching of silicon.

Chapter 2 provides experimental details for the Resonance Enhanced Multiphoton Ionization (REMPI) technique, plasma deposition of F-SiO_2 and a-Si:H,F materials, the Imaging of Radicals Interacting with Surfaces (IRIS) technique, and a variety of film and gas-phase analysis techniques used.

The remaining chapters report results from these characterizations and are papers either submitted or published in scientific journals. Chapter 3 reports the initial measurements of gas phase SiF in SiF_4 and SiF_4/H_2 plasma systems. In this chapter, gas phase SiF is measured as a function of plasma power and gas flow conditions. Chapter 4 discusses the effect of plasma parameters (power, gas ratio, gas flow) upon thin film deposition of a-Si:H,F and molecule-surface reactivity (SiF and SiF_2) under both etch and deposition conditions. The thin film and surface reactivity data are correlated to offer insight into deposition mechanisms. Additionally, special emphasis is given to the effect of ion bombardment on both etching and deposition. Chapter 5 looks specifically at the effect of substrate temperature (T_s) on SiF_x scatter in the same fluorosilane systems. Since rotational temperature (Θ_R) can be directly affected by surface equilibration, Θ_R for SiF and SiF_2 are measured and discussed

Reproduced with permission of the copyright owner. Further reproduction prohibited without permission.

with respect to changes in surface scatter at different T_S. Finally, Chapter 6 provides a comparison study between six different SiO_2:F,C depositing systems. The effect of source gas, gas ratios, and plasma power were examined in the six plasma systems. In these plasmas, the silicon precursor gas was varied between tetraethylorthosilicate (TEOS) and hexamethyldisiloxane (HMDSO). Hexafluoropropylene oxide (HFPO), CF_4, and C_2F_6 were used as the fluorine and carbon sources, and O_2 was the single source for the oxidant. This film study demonstrates the importance of chemical composition as well as bonding environment on the physical attributes of a material. Additionally, it demonstrates the ability of PECVD processes to tailor film properties with changing plasma parameters.

Reproduced with permission of the copyright owner. Further reproduction prohibited without permission.

References

1. M. A. Lieberman, A. J. Lichtenberg *Principles of Plasma Dishcharges and Material Processing*, Wiley and Sons: New York, (1994).
2. A. Grill *Cold Plasma in Materials Fabrication*, IEEE Press: Piscataway, NJ, (1994).
3. S. J. Ullal, A. R. Godfrey, E. Edelberg, L. Braly, V. Vahedi, E. Aydil *J. Vac. Sci. Technol A* **20**, 43 (2002).
4. G. Francis *Ionization Phenomena in Gases*, Butterworths: London, (1960).
5. G. Cicala, G. Bruno, P. Capezzuto *J. Vac. Sci. Technol. A* **16**, 2762 (1998).
6. G. Bruno, P. Capezzuto, G. Cicala *J. Appl. Phys.* **69**, 7256 (1991).
7. K. H. A. Bogart, S. K. Ramirez, L. A. Gonzales, G. R. Bogart, E. R. Fisher *J. Vac. Sci. Technol. A* **16**, 3175 (1998).
8. K.-M. Byun, W.-J. Lee *Metals Mater.* **6**, 155 (2000).
9. P. Favia, G. Caporiccio, R. D'Agostino *J. Polymer Sci. A* **32**, 121 (1994).
10. T. Gungor, H. Tolunay *Turk. J. Phys.* **26**, 269 (2002).
11. G. Cicala, M. Losurdo, P. Capezzuto, G. Bruno *Plasma Sources Sci. Technol.* **1**, 156 (1992).
12. R. d'Agostino, F. Cramarossa, F. Fracassi, F. Illuzzi In *Plasma Deposition, Treatment, and Etching of Polymers*; d'Agostino, R., Ed.; Academic Press: San Diego, CA, 1990, pp 95-162.
13. K. H. A. Bogart, N. F. Dalleska, G. R. Bogart, E. R. Fisher *J. Vac. Sci. Technol. A* **13**, 476 (1995).

Reproduced with permission of the copyright owner. Further reproduction prohibited without permission.

14. D. Denison, A. Saproo, D. Hodul *U.S. Patent* **application: USS 97-886148 19970630**, 12 (1999).

15. F. Fracassi, R. d'Agostino, P. Favia *J. Electrochem. Soc.* **139**, 2636 (1992).

16. S. M. Han, E. S. Aydil *J. Vac. Sci. Technol. A* **15**, 2893 (1997).

17. S. M. Han, E. S. Aydil *J. Appl. Phys.* **83**, 2172 (1998).

18. S. Hasegawa, T. Tsukaoka, T. Inokuma, Y. Kurata *J. Non-Cryst. Solids* **240**, 154 (1998).

19. B.-G. Yu, K.-H. Kim, K. S. Suh, J. T. Baek *Jpn. J. Appl. Phys., Part 2* **35**, L745 (1996).

20. A. Sonnenfeld, T. M. Tun, L. Zajickova, K. V. Kozlov, H.-E. Wagner, J. F. Behnke, R. Hippler *Plasmas Polym.* **6**, 237 (2001).

21. N. Selamoglu, J. A. Mucha, D. E. Ibbotson, D. L. Flamm *J. Vac. Sci. Technol B* **7**, 1345 (1989).

22. J. Lubguban, A. Saitoh, Y. Kurata, T. Inokuma, S. Hasegawa *Thin Solid Films* **337**, 67 (1999).

23. J. Lubguban, Y. Kurata, T. Inokuma, S. Hasegawa *J. Appl. Phys.* **87**, 3715 (2000).

24. J. Lubguban, Y. Kurata, T. Inokuma, S. Hasegawa *Mat. Res. Soc. Symp. Proc.* **606**, 57 (2000).

25. G. B. Raupp, T. S. Cale, H. P. W. Hey *J. Vac. Sci. Technol. B* **10**, 37 (1992).

26. V. Pankov, J. C. Alonso, A. Ortiz *J. Appl. Phys.* **86**, 275 (1999).

27. L. Martinu, D. Poitras *J. Vac. Sci. Technol. A* **18**, 2619 (2000).

28. P. Capezzuto, G. Bruno *Pure Appl. Chem.* **60**, 633 (1988).

Reproduced with permission of the copyright owner. Further reproduction prohibited without permission.

29. G. Cicala, G. Bruno, P. Capezzuto *Pure & Appl. Chem.* **68**, 1143 (1996).

30. S. Kasouit, S. Kumar, R. Vanderhaghen, I. Roca, P. Cabarrocas, I. French *J. Non-Crystalline Solids* **299-302**, 113 (2002).

31. Y.-H. Kim, M. S. Hwang, H. J. Kim *J. Appl. Phys.* **90**, 3367 (2001).

32. K. R. Kull, M. L. Steen, E. R. Fisher *J. Membr. Sci.*, manuscript in preparation.

33. H. Lee, J. P. Deneufville, S. R. Ovshinsky *J. Non-Crystalline Solids* **59 - 60**, 671 (1983).

34. H. Lee, J. P. Deneufville *J. Non-Crystalline Solids* **66**, 39 (1984).

35. H. Koinuma, T. Manako, H. Natsuaki, H. Fujioka, K. Fueki *J. Non-Crystalline Solids* **77 - 78**, 801 (1985).

36. T. Nakanishi, Y. Marukawa, S. Takahashi *Electrophotography* **28**, 274 (1989).

37. A. Madan, S. R. Ovshinsky, E. Benn *Philos. Mag. B* **40**, 259 (1979).

38. A. A. Langford, B. P. Nelson, M. L. Fleet, R. S. Crandall *Phys. Rev. B* **42**, 7245 (1990).

39. A. A. Langford, A. H. Mahan, M. L. Fleet, J. Bender *Phys. Rev. B* **41**, 8359 (1990).

40. K. L. Williams, E. R. Fisher *J. Vac. Sci. Technol. A*, submitted for publication (2003).

41. S. Ray, S. C. De, G. Ganguly, A. K. Barua *J. Appl. Phys.* **65**, 4024 (1989).

42. S. Oda, S. Ishihara, N. Shibata, H. Shirai, A. Miyauchi, K. Fukuda, A. Tanabe, H. Ohtoshi, J. Hanna, I. Shimizu *Jpn. J. Appl. Phys.* **25**, L188 (1986).

Reproduced with permission of the copyright owner. Further reproduction prohibited without permission.

43. W. M. M. Kessels, M. C. M. van de Sanden, D. C. Schram *J. Vac. Sci. Technol. A* **18**, 2153 (2000).

44. R. Gottscho *Phys. World* **6**, 39 (1993).

45. P. G. M. Sebel, L. J. F. Hermans, H. C. W. Beijerinck *J. Vac. Sci. Technol. A* **18**, 2759 (2000).

46. E. Kay, A. Dilks *Thin Solid Films* **78**, 309 (1981).

47. D. E. Ibbotson, D. L. Flamm, J. A. Mucha, V. M. Donnelly *Appl. Phys. Lett.* **44**, 1129 (1984).

48. K. P. Giapis, T. K. Minton *Mat. Res. Soc. Symp. Proc.* **406**, 33 (1996).

49. D. L. Flamm, V. M. Donnelly, J. A. Mucha *J. Appl. Phys.* **52**, 3633 (1981).

50. R. d'Agostino, F. Cramarossa, V. Colaprico, R. d'Ettole *J. Appl. Phys.* **54**, 1284 (1983).

51. A. Tasaka, K. Takahashi, K. Tanaka, K. Shimizu, S. Mori, S. Tada, W. Shimizu *J. Vac. Sci. Technol A* **20**, 1254 (2002).

52. J.-H. Min, S.-W. Hwang, G.-R. Lee, S. H. Moon *J. Vac. Sci. Technol A* **20**, 1574 (2002).

53. G. K. Herb, R. A. Porter, P. D. Cruzan, K. Agraz-Guerena, B. R. Soller *Electrochem. Soc. Ext. Abstr.* **81-2**, 710 (1981).

54. K. L. Williams, E. R. Fisher *J. Vac. Sci. Technol. A*, submitted for publication (2003).

55. K. L. Williams, I. T. Martin, E. R. Fisher *J. Am. Soc. Mass. Spectrom.* **13**, 518 (2002).

56. H. K. Yasuda *Plasma Polymerization*, Academic Press: New York, (1985).

Reproduced with permission of the copyright owner. Further reproduction prohibited without permission.

CHAPTER 2

EXPERIMENTAL METHODS

This dissertation chapter contains two main sections, which describe the methods by which data discussed in the following chapters were collected. Section one describes gas phase techniques. This includes resonance enhanced multiphoton ionization mass spectrometry (REMPI-MS), the Imaging of Radicals Interacting with Surfaces (IRIS) technique, as well as various other common gas phase techniques. The REMPI-MS method was used to characterize gas-phase SiF production in SiF_4 and SiF_4/H_2 plasmas. The IRIS technique and the other gas-phase analytical techniques were used to identify and measure multiple species in the gas phase. The second section of this chapter provides a detailed description of the methods by which silicon alloy films were deposited in SiF_4-containing plasma systems and details the analytical techniques used to fully characterize these materials.

Reproduced with permission of the copyright owner. Further reproduction prohibited without permission.

2.1. Gas-phase analytical techniques

2.1.1. REMPI-MS technique. Figure 2.1 shows a schematic of our home-built apparatus constructed to detect and characterize ion and radical species using mass spectrometry. This instrument consists of three main regions: low-pressure plasma source, differentially pumped high vacuum chamber where the species of interest is ionized and extracted into the third region, which is a time of flight (TOF) mass spectrometer (MS). In each experiment, feed gases enter a glass tube, rf power is applied to an inductor coil, and a plasma is produced. Expansion of the plasma into a differentially pumped vacuum chamber, and ultimately into a high-vacuum region, generates an effusive molecular beam consisting of virtually all species present in the plasma, including the species of interest. A tunable laser beam intersects the molecular beam 25 cm downstream from the plasma source, excites, and ionizes the species of choice. For the present experiments, the extraction plates are continually biased. In this configuration, native ions are deflected by the extraction plates such that they do not enter the interaction region and only radicals ionized by resonance enhanced multiphoton ionization (REMPI) are detected. To examine native plasma ions, pulsed biasing of extraction plates can be employed with no laser ionization of radical species. This method is described in further detail elsewhere.[1] Ion signals are collected by a dual microchannel plate detector.

In the work presented in chapter 3, the source of the molecular beam is a plasma consisting of 100% SiF_4 (Matheson, 99.9%), SiF_4/H_2 (General Air, 99.99%), or $SiF_4:O_2$ (General Air, 99.99%) feed gases in various ratios. Total pressure in the source is 11-16 mtorr for all systems as measured by a capacitance

Reproduced with permission of the copyright owner. Further reproduction prohibited without permission.

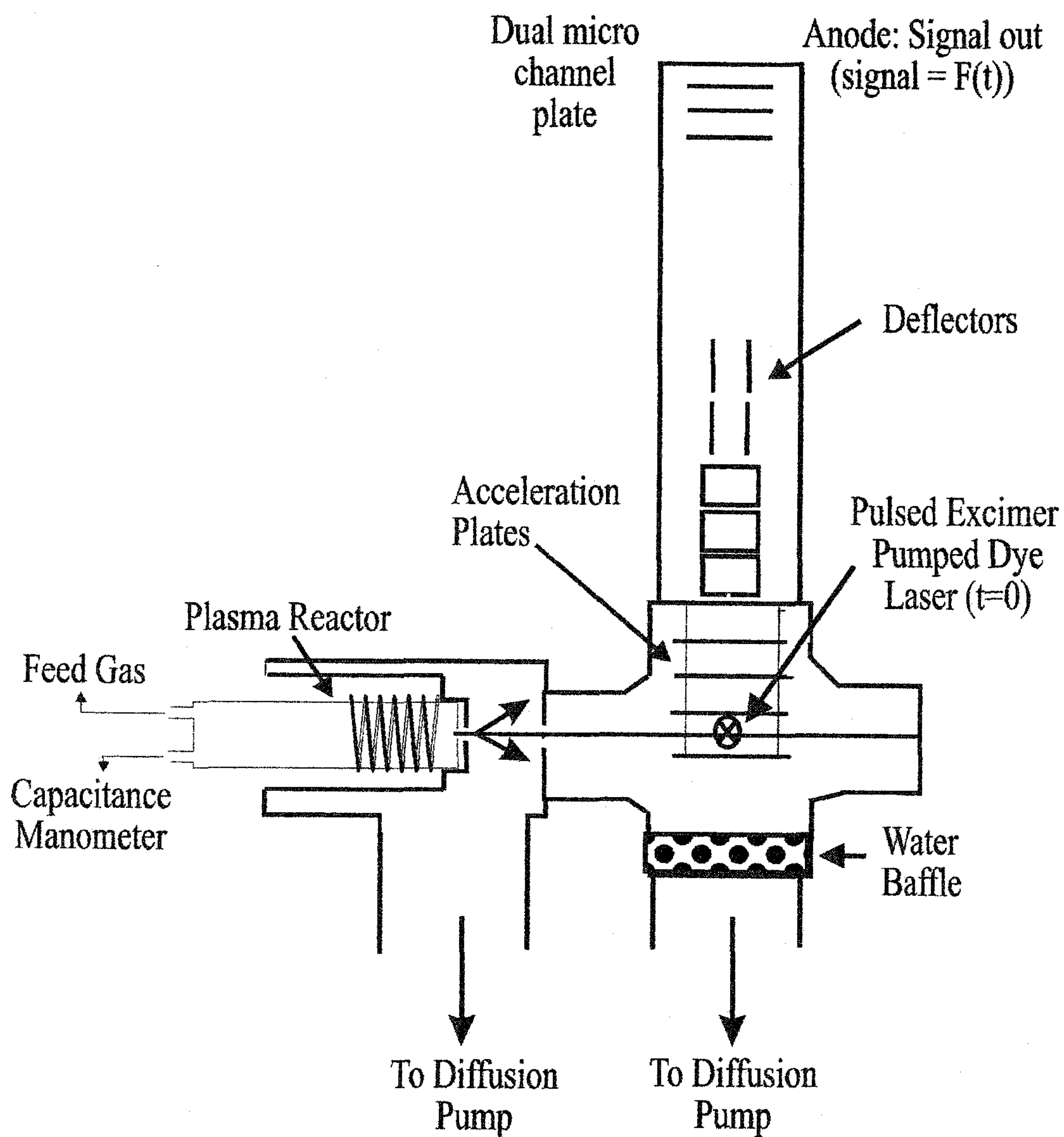

Figure 2.1. Schematic for the plasma molecular beam REMPI/TOF apparatus.

Reproduced with permission of the copyright owner. Further reproduction prohibited without permission.

manometer. The plasma is produced by the inductive coupling of 13.56 MHz rf power (140 and 180W) and is tuned by an rf matching network. The molecular beam is collimated by a slit, 2.5 mm wide, and irradiated with a focused dye laser. Tunable laser light in the 435-440 nm range (2 mJ/pulse) is produced by an excimer pumped (XeCl, 50 mJ, 40 Hz) dye laser system with Coumarin 120. No corrections for fluctuations in laser power were made. Ionized species are extracted from the molecular beam, accelerated to 2.5 kV to travel through a field-free drift tube (50 cm), and are detected using a dual microchannel plate detector (2.6 and 3kV) situated at the end of the TOF tube. Ion signals are collected for 10 acquisitions consisting of 200 scans each. Multiple sets of data are taken for each experiment.

One advantage of REMPI is that quantitative information on the density of a particular species in a complex molecular beam can be obtained using Eq. (2.1),[2]

$$n = \frac{I}{\left[I_{las} / \pi r^2\right]^m \sigma_2 (\sigma_i / \tau_L) q \pi r^2 h \left[1 - e^{-\tau_{es}/\tau_L}\right]} \qquad (2.1)$$

where I is the ion current measured by the microchannel plates, I_{las} is the dye laser intensity (photons per pulse), σ_i is the ionization cross section for SiF, σ_2 is the two photon excitation cross section for SiF, τ_{es} is the lifetime of the SiF $C''\ ^2\Sigma^+$ state, τ_L is the pulse width of the dye laser, and m is the total number of photons required for excitation and ionization.

Clearly, use of Eq. (2.1) requires knowledge of the cross sections for the multiphoton processes and the lifetime of the excited molecular state. Unfortunately, these values are not readily obtainable for SiF radicals. In this work, $I_{las} = 4.408 \times 10^{15}$ photons/pulse, r = 0.1 cm, h = 0.25 cm, and $\tau_L = 17$ ns. σ_i for SiF has previously

Reproduced with permission of the copyright owner. Further reproduction prohibited without permission.

been reported to be 7.13 x 10^{-17} cm^2 for the laser energy.[3] Values for σ_2 and τ_{es} for the SiF C″ $^2\Sigma^+$ state are not available in the literature. τ_{es}, however, was estimated from experimental results, which showed that the FWHM of our SiF signal was ~ 5 ns. This value has been used as an upper limit to the actual τ_{es} for the C″ state. To obtain a reasonable estimate for the density of SiF radicals in these experiments, $\sigma_2 \approx$ 4 x 10^{-42} cm^4 was used.[4] Although number densities for all of the data figures have not been explicitly calculated, the following are estimated densities for the given conditions: 4.6 x 10^{10} cm^{-3} for a 100% SiF_4 plasma at 180 W, 4.5 x 10^9 cm^{-3} for a 100% SiF_4 plasma at 50 W, and 1.8 x 10^9 cm^{-3} for 140 W SiF_4/H_2 plasmas with 10% H_2 and 2.0 x 10^9 cm^{-3} with 50% H_2 added.

2.1.2. IRIS data collection. The IRIS method, Fig. 2.2, has been described in detail previously.[5] In a typical IRIS experiment, feed gases enter at the rear of a glass reactor tube, rf power is applied to an inductor coil, and a plasma is produced. Expansion of the plasma into a differentially pumped vacuum chamber, and ultimately into a high vacuum region, generates an effusive molecular beam consisting of virtually all species present in the plasma, including the species of interest. A tunable laser beam intersects the plasma molecular beam downstream from the plasma source and excites the radical of interest. Spatially resolved LIF signals are collected by an electronically gated, intensified charge-coupled device (ICCD) located directly above the interaction region, perpendicular to both the molecular beam and the laser beam. A substrate is rotated directly into the path of the molecular beam and LIF signals are again collected. Differences between spatial

Reproduced with permission of the copyright owner. Further reproduction prohibited without permission.

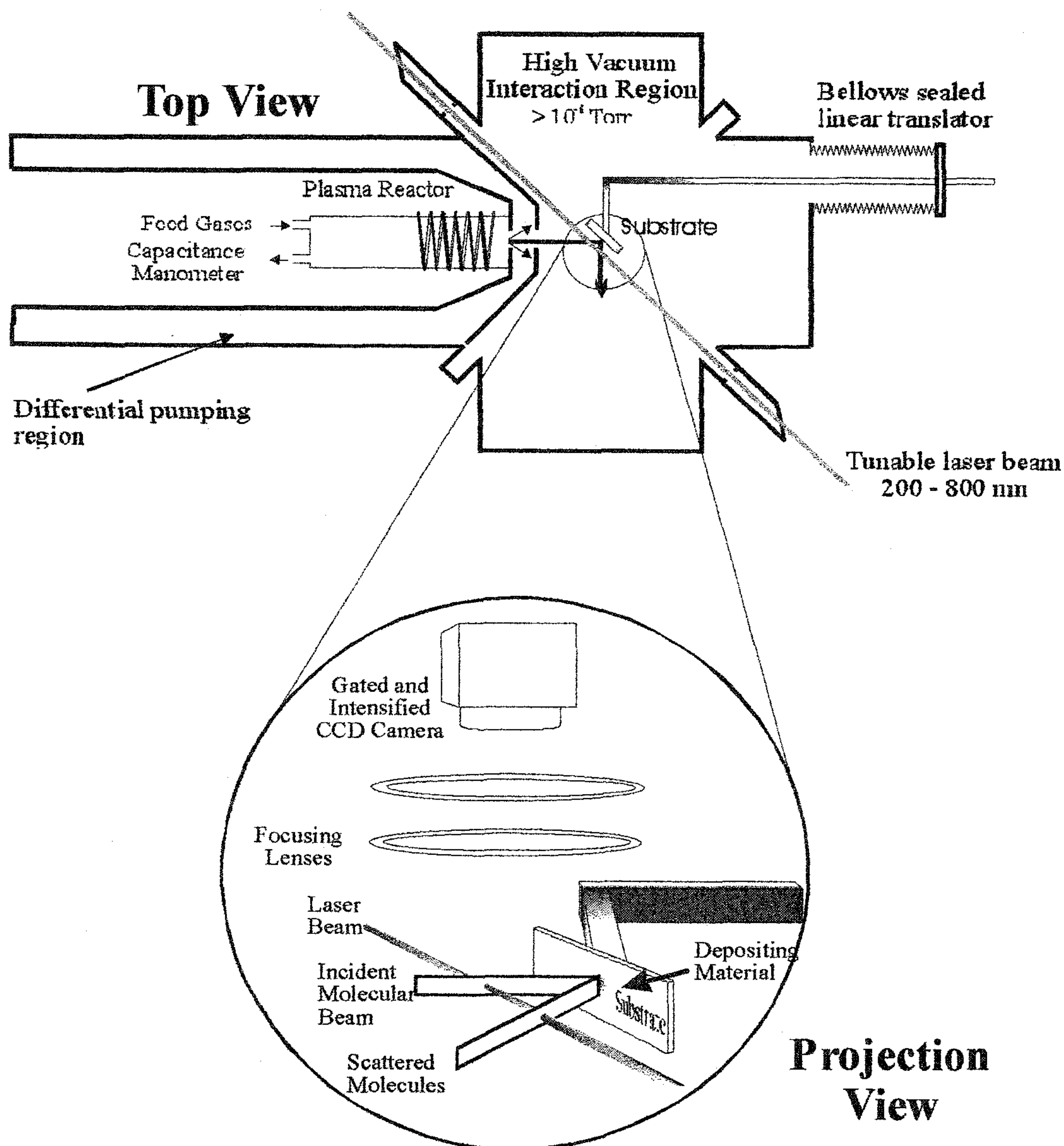

Figure 2.2. Schematic of the IRIS apparatus. The ICCD camera is located orthogonal to the plane of intersection and directly above the interaction region. In the ion perturbation experiments, a grounded mesh was placed on the chamber-side slit mounted to the liquid N_2 cold shield.

Reproduced with permission of the copyright owner. Further reproduction prohibited without permission.

distributions with the surface in and out of the molecular beam are used to measure radical-surface reactivity.

In the present work, the source of the molecular beam is a plasma consisting of either 100% SiF_4 (Matheson, 99.9%) or SiF_4 and H_2 (General Air, 99.9%) with a 50% or 10% H_2 mixture. Total pressure in the source is ~50 mTorr for the 15 sccm total flow experiments and ~100 mTorr for the 30 sccm total flow experiments, as measured by a capacitance manometer. The plasma is produced by the inductive coupling of 13.56 MHz rf power (P = 20, 40, 80, and 170 W) and is tuned by an rf matching network. The molecular beam was collimated by two slits, 1.6 and 1.7 mm wide. These slits were mounted on a liquid nitrogen cold shield, which was maintained at -178 °C during data collection.[6]

Substrates used here were 25 × 40 mm p-type silicon (100) wafers with ~20 Å of native oxide. The substrate was mounted with polished side facing the plasma molecular beam and positioned 3.0 - 6.0 mm away from the laser. For the substrate temperature (T_S) dependence experiments discussed in Chapter 4, substrate heating was obtained using a commercially available resistive heating element obtained from HeatWave, which was placed in direct contact with the metal face on which the substrate was held and thermally isolated from the substrate holder arm. Substrate temperatures were monitored using a thermocouple gauge attached to the front of the substrate and were maintained at the desired temperature (± 10 K).

For SiF experiments, tunable laser light in the 436.5 - 437.5 nm range (10 mJ/pulse) was produced by the output of an excimer pumped (XeCl, 100 mJ/pulse, 100 Hz) dye laser system with Coumarin 120. Additionally, frequency doubling was

Reproduced with permission of the copyright owner. Further reproduction prohibited without permission.

used to produce tunable laser light from 219 to 224 nm for all SiF_2 experiments (0.8 mJ/pulse). Because of the relatively low laser energy used for SiF_2 LIF collection, LIF data were collected as a function of laser power to determine laser saturation, Fig. 2.3. As a result, all SiF_2 data were collected at laser energies above 0.3 mJ/pulse. Excitation spectra of SiF_2 and SiF, shown in Chapter 4, have previously been well characterized, allowing clear identification of the spectral bands used for our IRIS experiments.[7,8] Reactivity measurements were made with the laser tuned to 437.416, 437.345, and 437.296 nm corresponding to the 9.5, 4.5, and 0.5 J states (PQ_{12} or Q_1 branches) of the (0,0) band of the SiF $A^2\Sigma^+ \rightarrow X^2\Pi$ electronic transition, respectively. For SiF_2 reactivity measurements, the laser was tuned to 221.53 nm, 220.40 nm, or 219.178 nm, corresponding to the 2^4_0, 2^5_0, or 2^6_0 vibronic band of the $A^1B_1 - X^1A_1$ transition, respectively. The LIF signal was imaged directly onto the ICCD camera, which has a 586 × 384 pixel display, yielding an imaged area of 109 mm^2. Pixels were binned (4 x 4) to increase signal-to-noise and reduce processing time. No corrections for fluctuations in laser power were made.

The gate width for the ICCD camera was set to 0.8 μs for SiF_2 and to 0.3 μs for SiF. These gate widths were selected based on the radiative lifetime of the two molecules. For SiF, the literature value of 230 ns was used.[8] For SiF_2, a range of radiative lifetime values (from 50 ns to 6μs) is available in the literature.[7] To help clarify this in our system, a lower limit to the radiative lifetime has recently been measured ~250 ns in the SiF_4 plasma system.[9] Because SiF_2 LIF signal can be collected for significantly longer times than for SiF, it is believe the radiative lifetime of SiF_2 is somewhat higher than this value. For both molecules, LIF signal was

Reproduced with permission of the copyright owner. Further reproduction prohibited without permission.

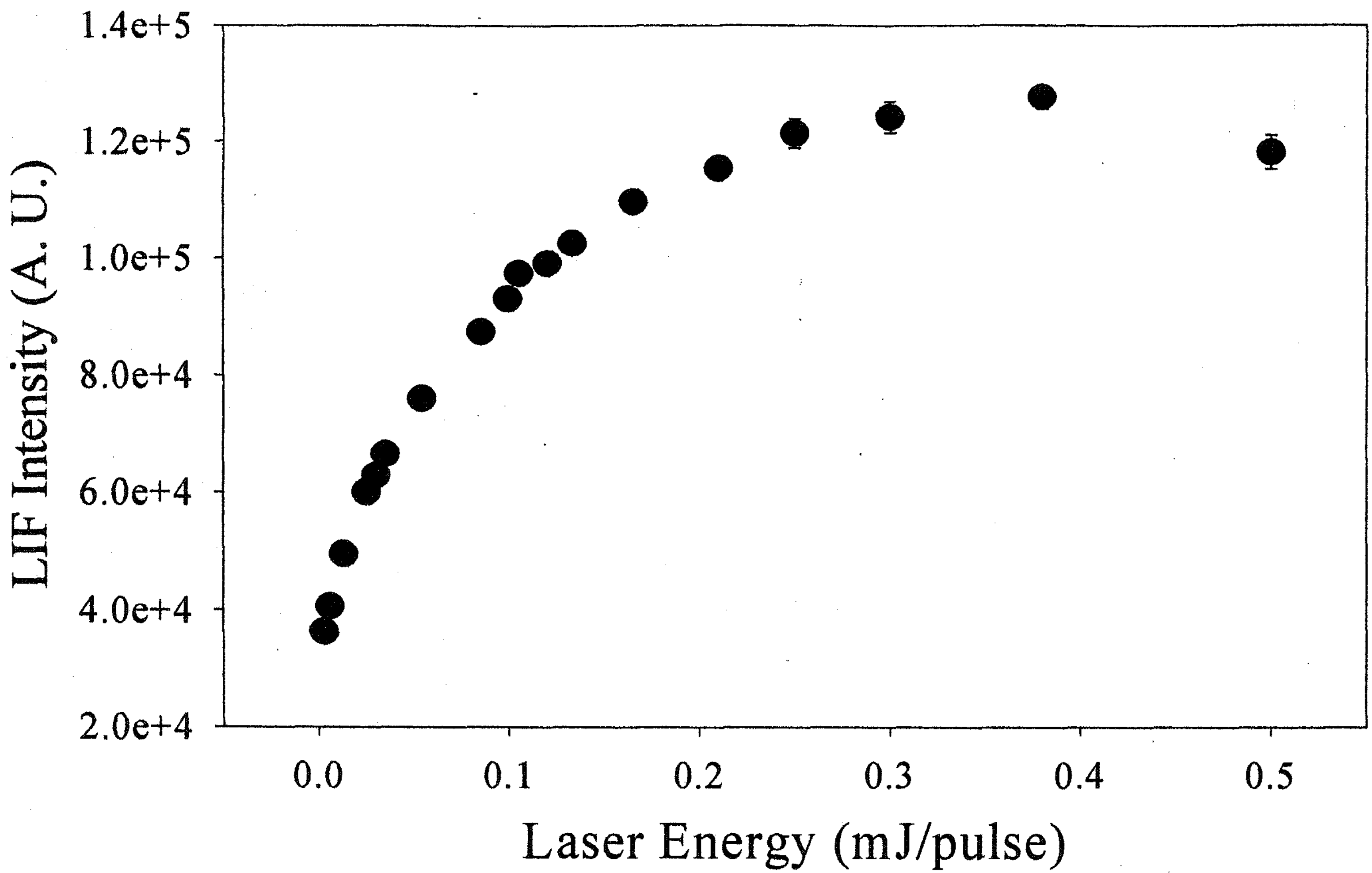

Figure 2.3. SiF_2 LIF intensity as a function of laser energy. All SiF_2 LIF data were collected at laser energies above 0.3 mJ/pulse.

Reproduced with permission of the copyright owner. Further reproduction prohibited without permission.

collected for 10 to 20 accumulations of 30 s exposures each. Multiple sets of data were taken for each experiment. Background images were taken with the laser tuned to an off-resonance frequency and were subtracted from the data image. A 1-D cross-section of each image was made by averaging a column 20 pixels wide (7.74 mm) containing the LIF signal and plotting signal intensity as a function of distance along the laser beam path.

Spatially resolved LIF data are interpreted using a quantitative model of the experiment, which reproduces the scattering data in one dimension. A detailed description of the simulation is given elsewhere.[10] Briefly, the simulation is based on the known geometry of the experiment and calculates the spatial distribution of the radical number density in the molecular beam at the interaction region. This model also calculates the radical number density along the laser beam for molecules scattering from the substrate surface. To adequately describe the spatial distribution of molecules desorbing from a surface, a specific scattering mechanism must be assumed. This simulation allows for either specular or adsorption-desorption scattering. In the present work, only adsorption-desorption scattering is observed. The calculated curve for this type of scatter assumes that all incident radicals leave the surface with a cosine distribution about the surface normal. To determine surface reactivity of a specific molecule, the fraction of radicals scattering from the surface, S, relative to those in the molecular beam is adjusted to best fit the experimental data. Since surface production of SiF_2 occurs for most experimental conditions, our results are presented in terms of S which is related to the surface reaction probability (R) by $R = 1 - S$.

Reproduced with permission of the copyright owner. Further reproduction prohibited without permission.

IRIS experiments measure the relative densities of molecules in the incident molecular beam and scattered from a surface. If the velocity distributions of the two populations (i.e. the molecular beam molecules and the scattered molecules) are significantly different, this can affect their densities in the laser. This can be accounted for by scaling S by the ratio of the velocities, equation 1:

$$S_{corr} = \frac{v_{mb}}{v_{scat}} \tag{1}$$

where v_{mb} is the velocity of molecules in the molecular beam and v_{scat} is the velocity of molecules scattered from the surface. SiF and SiF_2 velocities in SiF_4 plasmas have previously been measured in our laboratory and are used here to correct for surface equilibration.[9] Note that for the velocity distributions of scattered molecules, we assume thermal equilibration with the surface has occurred. Thus, the velocity of scattered molecules is characterized by T_S.

In Chapter 5, ion effects on SiF_x reactivity were investigated by two methods. First, the substrate was biased at ±200 V_{dc}. This is expected to perturb only charged species in the plasma molecular beam. A +200 V_{dc} bias should deflect all positive ions present in the molecular beam away from the Si substrate, while a -200 V_{dc} bias will accelerate all positive ions toward the Si substrate. In the second experiment, the plasma molecular beam was passed through a grounded mesh (g.m.) mounted onto the second slit (main chamber side), effectively reducing the density of all charged species. In this configuration, the grounded mesh does not perturb the energetics of neutral plasma species.[11]

2.1.3. Mass spectrometry experiments. Gas phase measurements of plasma species in the molecular beam[12] were conducted using a Dycor LC200S quadrupole

Reproduced with permission of the copyright owner. Further reproduction prohibited without permission.

mass spectrometer (MS). The MS was mounted onto the IRIS instrument to sample species at the position of the substrate holder, Fig. 2.4. This positioned the MS detector directly in-line with the plasma molecular beam approximately ~20 cm downstream from the plasma source. A 30 eV ionization energy was used to characterize all neutral species as a function of both $\%H_2$ in the feed gas and applied rf power. Atmospheric H_2O and hydrocarbon contamination (pump oil) were found in low concentrations. These sources of hydrogen can react to produce both HF and $HSiF_2$ signals for the 100% SiF_4 plasma systems. All measurements were background corrected by subtracting a mass spectrum of the source gas. This accounts for signal resulting from monomer cracking in the mass spectrometer.

2.1.4. Optical emission spectroscopy. The reactor detailed in the following section (Fig. 2.5) was fitted with a replaceable quartz window located at the end of the plasma reactor tube away from the reactor coil. The orientation of this window allowed for collection of plasma emission down the full length of the reactor tube minimizing the integration time necessary for data collection. An Ocean Optics S2000 triple spectrometer was used for all optical emission spectroscopy (OES) experiments. Three separate fiber optic bundles were used to collect a total wavelength range of 240 – 700 nm. Light from each optical fiber bundle was imaged through a 10 μm entrance slit onto holographic gratings (1800 grooves/cm). The separated wavelengths were then projected onto three 2048 element linear charged coupled device-array detectors for high-resolution detection of atomic and molecular emission lines. Signals were integrated for times between 2 and 60 s.

Reproduced with permission of the copyright owner. Further reproduction prohibited without permission.

Reproduced with permission of the copyright owner. Further reproduction prohibited without permission.

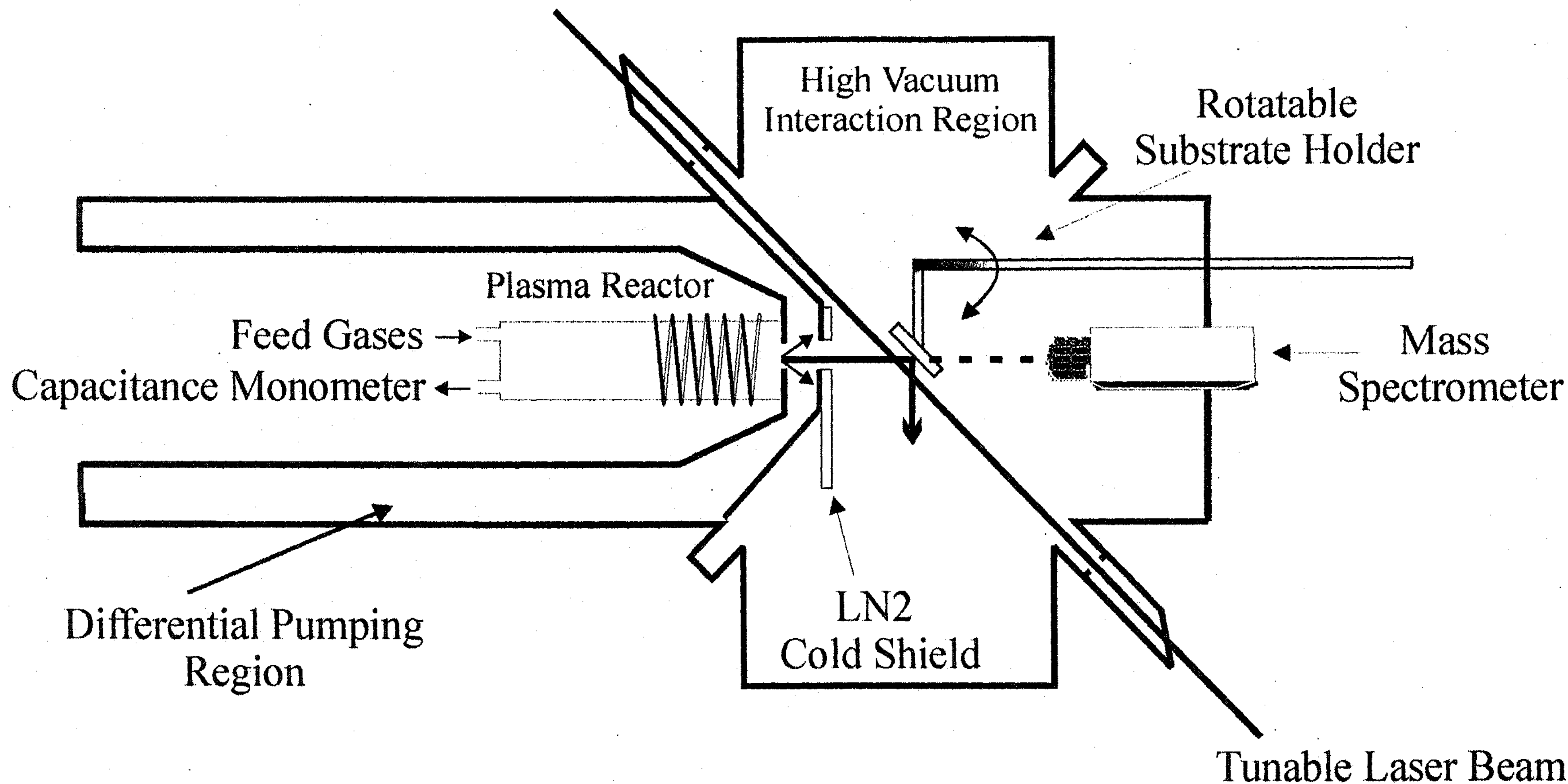

Figure 2.4. Schematic of MS mounted to IRIS chamber. For MS studies, the substrate holder flange is removed and replaced with one containing the quadrupole mass spectrometer directly in-line with the plasma molecular beam.

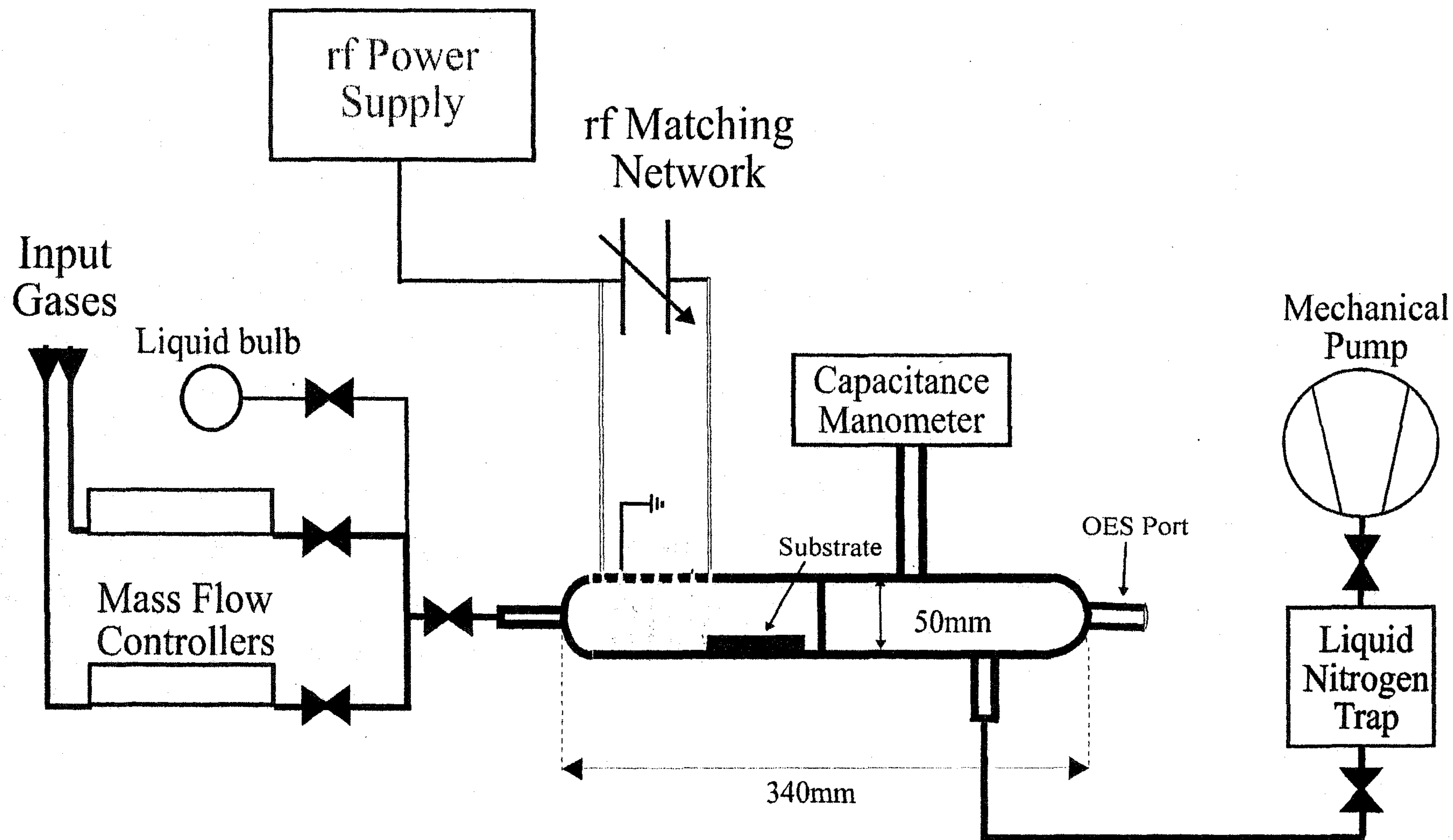

Figure 2.5. Schematic of the plasma reactor used for deposition of a-Si:H,F and SiO_2:F,C materials. Optical Emission spectroscopy was performed using the quartz OES window located at the end opposite the reactor coil.

Reproduced with permission of the copyright owner. Further reproduction prohibited without permission.

2.2. Surface characterization methods

All of the plasma generated materials studied in this work were produced in a home-built tubular glass inductively coupled rf plasma reactor, Fig. 2.5. The reactor consisted of two cylindrical Pyrex tubes held together by a 50 mm o-ring joint and a Thomas pinch clamp. Glass sleeves were employed to reduce deposition on the reactor walls. An 8 ½ turn, 10 gauge nickel-coated copper wire was used for the inductor coil. Gases were introduced through a single ¾ inch port located directly in front of the inductor coil. Gas products were removed from the system through a liquid N_2 cold trap by an Alcatel 2012A mechanical pump at a speed of 4.2 Ls^{-1}. Power was supplied to the inductor coil by an Advanced Energy RFPP 5s power supply, which has a 13.56 MHz power range of 0 - 500 W.

2.2.1. Amorphous Si:H,F deposition. All a-Si:H,F films were deposited in the plasma reactor described above, using inductively coupled rf (13.56 MHz) plasma enhanced chemical vapor deposition (PECVD).[13] Film deposition conditions were nearly identical to those in the IRIS molecular beam source. SiF_4 (Matheson, 99.9%) and H_2 (General Air, 99.9%) were admitted into the plasma chamber through MKS mass flow controllers such that the total gas flow was 30 sccm and the total pressure in the reactor remained ~400 mTorr, as measured with an MKS Baratron capacitance manometer. In addition, ion effects upon film deposition were investigated by depositing films on substrates placed between biased copper plates (one biased to +200 V, the other grounded). With this configuration, ions are effectively prevented from reaching the substrate surface.

Reproduced with permission of the copyright owner. Further reproduction prohibited without permission.

Substrates were silicon wafers (p-type, ⟨100⟩) with a native oxide thickness of ~12 Å that were scribed to dimensions of ~10 × 10 mm. The substrates were oriented parallel to the gas flow and placed in the center of the coil region. Amorphous Si:H,F films were deposited as a function of both percent H_2 in the feed gas (0-50%) and plasma power (P) from 5 - 170 W. Deposition times were 20 minutes for films analyzed by FTIR and 5 minutes for films analyzed by ellipsometry and XPS.

2.2.2. SiO_2:F,C deposition. All films were deposited in our home built inductively coupled rf plasma reactor, Fig. 2.5. For all depositions, the applied rf power was held constant at 80 W. The pressure in the chamber was monitored with an MKS Baratron capacitance manometer, which is insensitive to differing gas compositions and was stabilized to the desired pressure prior to plasma ignition. Because three feed gases were used in these experiments, partial pressures were used to determine the relative concentrations of each gas for a given deposition. Hexamethyldisiloxane, HMDSO (Aldrich, 99.99%), was placed in a 100 mL Pyrex glass sidearm vacuum flask with a Teflon stopcock and underwent three freeze-pump-thaw cycles to remove dissolved gases. Tetraethoxysilane, TEOS (Schumacher Extrema, 99.9999%), was supplied in a stainless steel tank that underwent a similar gas-removal procedure. Both TEOS and HMDSO were admitted to the plasma through room temperature gas lines, and their vapor pressures were maintained at 50 and 75 mtorr (±2%), respectively, using a Nupro bellows-sealed valve. The silicon precursor pressure in the reactor was allowed to stabilize prior to the addition of oxidant and fluorocarbon sources. O_2 (General Air, 99.993%) and the fluorocarbon precursors, CF_4 (Matheson, 99.99%), C_2F_6 (Matheson, 99.99%), and

Reproduced with permission of the copyright owner. Further reproduction prohibited without permission.

hexafluoropropylene oxide (HFPO, Aldrich, 98%), were added to the existing alkoxysilane flow through MKS mass flow controllers. The O_2 and FC percentages are calculated from the partial pressure of a given precursor divided by the total pressure. For the O_2 dependence studies, the flow was adjusted so that the O_2 pressure varied between 0 and 930 mtorr (0 - 90%), while the silicon and fluorocarbon (20-150 mtorr) sources were held constant. For FC dependence studies, the fluorocarbon flow was adjusted so that it did not exceed 50% of the total gas concentration and was varied while O_2 was held constant at ~500-750 mtorr, depending on the system. Partial pressures and percentages for feed gas conditions used to acquire the FTIR and high-resolution XPS data presented here are listed in Table 2.1.

Substrates were 5 x 5 cm pieces of silicon wafers (p-type, ⟨100⟩) with ~12 Å of native oxide (used for ellipsometry measurments); 1 x 1 cm pieces of silicon wafers (p-type, ⟨100⟩) with ~300 Å TiO_2 (used for XPS analysis); and KBr pellets (used for FTIR measurements). All substrates were oriented parallel to the gas flow and placed ~10 cm downstream from the rf coil. The deposited SiO:F,C films were analyzed *ex situ* by FTIR and XPS for film composition and by spectroscopic ellipsometry (SE) for film thickness and refractive index.

Reproduced with permission of the copyright owner. Further reproduction prohibited without permission.

Table 2.1. Feed gas concentrations for FTIR and XPS data.[a]

Figure	P_{Si} (mtorr)	%Si	P_{O2} (mtorr)	$\%O_2$	P_{FC} (mtorr)	% FC	P_{total} (mtorr)
1a (HMDSO)	75	41.7	0	0.0	105	58.3	180
1b (HMDSO)	75	21.7	171	49.4	100	28.9	531
1c (HMDSO)	75	11.0	500	73.0	110	16.0	685
1d (HMDSO)	75	7.6	800	81.0	113	11.4	988
2a (HMDSO)	75	9.0	738	88.5	21	2.5	834
2b (HMDSO)	75	8.8	738	87.0	36	4.2	849
2c (HMDSO)	75	8.0	738	79.1	120	12.9	933
8a, 10a, 10b (TEOS)	50	34.3	0	0.00	96	65.7	146
8b (TEOS)	50	25.0	50	25.0	100	50.0	200
8c (TEOS)	50	15.6	180	56.3	90	28.1	320
8d, 10c, 10d (TEOS)	50	5.6	750	84.3	90	10.1	890

[a]Partial pressures and concentrations (%) of the three gas precursors for the FTIR and XPS data shown in the given figures.

Reproduced with permission of the copyright owner. Further reproduction prohibited without permission.

2.2.3. Fourier transform infrared spectroscopy. KBr pellets were used as substrates for plasma deposition of silicon alloy films. Transmission FTIR spectra were obtained *ex situ* using a Nicolet 760 FTIR spectrometer. N_2 purging was used to reduce absorption from atmospheric moisture and CO_2. All spectra were collected using 8 cm^{-1} resolution and averaging over 128 scans. Corrections were made for a sloping baseline and atmospheric CO_2 absorption.

2.2.4. Scanning electron microscopy. SEM images were obtained using a Phillips 505 microscope with an accelerating voltage of 20 – 30 keV and a 50 nm spot size. Either a silicon wafer or a copper wire was used as the substrate for plasma deposition. Preparation for SEM analysis involved, first, affixing the sample to a standard SEM sample stub using double-sided copper tape (3M). To prevent surface charging during imaging, a ~20 nm Au film was sputter coated onto the surface of all samples. Films deposited onto silicon substrates were imaged at a 60° angle (with respect to surface normal) for better contrast. Coated wires, however, were imaged at 0 degrees.

2.2.5. X-ray photoelectron spectroscopy. XPS analyses were performed on a Physical Electronics PE5800 system, equipped with a 2 mm monochromatic Al K_α X-ray source, hemispherical analyzer, and multichannel detector. A low energy (~1 eV) electron neutralizer was used for charge neutralization. Survey spectra were collected using an analyzer pass energy of 93.90 eV and high resolution C_{1s} spectra were acquired using a pass energy of 23.50 eV and were fit using Gaussian functions. A photoelectron take-off angle of 45°, which corresponds to ~40 Å sampling depth, was used. Binding energy scales were referenced by setting the C-C peak maximum

Reproduced with permission of the copyright owner. Further reproduction prohibited without permission.

in the C_{1s} spectra to 284.8 eV, and the Si-O peak maximum in the Si_{2p} spectra to 103.7 eV.[14]

2.2.6. Variable angle spectroscopic ellipsometry. Films deposited on silicon wafers were analyzed using a J. A. Woolam VASE variable angle spectroscopic ellipsometer. Spectra from 300 to 1500 nm in 20 nm increments were collected at 75° and 85° for three locations per sample. Experimental data were modeled using a Cauchy model for non-absorbing low k dielectric materials. Film thickness and refractive index were determined using the model. Profilometry was used to independently confirm film thickness. For these measurements, a portion of the Si substrate was masked using Scotch tape, which was removed after deposition. The resulting step edge was then measured with a Sloan-Dektak IIA profilometer. With both measurement types, deposition rates were calculated by dividing the average film thickness by the deposition time. All deposition rates are the average of three different samples using measurements taken from two different spots on each film.

Reproduced with permission of the copyright owner. Further reproduction prohibited without permission.

References

1. W. C. Flory, K. L. Williams, E. R. Fisher, (unpublished work).
2. G. Scoles *Atomic and Molecular Beam Methods*, Oxford University Press: New York, (1988).
3. T. R. Hays, R. C. Wetzel, F. A. Baiocchi, R. S. Freund *J. Chem. Phys.* **88**, 823 (1988).
4. P. M. Johnson *Acc. Chem. Res.* **13**, 20 (1980).
5. P. R. McCurdy, K. H. A. Bogart, N. F. Dalleska, E. R. Fisher *Rev. Sci. Instrum.* **68**, 1684 (1997).
6. P. R. McCurdy, V. A. Venturo, E. R. Fisher *Chem. Phys. Lett.* **274**, 120 (1997).
7. Y. M. Khanna, G. Besenbruch, J. L. Margrave *J. Chem. Phys.* **46**, 2310 (1967).
8. S. J. Davis, S. G. Hadley *Phys. Rev. A* **14**, 1146 (1976).
9. J. Zhang, K. L. Williams, E. R. Fisher *J. Phys. Chem. A*, submitted for publication. (2002).
10. K. H. A. Bogart, J. P. Cushing, E. R. Fisher *Chem. Phys. Lett.* **267**, (1997).
11. P. R. McCurdy, C. I. Butoi, K. L. Williams, E. R. Fisher *J. Phys. Chem. B* **103**, 6919 (1999).
12. Only 15 sccm total gas flow was used to maintain proper working conditions of the mass spectrometer.
13. N. M. Mackie, D. G. Castner, E. R. Fisher *Langmuir* **14**, 1227 (1998).

Reproduced with permission of the copyright owner. Further reproduction prohibited without permission.

14. J. F. Moulder, W. F. Stickle, P. E. Sobel, K. D. Bomben *Handbook of X-Ray Photoelectron Spectroscopy*, Physical Electronics: Minneapolis, MN, (1995).

Reproduced with permission of the copyright owner. Further reproduction prohibited without permission.

CHAPTER 3

MULTIPHOTON IONIZATION DETECTION OF SiF RADICALS

Reprinted with permission from : Keri L. Williams, Vincent A. Venturo, J. A. Bray, and Ellen R. Fisher, *Chemical Physics Letters*

This dissertation chapter contains results from a paper published in the journal of *Chemical Physics Letters*. The manuscript was written by Keri L. Williams and edited by Ellen R. Fisher. Vincent A. Venturo is responsible for building the REMPI-TOF instrument. J. A. Bray developed the equation for calculating number density, and all data was collected and analyzed by Keri L. Williams. This chapter describes the effect of plasma parameters such as rf power and source gas ratios on the gas-phase production of SiF radicals. Additionally, this paper is a proof of concept for the REMPI-MS technique developed in the Fisher laboratory.

Reproduced with permission of the copyright owner. Further reproduction prohibited without permission.

3.1. Introduction

Silicon-fluorine etching and fluorinated amorphous silicon (a-Si:F) deposition processes are important in the microelectronics industry as well as in the production of other materials. Specifically, amorphous hydrogenated, fluorinated silicon (a-Si:H,F) films deposited from SiF_4/H_2 plasmas have been used in the fabrication of solar cells.[1] In addition, fluorinated SiO_2 films deposited from SiF_4/O_2 plasmas, have become the substance of choice for intermetal dielectric (IMD) materials used in electronic devices.[2] This is largely because of significantly improved material properties[3] such as thermal stability,[4] improved photoconductivity,[5] and decreased dielectric constant[6] offered by fluorinated a-Si films (a-Si:H,F, F-SiO_2) over that of traditional a-Si films.[7-9]

Unfortunately, little is known about many mechanistic aspects of both a-Si:H,F film deposition and selective etching of Si,[7,8,10,11] SiO_2,[8,10] and Si_3N_4[8,10] films. Hence, there has been a continued effort to elucidate the roles of different ion, neutral, and radical species involved in deposition and etching processes.[1,6,12-15] These methods, however, often perturb the plasma, require *ex situ* analysis, or do not offer detection of all plasma species. Resonance enhanced multiphoton ionization (REMPI) coupled with time of flight mass spectrometry (TOFMS), on the other hand, is well suited for selective, *in situ* identification of many gas phase species.[16-18] Other non-intrusive methods for detection of small molecules like SiF (and SiCl in analogous $SiCl_4$ plasmas) include optical emission spectroscopy (OES), laser induced fluorescence (LIF), and electron impact (EI) or multiphoton ionization (MPI) mass spectrometry. REMPI is complementary to these methods because it directly

Reproduced with permission of the copyright owner. Further reproduction prohibited without permission.

measures ground state molecule densities as opposed to excited species (as with OES), it does not induce fragmentation of the species (a potential problem with EI), and is more sensitive than MPI. Although LIF and REMPI are comparable optical techniques for the detection of radical species, REMPI offers the added benefit of high sensitivity for non-fluorescing species. As SiF can also be observed using LIF, in the present work we have used the detection of this radical to demonstrate our REMPI capabilities while still being able to compare these results with those measured using LIF, which are presented in Chapter 5.

Thus, we have employed [2 + 1] REMPI/TOFMS for the first time in the detection of the SiF radical produced in SiF_4, SiF_4/H_2, and SiF_4/O_2 rf plasmas. SiF is an important intermediate in the deposition of a-Si:F materials and in the etching of silicon by fluorinated gases.[19] As an extension of our imaging of radicals interacting with surfaces (IRIS) technique,[20] described in Chapter 2, we have constructed a new molecular beam apparatus designed for measurement of plasma species employing REMPI/TOFMS detection. The first stage of implementation for this instrument is the identification of plasma species through collection of mass spectra and excitation spectra. In this chapter, gas phase densities for SiF in these plasmas have been measured as a function of plasma parameters, including $\%H_2$, $\%O_2$, and applied rf power. The laser-induced ionization of SiF is achieved by a one-photon resonance transition from the (1, 0) $C'' \, ^2\Sigma^+$ Rydberg state, whereas excitation is obtained by the two-photon resonance transition from the (1, 0) $C'' \, ^2\Sigma^+ \leftarrow X \, ^2\Pi_{1/2}$ band with additional resonance enhancement involving one-photon transitions from the $A \, ^2\Sigma^+ \leftarrow X \, ^2\Pi_{1/2}$ and $C'' \, ^2\Sigma^+ \leftarrow A \, ^2\Sigma^+$ states.[16,18]

Reproduced with permission of the copyright owner. Further reproduction prohibited without permission.

3.2. Results and Discussion

3.2.1 Mass and excitation spectra. Figure 3.1 shows a mass spectrum taken for a 180 W, 100% SiF_4 rf plasma. It is clear from the completely resolved ^{28}SiF, ^{29}SiF, and ^{30}SiF isotope peaks in this figure that our mass spectrometer is better than 0.5 amu in this mass range. Using these data, a rough estimate of the resolution of the instrument shows $R > 250$. Moreover, the isotopic ratios of these peaks (92.6%, 4.6%, and 2.8%, respectively) agree well with the known literature values of 92.23%, 4.67%, and 3.10% for ^{28}Si, ^{29}Si, and ^{30}Si.[21] No mass peaks due to fragmentation of the parent SiF^+ are observed at this wavelength.

An excitation spectrum for SiF, obtained by tuning the laser in 0.005 nm increments from 435 – 440 nm (1 s/step) and integrating only over the ^{28}SiF peak, is shown in Fig. 3.2. This spectrum is in good agreement with those reported earlier.[16-18] All data presented here were taken with the laser tuned to the band at 438.1 nm corresponding to the (1,0) $C''\ ^2\Sigma^+ \leftarrow X\ ^2\Pi_{1/2}$ SiF transition. The extreme intensity of this transition can be accounted for by noting that the one photon LIF spectrum of the SiF (0, 0) $A\ ^2\Sigma^+ \leftarrow X\ ^2\Pi_{1/2}$ band reported by Davis and Hadley[22] displayed a red degraded band head at 436.8 nm. Hence, the REMPI band observed is enhanced by sequential one photon transitions between real states.

3.2.2 Power Dependence. Since increasing the plasma rf power can convert the overall plasma process from deposition to etching, the effects of rf power upon SiF production have been investigated. SiF^+ intensity as a function of rf power for both a 100% SiF_4 plasma and a 75:25 SiF_4:O_2 plasma are shown in Fig. 3.3. Below

Reproduced with permission of the copyright owner. Further reproduction prohibited without permission.

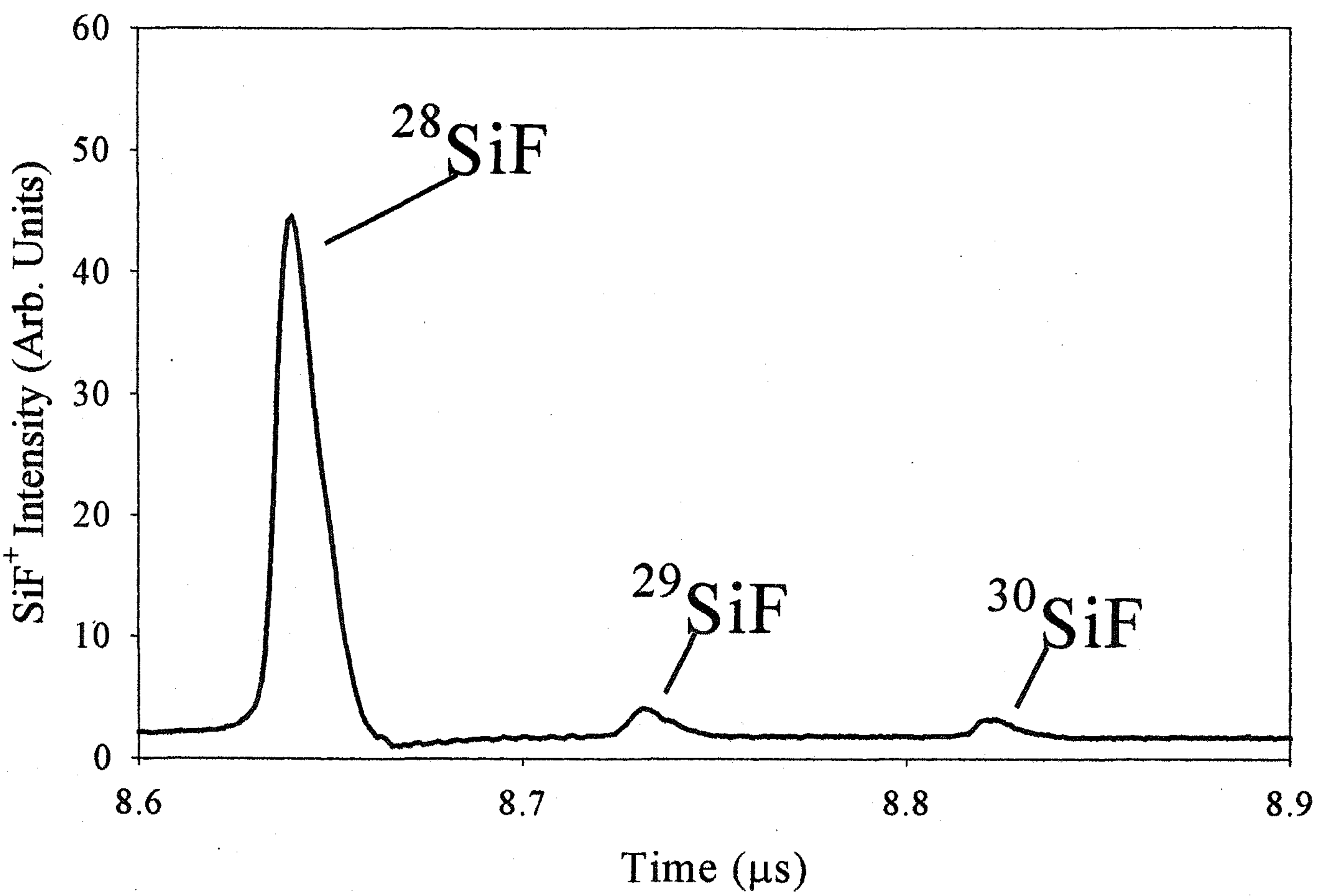

Figure 3.1. Mass resolved time of flight spectrum of 100% SiF_4. The applied rf power to the plasma was 180 W.

Reproduced with permission of the copyright owner. Further reproduction prohibited without permission.

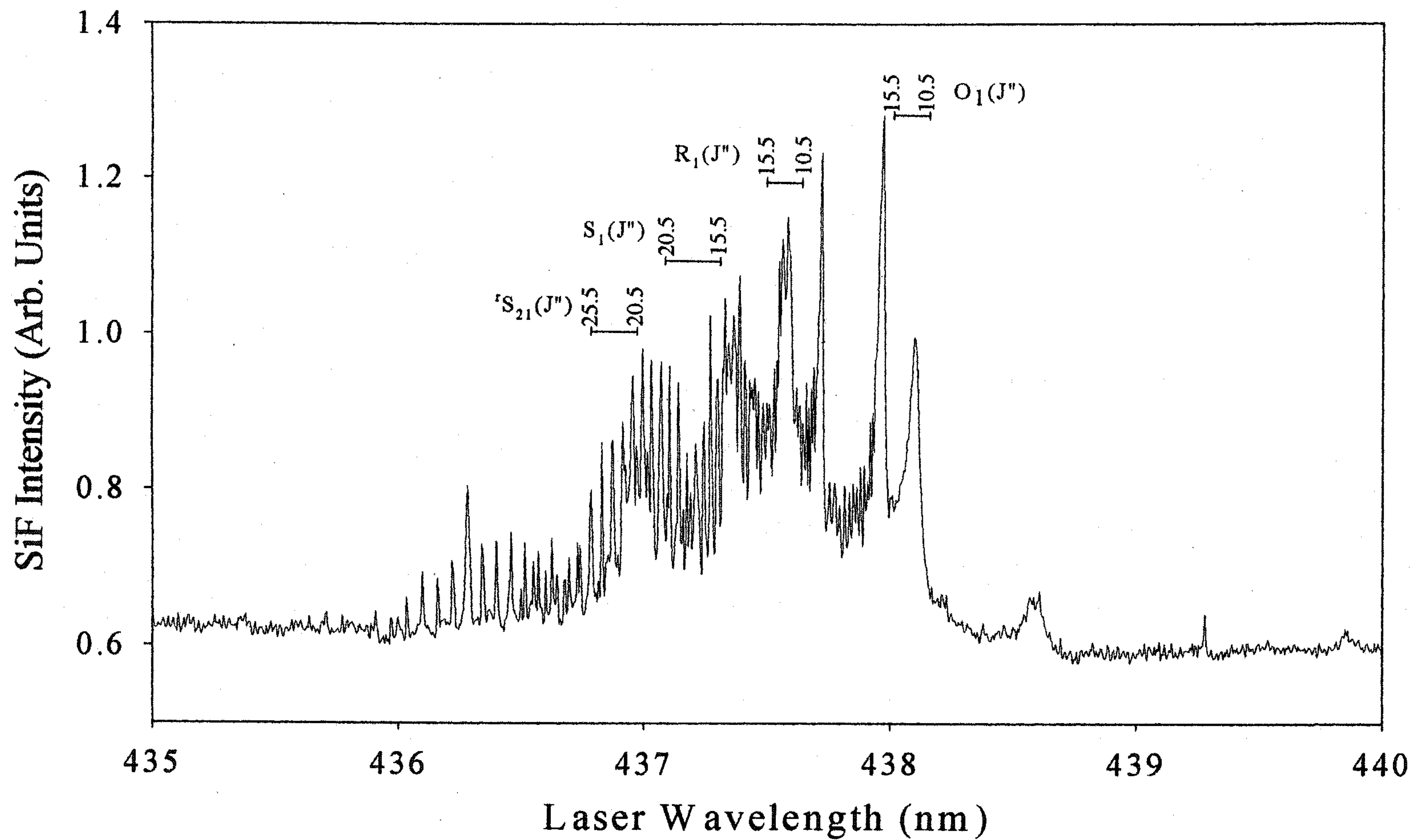

Figure 3.2. REMPI excitation spectrum corresponding to the SiF (1,0) C″ $^2\Sigma^+ \leftarrow$ X $^2\Pi_{1/2}$ transition. Individual states are labeled appropriately.

Reproduced with permission of the copyright owner. Further reproduction prohibited without permission.

Reproduced with permission of the copyright owner. Further reproduction prohibited without permission.

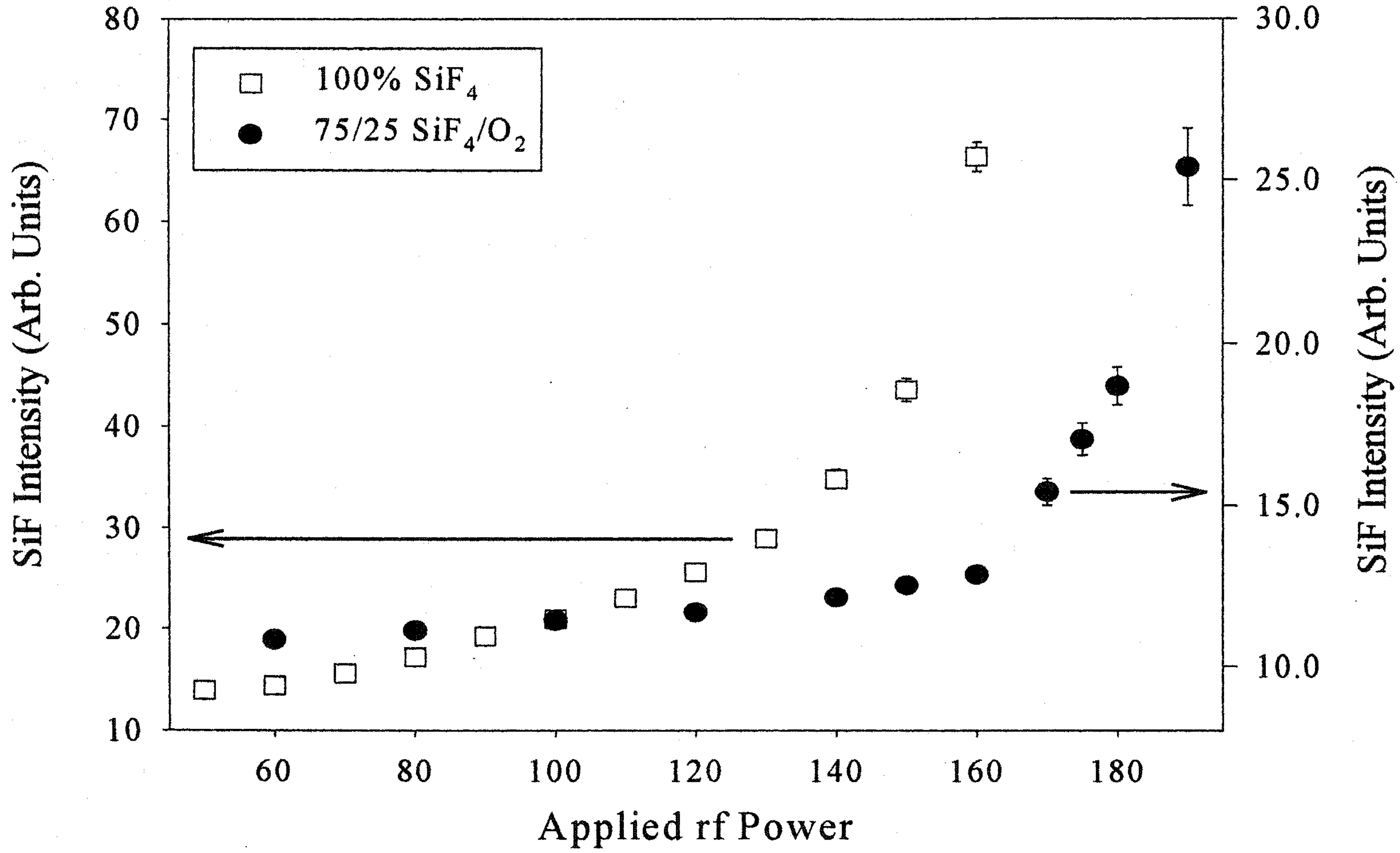

Figure 3.3. Relative SiF density as a function of rf power for 100% SiF_4 (□) and 75:25 SiF_4/H_2 (●) plasmas.

120 W, there is little SiF production in both plasmas and no real power dependence. Above 120 W, however, the SiF density in the SiF_4 plasmas increases dramatically with increasing rf power. A similar increase is observed at powers >140 W in the SiF_4:O_2 system. Previous studies have shown that higher rf power results in greater fragmentation of the feed gas in many plasma systems.[23,24] Our results are consistent with this in that one likely pathway for production of SiF is dissociation of SiF_x ($x > 1$) species. Our results also agree with the Walkup et al. observation of SiF production when a silicon substrate was placed in a CF_4 plasma.[13] They believe that SiF is primarily the product of cracking of a stable etch product such as SiF_4 or SiF_2 in their system.

3.2.3. Constant total gas flow. SiF_4/H_2 and SiF_4/O_2 plasmas with constant total flow have also been studied to investigate the effect of gas ratios on the production of SiF in these systems. Fig. 3.4a shows the relative SiF density as a function of $\%O_2$ and $\%H_2$ in the plasma. A significant decrease in the production of SiF radicals is seen in SiF_4/O_2 plasmas with increased O_2 addition. It is believed that the addition of O_2 leads to the production of SiO,[25] and $SiOF_2$ ($\Delta H_f = -959.8$ kJ/mol)[26] in the gas phase because of the thermodynamic stability of the Si=O bond. Indeed, we have identified SiO in SiF_4/O_2 plasmas at 180 W rf power using optical emission spectroscopy (OES).[27] $SiOF_2$ was not observed in the OES spectrum of the plasma. Formation of this species may still be occurring, however, as OES only provides information on excited state plasma species that emit radiation. In the analogous CF_4 plasmas, similar decreases in intensity of CF radicals have been observed upon addition of O_2.[28] The decreases in this system have been ascribed primarily to the production of the analogous, thermodynamically stable COF_2 ($\Delta H_f^\circ = -624$ kJ/mol),[29] as well as COF and CO.

Reproduced with permission of the copyright owner. Further reproduction prohibited without permission.

Reproduced with permission of the copyright owner. Further reproduction prohibited without permission.

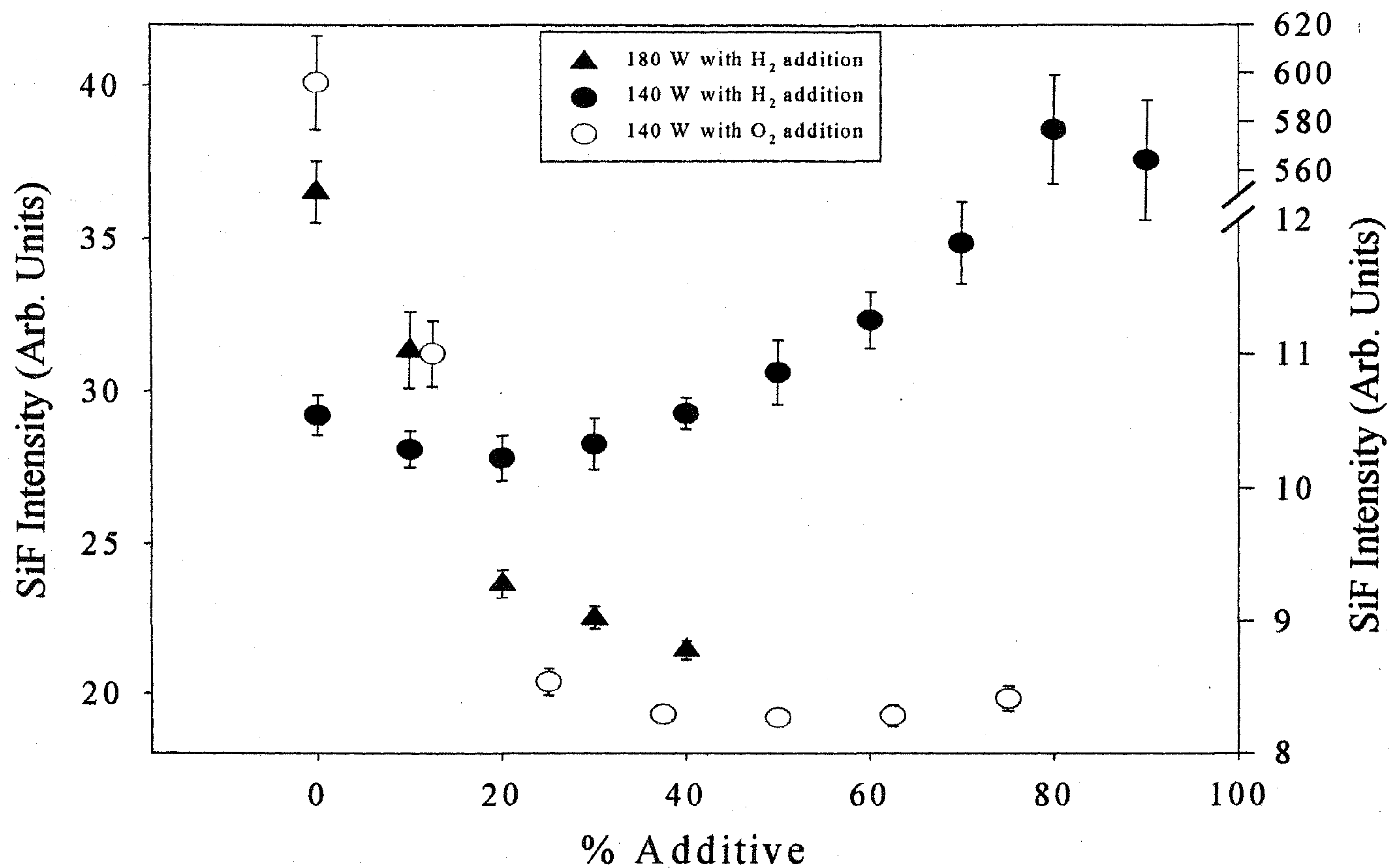

Figure 3.4. (a) Relative SiF density with a constant total flow as a function of % O_2 addition (140 W [O]) and %H_2 addition (140 W [●] and 180 W [▲]).

Reproduced with permission of the copyright owner. Further reproduction prohibited without permission.

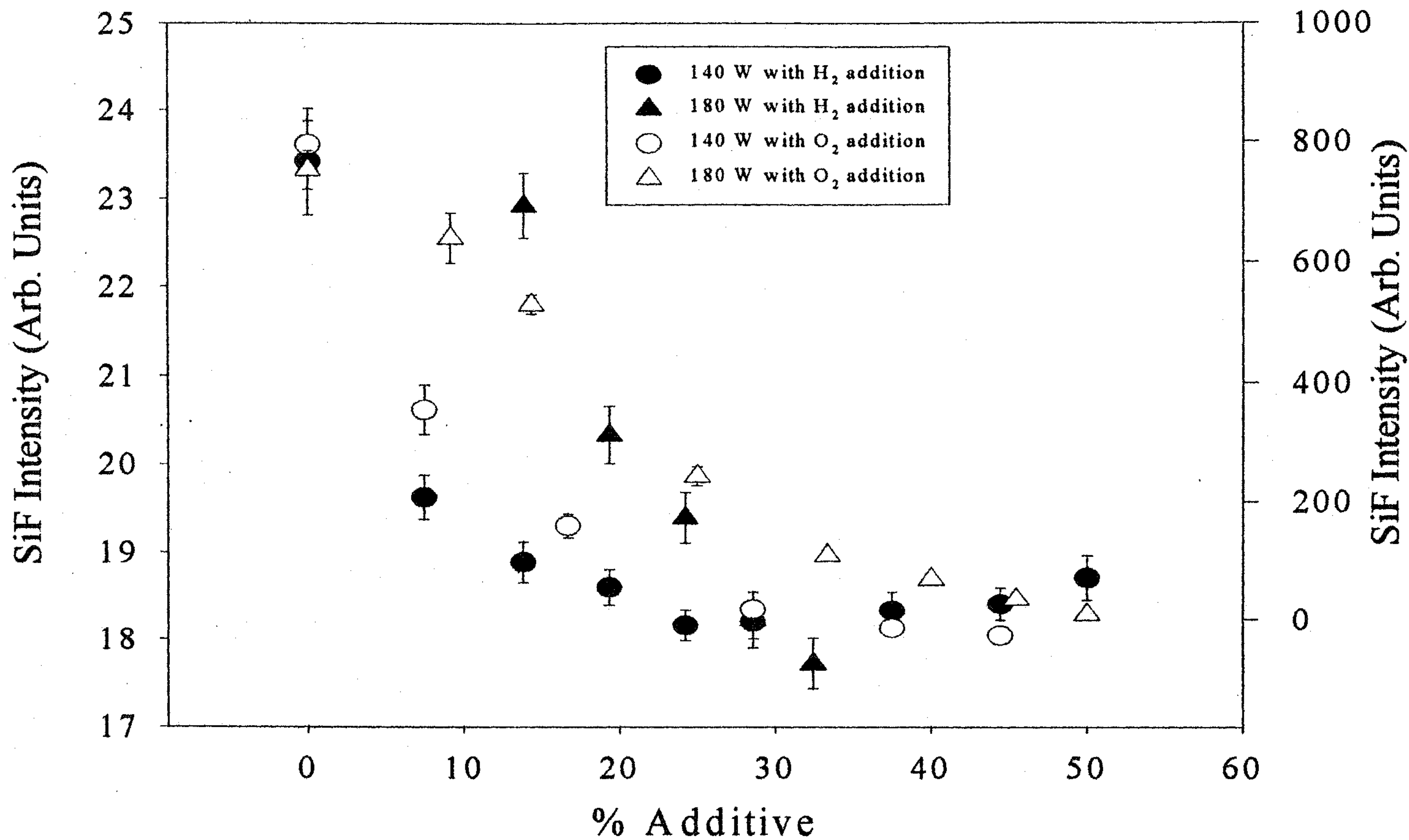

Figure 3.4. (b) Relative SiF density with a constant SiF_4 flow as a function of %O_2 addition (140 W [O] and 180 W [Δ]) and % H_2 addition (140 W [●] and 180 W [▲]). The left vertical axes correspond to values for the H_2 addition data. The right vertical axes correspond to values for the O_2 addition data.

In contrast, in the SiF_4/H_2 system at both 140W and 180 W applied rf power, SiF production decreases with increased H_2 concentrations up to 20% H_2. This is likely the result of the favorable recombination of F with H dominating over other formation processes for SiF. At concentrations above ~40% H_2, there is an increase in SiF production for the 140 W data. For the 180 W plasma system, no data were taken above 40% H_2 since an equivalent plasma glow could not be maintained. We have, however, observed a similar increase in SiF production at high H_2 concentrations using high power plasmas (170 W) in our laser-induced fluorescence (LIF) IRIS experiments presented in Chapter 5. In those investigations, pressure increases in the source were not an issue.

The decrease in SiF production observed upon addition of small amounts of H_2 (< 20%) in agreement with Lee and Deneufville[1] who observed a decrease for a 10 W, 100 kHz SiF_4/H_2 parallel plate system. Likewise, Tanaka et al. found that addition of H_2 to their glow discharge system led to production of $SiHF_3$ and complete loss of SiF signal.[30] Furthermore, Cicala et al. note that the emission from SiF* is lower in a 90:10 SiF_4/H_2 plasma than in a 100% SiF_4 plasma.[9] Since the density of SiF_x radicals in SiF_4 plasmas is controlled by the reaction of SiF_x species and F atoms, addition of H_2, which scavenges F atoms, results in a decrease in the SiF_x production. It is clear from our data that the lowest concentrations of SiF for both plasma powers occur at ~10 – 20% H_2 addition. SiF production increases, however, at higher H_2 additions (> 40%). This increase could be the result of SiF production through the fragmentation of etch products such as SiF_2 and SiF_4, as

Reproduced with permission of the copyright owner. Further reproduction prohibited without permission.

observed by Walkup et al. in a fluorocarbon etching plasma.[13] Another, possibly more likely, route to SiF at high H_2 concentrations is shown in Eq. 3.1.

$$SiF_2 + H \rightarrow SiF + HF \quad (3.1)$$

This reaction becomes accessible with excess hydrogen in the system after the F atoms in the system have been scavenged.[5,9,31] This is discussed in greater detail in Chapter 5.

3.2.4. Constant SiF_4 Gas Flow. SiF_4/H_2 and SiF_4/O_2 plasmas with constant SiF_4 flow have also been studied to eliminate the possibility that decreasing SiF_4 flow in the plasma source is the cause for the observed trends in SiF production. Figure 3.4b shows the relative SiF density as a function of $\%O_2$ and $\%H_2$ for the two applied plasma powers (140 and 180 W). Similar to the results found with a constant total gas flow, addition of O_2 resulted in significant decreases in SiF production at both powers. Furthermore, a much sharper decrease in SiF was observed at 140 W rf power relative to the 180 W rf power plasma. Likewise, trends similar to those observed in the constant flow system were observed at both powers for the SiF_4/H_2 plasma system. However, no data were taken beyond 50% dilution because the pressure in the source increases sufficiently to preclude additional measurements.

3.3. Conclusion

The detection of SiF radicals by REMPI/TOFMS has been investigated under various plasma and feed gas conditions using a newly constructed plasma molecular beam apparatus. We have shown that addition of different diluents greatly affects the chemistry and, thus, the production of SiF radicals, in each plasma system.

Reproduced with permission of the copyright owner. Further reproduction prohibited without permission.

Furthermore, plasma power has proven to greatly affect the degree of fragmentation seen in fluorosilane plasmas. Future experiments with this new apparatus will focus on surface interactions of SiF radicals as well as additional plasma species in other systems of interest to the semiconductor industry.

Reproduced with permission of the copyright owner. Further reproduction prohibited without permission.

References

1. H. Lee, J. P. Deneufville *J. Non-Crystalline Solids* **66**, 39 (1984).
2. S. M. Han, E. S. Aydil *J. Vac. Sci. Technol. A* **15**, 2893 (1997).
3. A. Madan, S. R. Ovshinsky, E. Benn *Philos. Mag. B* **40**, 259 (1979).
4. N. Mutsukura, M. Ohuchi, S. Satoh, Y. Machi *Thin Solid Films* **109**, 47 (1983).
5. G. Bruno, P. Capezzuto, G. Cicala *J. Appl. Phys.* **69**, 7256 (1991).
6. B. Petit, A. Durandet, J. Pelletier *Vacuum* **36**, 799 (1986).
7. H. F. Winters, I. C. Plumb *J. Vac. Sci. Technol. B* **9**, 197 (1991).
8. D. R. Sparks *J. Electrochem. Soc.* **139**, 1736 (1992).
9. G. Cicala, M. Losurdo, P. Capezzuto, G. Bruno *Plasma Sources Sci. Technol.* **1**, 156 (1992).
10. H. Boyd, M. S. Tang *Solid State Technol.* **22**, 133 (1979).
11. A. Darcy, A. Galijatovic, R. Barth, T. Kenny, K. D. Krantzman, T. A. Schoolcraft *J. Mol. Graphics* **14**, 260 (1996).
12. J. F. Morar, N. D. McFeely, G. Landgren, F. J. Himpsel *Appl. Phys. Lett.* **45**, 174 (1984).
13. R. Walkup, P. Avouris, R. W. Dreyfus, J. M. Jasinski, G. S. Selwyn *Appl. Phys. Lett.* **45**, 372 (1984).
14. R. Walkup, P. Avouris, R. W. Dreyfus, J. M. Jasinski, G. S. Selwyn *Soc. Symp. Proc.* **29**, 269 (1984).
15. E. Hirota *J. Phys. Chem. A* **87**, 3375 (1983).

Reproduced with permission of the copyright owner. Further reproduction prohibited without permission.

16. M. N. R. Ashfold, J. Pearson, J. W. Hudgens, R. D. Johnson III *Chem. Phys. Lett.* **263**, 138 (1996).

17. J. A. Dagata, D. W. Squire, C. S. Dulcey, D. S. Y. Hsu, M. C. Lin *Chem. Phys. Lett.* **134**, 151 (1987).

18. C. S. Dulcey, J. W. Hudgens *Chem. Phys. Lett.* **118**, 444 (1985).

19. H. F. Winters, J. W. Coburn *Surf. Sci. Rep.* **14**, 161 (1992).

20. P. R. McCurdy, K. H. A. Bogart, N. F. Dalleska, E. R. Fisher *Rev. Sci. Instrum.* **68**, 1684 (1997).

21. R. C. Weast *Handbook of Chemistry and Physics*, CRC: New York, (1966).

22. S. J. Davis, S. G. Hadley *Phys. Rev. A* **14**, 1146 (1976).

23. A. Grill *Cold Plasma in Materials Fabrication*, IEEE Press: Piscataway, NJ, (1994).

24. M. A. Lieberman, A. J. Lichtenberg *Principles of Plasma Discharges and Material Processing*, Wiley and Sons: New York, (1994).

25. Y. Matsuo, T. Nakajima, T. Kobayashi, M. Takami *Appl. Phys. Lett.* **71**, 996 (1997).

26. J. P. Stewart, M. S. Gordon, J. S. Frank *Phosphorus Sulfur Silicon Relat. Elem.* **47**, 105 (1990).

27. K. L. Williams, E. R. Fisher **unpublished work.**

28. N. M. Mackie, D. G. Castner, E. R. Fisher *Langmuir* **14**, 1227 (1998).

29. M. W. Urban, C. D. Craver *Structure-Property Relations in Polymers: Spectroscopy and Performance*, ACS: Washington DC, (1993).

30. K. Tanaka, Y. Akiyama, T. Tanaka *J. Mol. Spctrosc.* **137**, 55 (1989).

Reproduced with permission of the copyright owner. Further reproduction prohibited without permission.

31. G. Cicala, G. Bruno, P. Capezzuto *Pure & Appl. Chem.* **68**, 1143 (1996).

Reproduced with permission of the copyright owner. Further reproduction prohibited without permission.

CHAPTER 4

SUBSTRATE TEMPERATURE EFFECTS ON SURFACE REACTIVITY OF SiF_x ($x = 1, 2$) RADICALS IN FLUOROSILANE PLASMAS

Reprinted with permission from Keri L. Williams and Ellen R. Fisher, *J. Vac. Sci. Technol. A*

This dissertation chapter contains results from a full paper submitted to the Journal of Vacuum Science and Technology A in October 2002. The manuscript was written by Keri L. Williams and edited by Ellen R. Fisher. This chapter describes the effect of substrate temperature on SiF and SiF_2 reactivity on a Si surface during plasma etching and deposition of fluorinated silicon materials. Mechanisms responsible for surface evolution of SiF and SiF_2 at $T_S > 600$ K are discussed. Additionally, rotational temperatures (θ_R) for SiF and SiF_2 were measured in a 170 W plasma as 450 ± 50 K and 752 ± 100 K, respectively.

Reproduced with permission of the copyright owner. Further reproduction prohibited without permission.

4.1. Introduction

Fluorine-containing plasmas are useful in semiconductor device fabrication, primarily for silicon etching systems. They may also be used for the deposition of fluorinated thin films like amorphous, hydrogenated, fluorinated silicon (a-Si:H,F) and fluorocarbon films. Fluorosilane plasmas have been used to both etch and deposit a wide variety of materials.[1-5] In etching systems, F atoms are considered the primary etchant, producing SiF_2 and SiF_4 as gas-phase products. In addition to F atoms, SiF_x species are thought to be key components in the chemical processes that dictate the overall plasma regime—etching or deposition.[5,6] Whereas SiF_2 is a known etch product, SiF is considered a deposition precursor in fluorosilane depositing systems [5-12] In both plasma regimes, it is the surface reaction layer, including adsorption, product formation, and molecule desorption, that largely determines etch and deposition quality.[13]

Many plasma parameters, including applied rf power (P) feed gas composition, ion bombardment, and substrate temperature (T_S) directly affect the surface adlayer by shifting equilibrium concentrations of adsorbed radicals and adsorption-desorption dynamics.[6] Specifically, regulation of T_S has proven useful in directing the rate and selectivity of F atom etching of silicon.[4,7,14-16] Indeed, Si etching increases significantly when T_S is raised from room temperature to > 600 K.[6,7] Staffa and coworkers also observed increased etch rates at elevated T_S for both silicon nitride and silicon oxide. In addition, they observed an increase in etch selectivity of the nitride over the oxide with increased T_S.[4] Such empirical studies clearly illustrate the usefulness of T_S as a control for etch characteristics.

Reproduced with permission of the copyright owner. Further reproduction prohibited without permission.

A number of studies have demonstrated that the SiF_x surface adlayer concentrations during etching are significantly altered with increasing T_S. In those studies, at $T_S = 300$ K, the adlayer consists of a mixture of SiF_3, SiF_2, and SiF.[6,7,17] As T_S is increased, the amount of SiF_3 in the adlayer decreases, whereas the amount of SiF and SiF_2 increases. At $T_S > \sim 600$ K, the adlayer consists primarily of SiF. Characterization of the desorbing species during etching by Winters et al. indicated there is also a shift in the major etch product as a function of T_S.[6,11] In their experiments, more SiF_4 is produced at $T_S < 600$ K, whereas SiF_2 is the more abundant product at $T_S > 600$ K. This is consistent with the rate-limiting step for etching at low T_S being conversion of the SiF_3 to SiF_4, whereas the rate-limiting step at high T_S is the conversion of SiF to SiF_2.[17]

Sebel et al.[7] recently extended the work of Winters and Coburn[6] by characterizing desorbing SiF_x species as a function of T_S with and without ion bombardment. Under both conditions, they found that T_S was a major influence on the desorbing species, similar to the results of Winters and Coburn. They also found, however, that the principal effect of ion bombardment is to alter the relative abundance of the desorbing species, independent of T_S. The introduction of ions shifts the primary etch product towards SiF_2 and away from SiF_4. The Coburn and Winters[6] study and the Sebel et al.[7] study demonstrate the importance of T_S on silicon etching with and without ions in the system. To fully understand plasma etching of silicon, however, it is also important to characterize surface interactions of plasma species (including ions) as a function of T_S with the full range of plasma species impinging upon the surface.

Deposition of fluorinated silicon materials from SiF_4 plasmas can be achieved through H_2 dilution, which shifts the plasma regime away from etching.[5,18] The electrical

Reproduced with permission of the copyright owner. Further reproduction prohibited without permission.

and optical properties of these materials are often directly correlated to their deposition conditions, including T_S.[19] A primary benefit of T_S control during film deposition is improvement in control of chemical composition, resulting in improved electrical properties. For example, Madan and coworkers observed a strong, linear dependence of the dark conductivity with increasing T_S for SiF_4:H_2 plasma-deposited a-Si:H,F films used for solar cells.[19] Physical attributes such as crystallinity and hardness can also be improved with T_S control. Characterization of SiO_2 materials deposited as a function of T_S have shown that hardness of these films increases with T_S.[3] Another example comes from studies by Syed and coworkers[2] that demonstrated poly-Si deposited with no H_2 addition contains numerous microvoids and is easily oxidized, but crystallinity monotonically increases with T_S. It is clear from these findings that understanding the role of T_S allows for improved control of deposited materials and silicon etching.[2,3,20-25]

Many studies have characterized either gas phase or surface composition as a function of plasma parameters. Although these studies lend insight into the end products of either etching or deposition, they do not address the plasma-surface interface reactions occurring during processing. Much of the work that has investigated surface interactions has been conducted in a non-plasma environment (primarily with molecular beams) because of the complex nature of glow discharges.[4,7,9,10,16,26-31] Fluorosilane plasma research conducted in our laboratories using the Imaging of Radicals Interacting with Surfaces (IRIS) technique has sought to elucidate mechanisms involved in deposition and etching by studying radical reactivity amidst the full range of plasma species. Specifically, rf power, gas flows, and ion effects on interface reactions have been investigated for SiF_4 and SiF_4:H_2 plasmas, Chapter 5.[32,33] The IRIS data presented here

Reproduced with permission of the copyright owner. Further reproduction prohibited without permission.

complements these gas-phase and surface analyses by investigating the effects of T_S on SiF and SiF_2 surface reactivity during deposition and etching in SiF_4 and SiF_4:H_2 systems.

4.2. Results

4.2.1. Spectroscopy. Laser-induced fluorescence (LIF) offers a non-intrusive and highly selective study of one type of radical in a molecular beam populated by a variety of different species. The spectroscopy of both SiF and SiF_2 has been studied extensively using LIF.[34,35] Figure 4.1 shows a fluorescence excitation spectrum for the $A^1B_1 - X^1A_1$ transition of SiF_2 obtained from a 170 W, 30 sccm SiF_4 plasma molecular beam. The spectrum was obtained by tuning the laser in 0.025 nm increments from 219 to 225 nm (1s/step). A comparison to literature spectra verifies that the fluorescing species is indeed SiF_2.[34] Reactivity data were acquired by tuning the laser to one particular rovibrational band of SiF_2, either the 2^6_0, 2^5_0, or the 2^4_0 state discussed below, data were taken for all three states as a function of substrate temperature.

Figure 4.2 shows the experimental excitation spectrum for SiF in the same 100% SiF_4 plasma molecular beam. Calculated line positions for the (0,0) band of the SiF $A^2\Sigma^+ \rightarrow X^2\Pi$ electronic transition are also shown. Calculations are based on a computer simulation program developed by W. G. Brieland at Sandia National Laboratories. This program uses previously determined spectroscopic constants reported in literature to calculate a spectrum based upon temperature and laser resolution. There is excellent agreement between the calculated and experimental line positions, demonstrating that the fluorescing species is indeed SiF. All reactivity measurements were made with the laser

Reproduced with permission of the copyright owner. Further reproduction prohibited without permission.

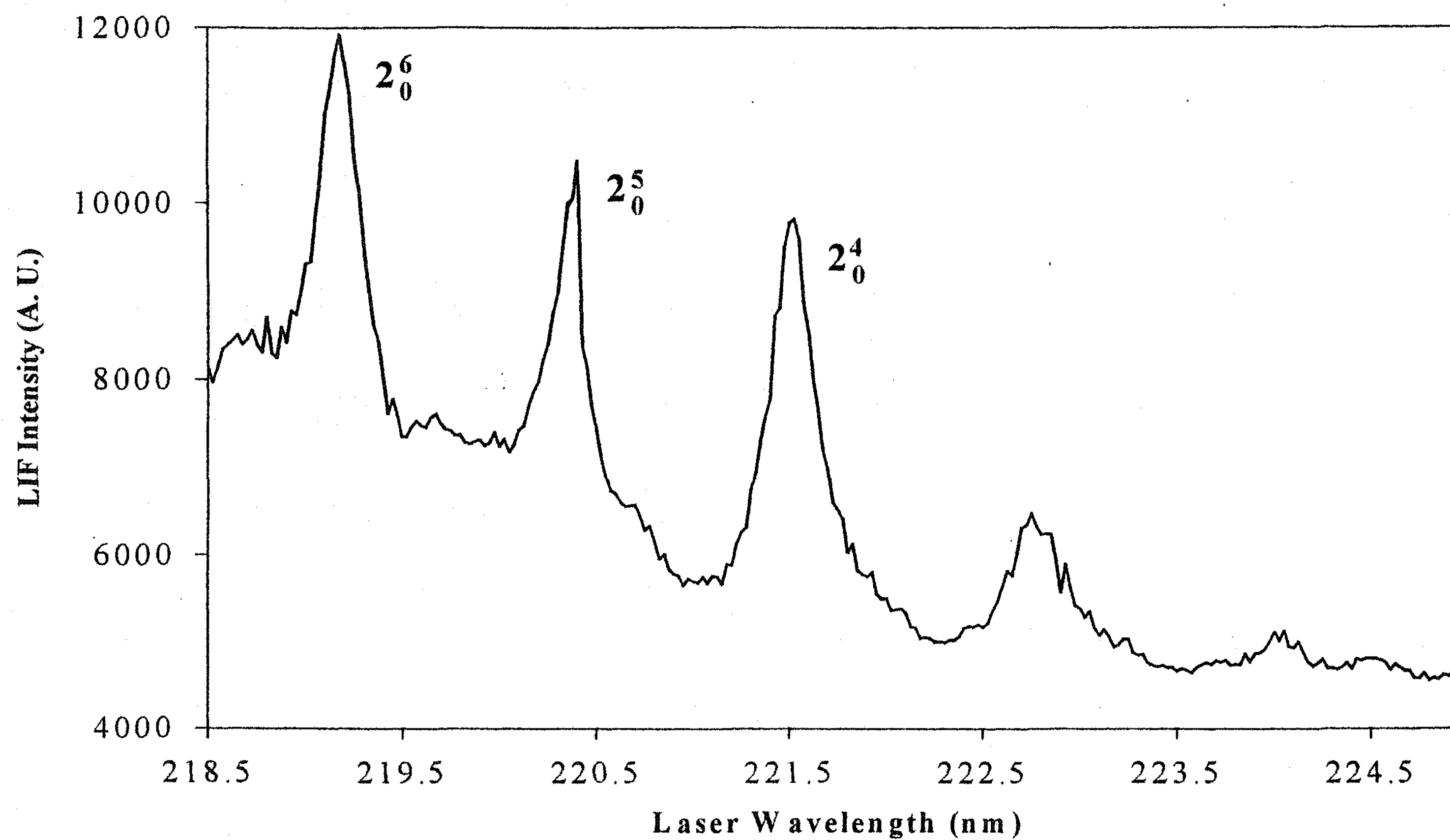

Figure 4.1. The experimental fluorescence excitation spectrum of SiF_2 in the molecular beam formed from a 100% SiF_4 plasma (170 W, 30 sccm). The three rovibronic states of SiF_2 used for IRIS experiments are labeled. The SiF_2 spectrum was taken using 0.025 nm steps from 218.5 to 224.6 nm.

Reproduced with permission of the copyright owner. Further reproduction prohibited without permission.

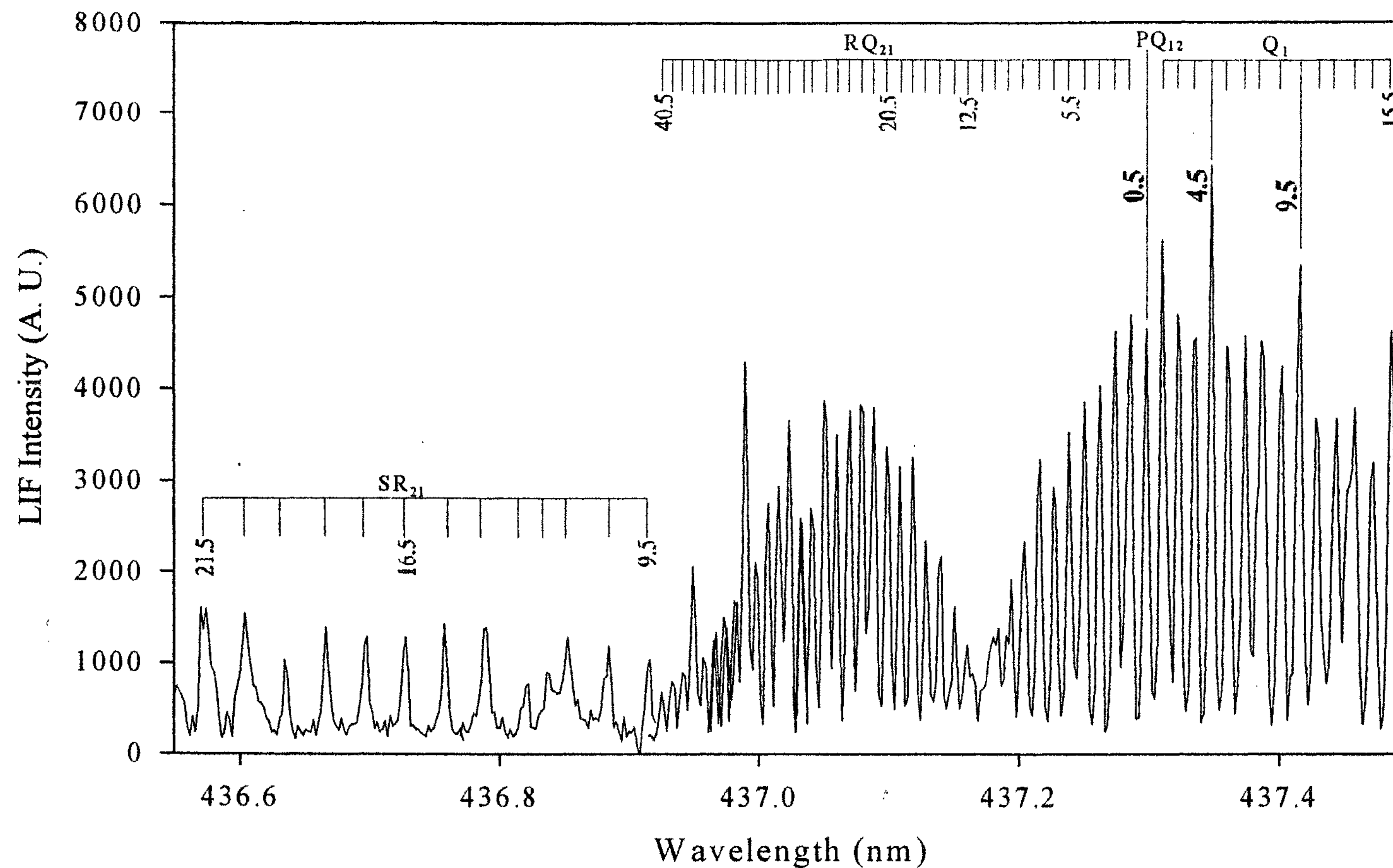

Figure 4.2. The experimental fluorescence excitation spectrum of SiF in the molecular beam formed from a 100% SiF_4 plasma (170 W, 30 sccm). Rotational lines used in IRIS reactivity experiments are denoted with a * and correspond to the 0.5, 4.5, and 9.5 J-states. The SiF spectral data was collected by stepping the dye laser in 0.003 nm increments from 436.5 to 437.5 nm.

Reproduced with permission of the copyright owner. Further reproduction prohibited without permission.

tuned to 437.292 nm, 437.345 nm, or 437.412 nm corresponding to the J = 0.5, 4.5, and 9.5 rotational lines of the PQ_{12} or Q_1 branches. Comparison of calculated and experimental spectra allows determination of the SiF rotational temperature, Θ_R. Comparing SiF spectra obtained for 100% SiF_4 plasmas at 40, 80, and 170 W (using the range 436.8 - 437.2 nm) to simulated spectra, we find $\Theta_R \sim 450 \pm 50$ K for all three plasma powers.

4.2.2. Temperature Dependence for Surface Reactivity of SiF and SiF_2. Investigations of T_s effects on the surface scatter of SiF and SiF_2 provide insight into the surface processes occurring during film deposition and etching. Furthermore, these data complement other work from our laboratory, which specifically addressed the effect of plasma parameters (power and feed gas composition) and bombarding ions on SiF_x surface interactions, Chapter 5.[32,33] Figure 4.3 shows a series of ICCD images of SiF_2 using a 90:10 SiF_4/H_2 plasma molecular beam (P = 170 W) impinging upon a 375 K Si substrate. The LIF signal from SiF_2 radicals in the incident beam is shown in Fig. 4.3a. Figure 4.3b is the LIF signal for both incident and scattered SiF_2 radicals obtained with a Si substrate rotated into the path of the molecular beam. Figure 4.3c is the difference between Fig. 4.3b and Fig. 4.3a, representing only SiF_2 desorbing from the substrate.

Figure 4.4a shows the 1-D cross-sections corresponding to images in Figs. 4.3a (incident SiF_2) and 4.3c (scattered SiF_2). The broad spatial distribution and the shift of the scattered signal peak maximum away from the molecular beam peak maximum indicate SiF_2 radicals scatter with a cosine angular distribution. Simulated curves for the incident beam and scattered molecules with S = 1.40 are also shown in Fig. 4.4a,

Reproduced with permission of the copyright owner. Further reproduction prohibited without permission.

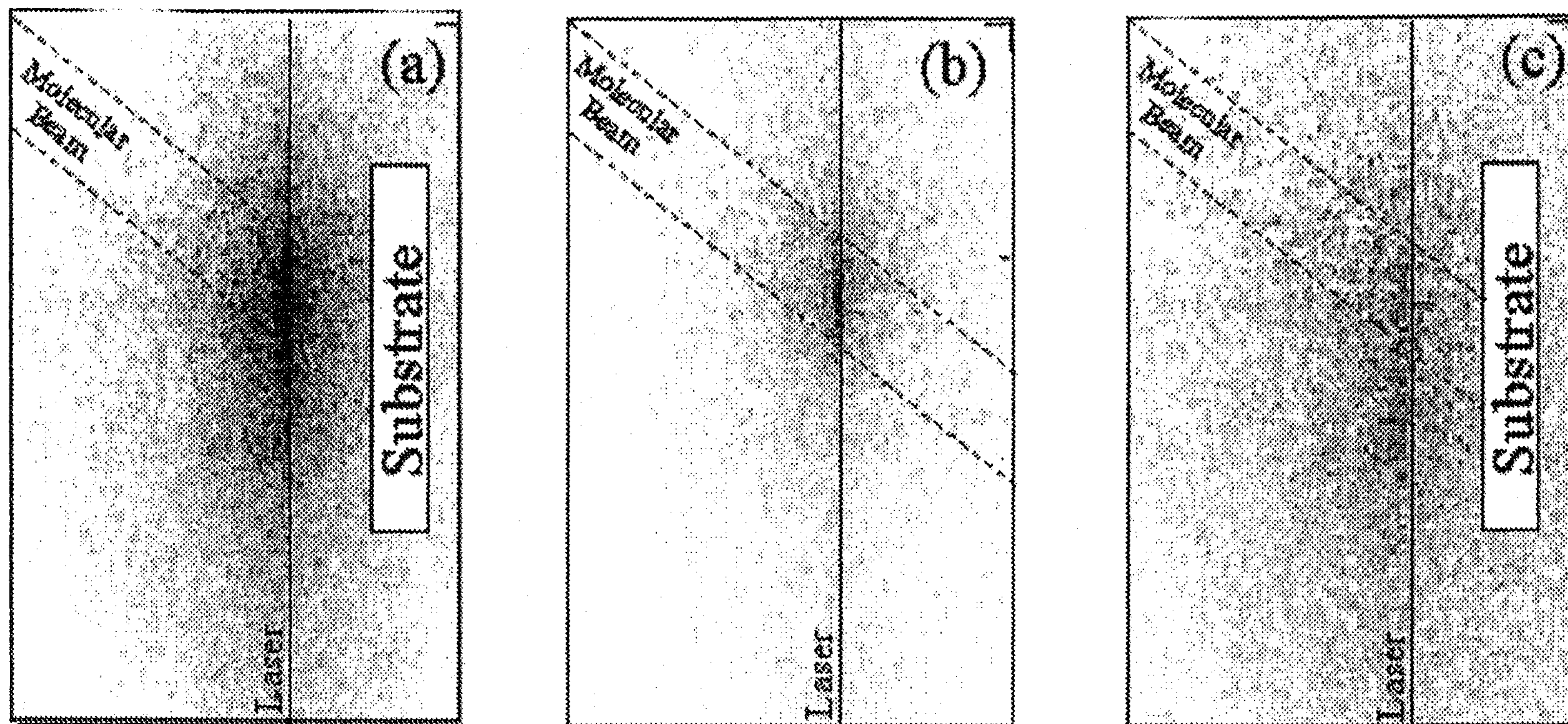

Figure 4.3. Spatially resolved, two-dimensional ICCD images of SiF_2 LIF signal for (A) a 90:10 SiF_4/H_2 (P = 170 W) plasma molecular beam with no substrate and (b) with a 375 K Si substrate rotated into the path of the molecular beam. Image (C) is the difference between images (A) and (B) and shows only the SiF_2 radicals scattered from the surface. Dashed lines indicate the molecular beam traveling across the image at a 45° angle and the laser beam propagating from the bottom to the top of the image.

Reproduced with permission of the copyright owner. Further reproduction prohibited without permission.

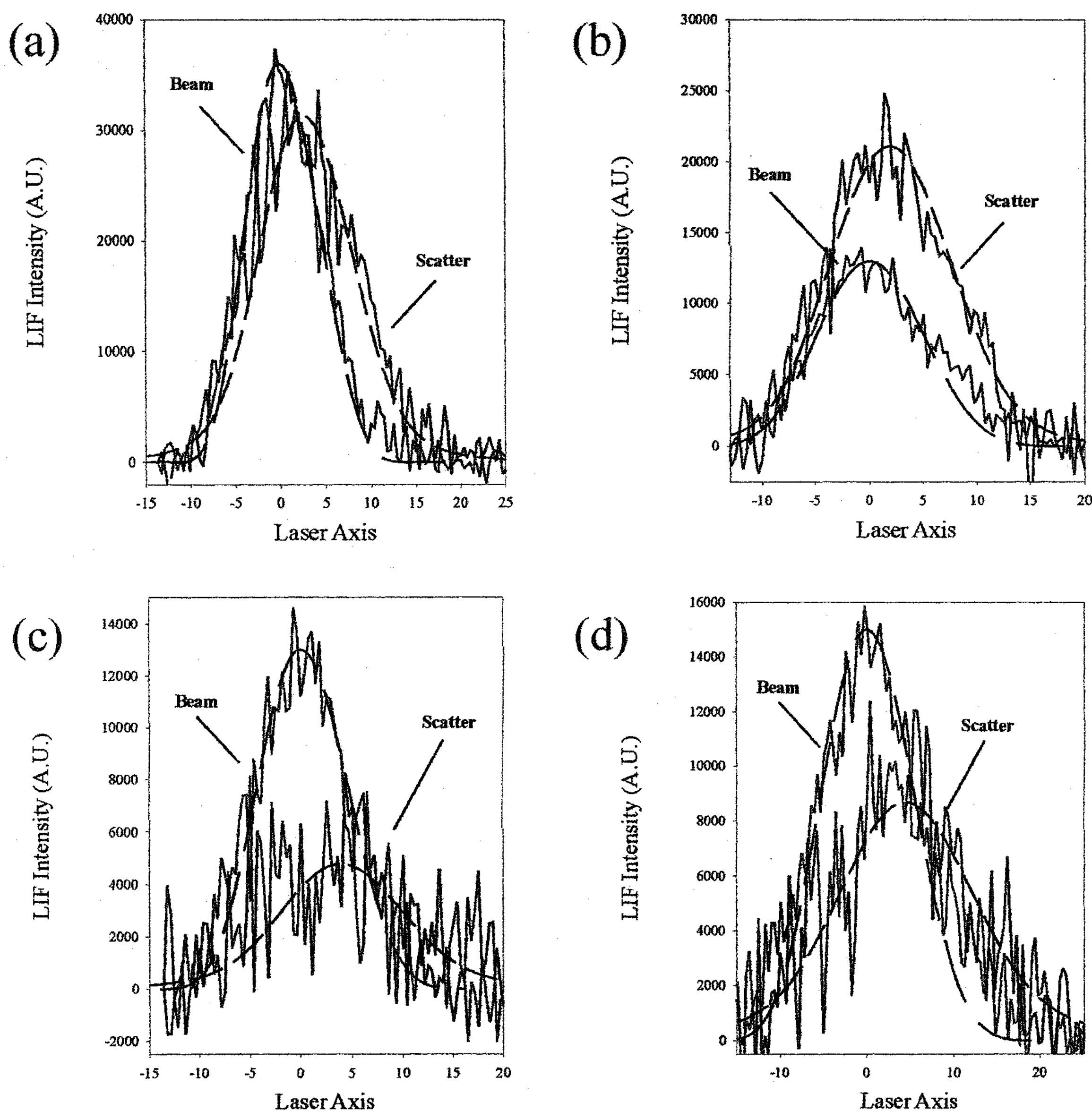

Figure 4.4. Cross-sectional data for LIF signals from 90:10 SiF_4/H_2 plasmas (P = 170 W) for (A) SiF_2, T_S = 375 K, (B) SiF_2, T_S = 675 K, (C) SiF, T_S = 375 K, and (D) SiF, T_S = 675 K. Cross sections from the experimental plasma molecular beam and scattered molecules are shown with simulated curves (dashed lines) produced from the reactivity model described in the text. The simulations plotted correspond to uncorrected scatter values of (A) 1.47 ± 0.06, (B) 1.90 ± 0.09, (C) 0.75 ± 0.09, and (D) 1.20 ± 0.07.

Reproduced with permission of the copyright owner. Further reproduction prohibited without permission.

confirming the cosine distribution for scattered molecules. Averaging several data sets yields $S = 1.47 \pm 0.06$. Note that an S value greater than unity indicates that surface production of a species contributes to the observed scattering signal. Possible mechanisms for surface generation of SiF_2 have been discussed previously.[18,32] Significant changes in scatter are observed with increasing T_s. Overall an increase in scatter can easily be seen by comparing the SiF_2 scatter cross section for a 375 K substrate (Fig. 4.4a) to that for a 675 K substrate (Fig. 4.4b), simulation of which yields $S = 1.90$. Similarly, the surface scatter for SiF also increases with increasing T_S, Figs. 4.4c and 4.4d. Calculated scatter coefficients for these data increase from 0.75 ± 0.25 to 1.20 ± 0.10, with $T_S = 375$ K and $T_S = 675$ K, respectively.

As noted in Chapter 2, changes in translational temperature, Θ_T, upon interaction with the substrate can cause significant changes in the observed scatter coefficients. Previous work in our group has determined the $\Theta_T(SiF_2)$ in the molecular beam to be ~430 K at 80 W rising to ~540 K at $P = 200$ W.[36] For SiF, Θ_T is ~570 K at $P = 80$ W, increasing to ~860 K for 200 W plasmas.[36] Using Θ_T values found using 40 W and 170 W plasmas, corrected scatter coefficients have been calculated for both SiF and SiF_2 assuming complete equilibration to T_S. Both corrected and uncorrected scatter values are given in Table 4.1 (SiF_2) and Table 4.2 (SiF) for T_S ranging from 298 to 875 K. These tables also contain data for two different plasma systems, 100% SiF_4 and 90:10 SiF_4:H_2, at $P = 170$ W and $P = 40$ W. This set of plasma conditions allows the investigation of T_S effects under different etching and depositing regimes.

Figure 4.5a shows the effect of T_S on SiF scatter for 100 % SiF_4 and 90:10 SiF_4:H_2 plasmas ($P = 170$ and 40 W). For each system, SiF scatter is essentially constant

Reproduced with permission of the copyright owner. Further reproduction prohibited without permission.

Table 4.1. Corrected Scatter Coefficients For SiF_2 as a function of T_s.[a]

T_S	Correction Factor[b]	S_{cor}			
		170 W, 100% SiF_4	170 W, 10% H_2	40 W, 100% SiF_4	40 W, 10% H_2
298	1.30	3.60 ± 0.10	1.92 ± 0.13	1.20 ± 0.01	0.42 ± 0.01
375	1.15	3.19 ± 0.14	1.70 ± 0.07	1.02 ± 0.07	0.43 ± 0.05
475	1.03	2.86 ± 0.10	1.52 ± 0.07	0.92 ± 0.06	0.34 ± 0.03
575	0.93	2.43 ± 0.16	1.32 ± 0.07	0.91 ± 0.06	0.32 ± 0.03
600	0.91	2.51 ± 0.06	1.41 ± 0.13	0.95 ± 0.05	0.46 ± 0.04
625	0.89	2.61 ± 0.12	1.52 ± 0.09	1.23 ± 0.07	0.61 ± 0.03
650	0.88	2.66 ± 0.07	1.58 ± 0.08	1.39 ± 0.07	0.71 ± 0.13
675	0.86	3.01 ± 0.06	1.64 ± 0.08	1.73 ± 0.08	0.83 ± 0.08

[a]Values obtained using our simulation of the experiment, assuming an adsorption-desorption scattering mechanism. Errors given are one standard deviation of the mean of several data sets.

[b]Correction factor is based on Equation 1 described in the text and assumes full thermal equilibration on the surface. Velocities for SiF and SiF_2 from previous measurements in our laboratory[36] are used in Equation 1.

Reproduced with permission of the copyright owner. Further reproduction prohibited without permission.

Table 4.2. Scatter Coefficients For SiF in Fluorosilane-based plasmas as a function of T_s.[a]

T_S	Corr. Factor, 170 W[b]	S_{cor}		Corr. Factor, 40 W[b]	S_{cor}	
		170 W, 100% SiF_4	170 W, 10% H_2		40 W, 100% SiF_4	40 W, 10% H_2
298	1.64	1.20 ± 0.13	1.28 ± 0.24	1.42	0.43 ± 0.14	0.21 ± 0.14
375	1.46	1.02 ± 0.10	1.10 ± 0.13	1.26	0.40 ± 0.08	0.25 ± 0.08
475	1.30	0.97 ± 0.09	1.00 ± 0.14	1.12	0.38 ± 0.08	0.26 ± 0.10
575	1.18	1.18 ± 0.08	0.86 ± 0.14	1.02	0.44 ± 0.08	0.36 ± 0.15
600	1.15	1.22 ± 0.07	1.14 ± 0.13	1.00	0.67 ± 0.08	0.50 ± 0.09
625	1.13	1.21 ± 0.09	1.29 ± 0.19	0.98	0.73 ± 0.10	0.73 ± 0.12
650	1.11	1.30 ± 0.07	1.22 ± 0.08	0.96	0.92 ± 0.07	0.82 ± 0.12
675	1.09	1.36 ± 0.09	1.31 ± 0.08	0.94	0.98 ± 0.09	0.85 ± 0.09

[a]Values obtained using our simulation of the experiment, assuming an adsorption-desorption scattering mechanism. Errors given are one standard deviation of the mean of several data sets.
[b]Correction factor is based on Equation 1 described in the text and assumes full thermal equilibration on the surface. Velocities for SiF and SiF_2 from previous measurements in our laboratory[36] are used in Equation 1.

Reproduced with permission of the copyright owner. Further reproduction prohibited without permission.

Reproduced with permission of the copyright owner. Further reproduction prohibited without permission.

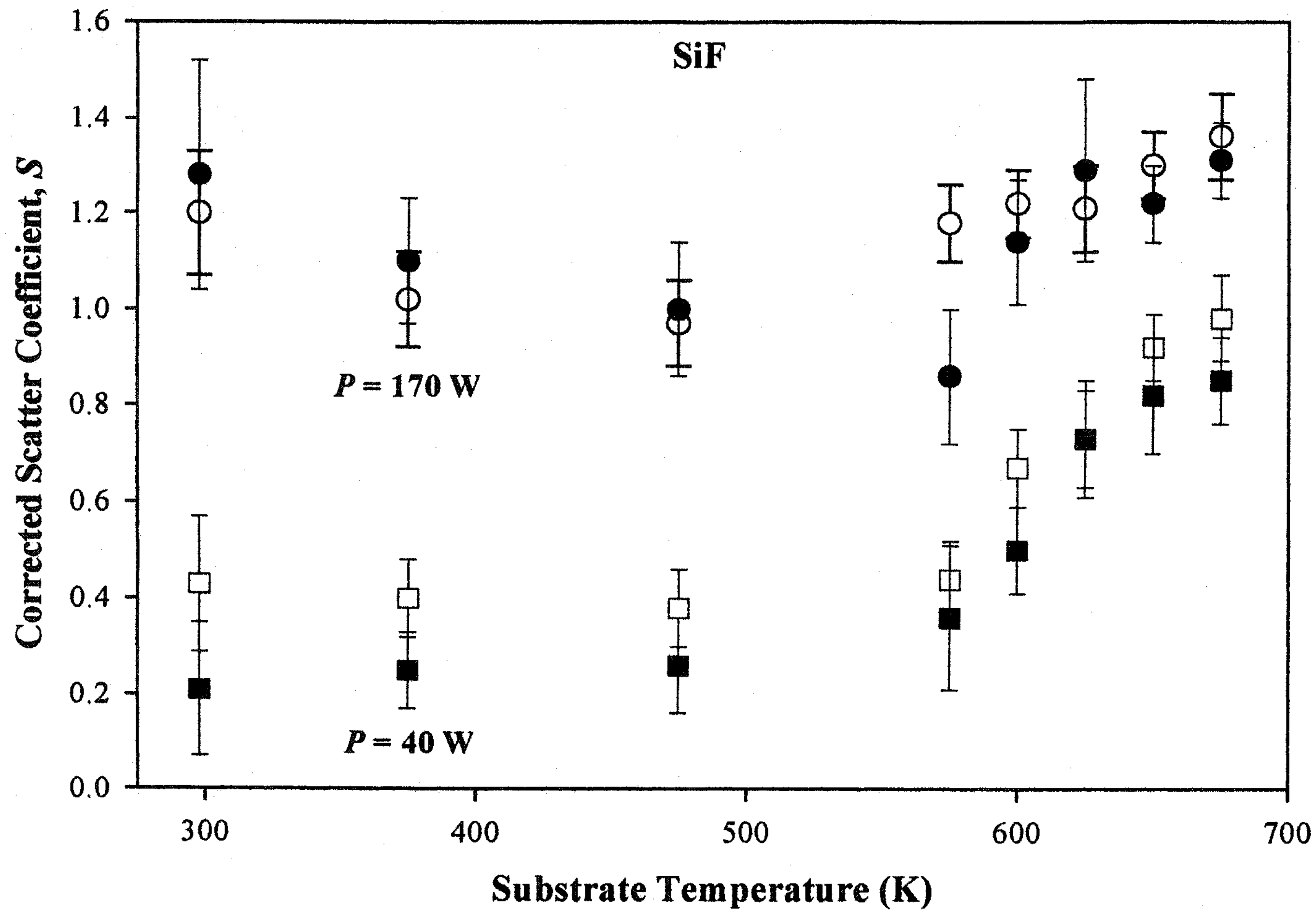

Figure 4.5. (A) Scatter coefficients for SiF ($J = 4.5$) in 100% SiF_4 (open symbols) and 90:10 SiF_4:H_2 (closed symbols) plasmas at 170 W (circles) and 40 W (squares) as a function of T_S.

Reproduced with permission of the copyright owner. Further reproduction prohibited without permission.

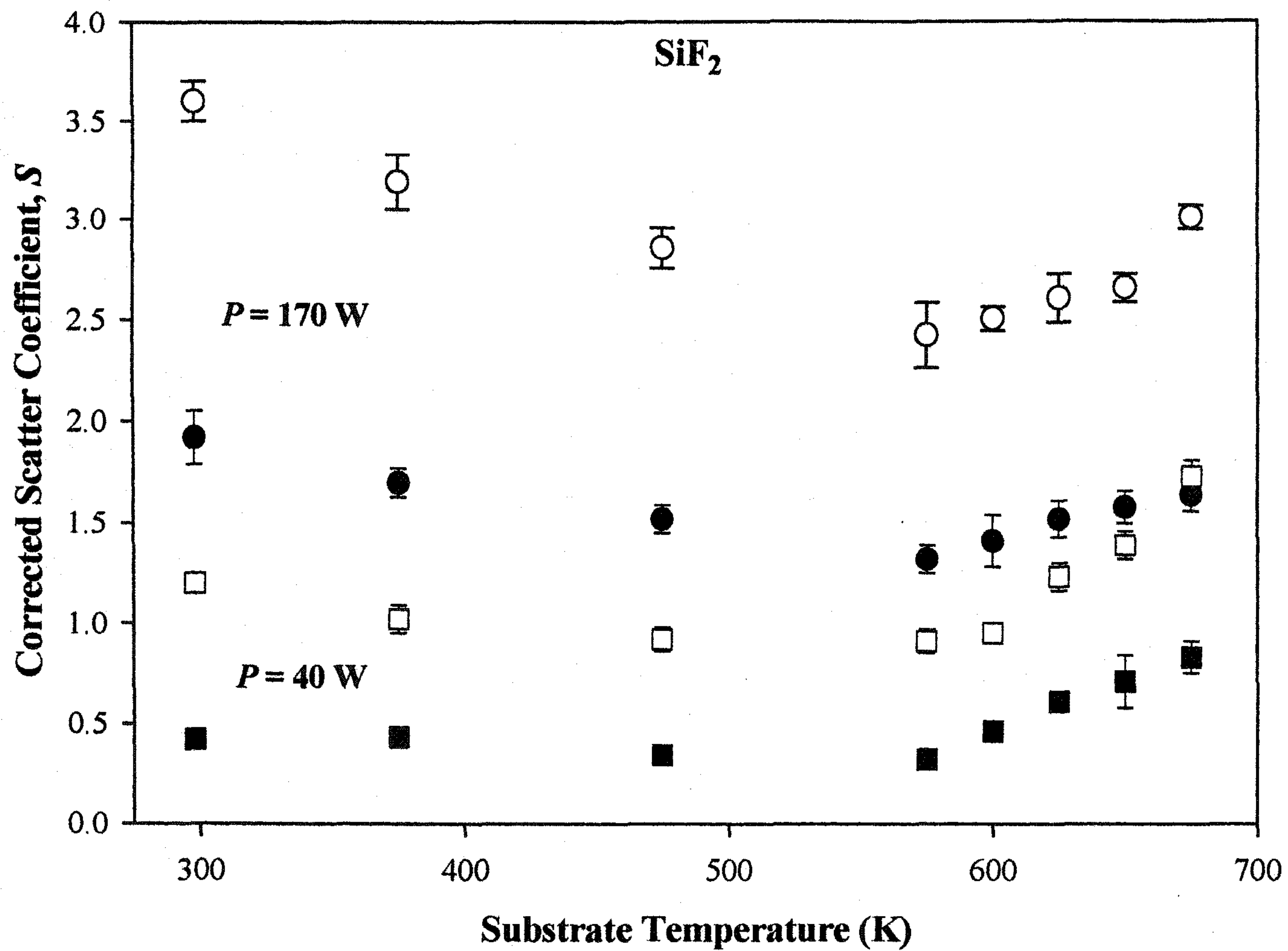

Figure 4.5. (B) Scatter coefficients for SiF_2 (2_0^4) in 100% SiF_4 (open symbols) and 90:10 SiF_4:H_2 (closed symbols) plasmas at 170 W (circles) and 40 W (squares) as a function of T_S.

at $T_S < 575$ K. Above this temperature, however, SiF scatter increases linearly for all four plasma systems but at different rates of increase. Linear regression analysis of the SiF scatter in both of the 170 W plasmas yields a slope of 1.86×10^{-3} ($r^2 = 0.970$). Analysis of the 40 W plasma systems reveals a slightly larger slope for the SiF scatter, m $= 5.32 \times 10^{-3}$ ($r^2 = 0.958$), suggesting a greater dependence on T_S at the lower *P*. These differences in scatter dependence on T_S as a function of plasma power is likely the result of changing adlayer composition and will be discussed in further detail in Section 4.3. Interestingly, at the same *P* and T_S, *S*(SiF) values measured in the SiF_4 plasma are nearly identical to those measured in the 90:10 SiF_4/H_2 system.

The surface interactions of SiF_2 are highly dependent on both the T_S and the plasma composition. Similar to results for SiF, *S*(SiF_2) increases at $T_S > 575$ K for all four plasma systems, Figure 4.5b. Linear regression analysis of the SiF_2 scatter for elevated T_S again indicates a slightly stronger dependence on T_S for the 40 W plasmas (m $= 5.08 \times 10^{-3}$, $r^2 = 0.995$) than for the 170 W systems ($m = 3.00 \times 10^{-3}$, $r^2 = 0.974$). From $T_S = 300$ K to $T_S = 575$ K, we observe a small but significant decrease in *S*(SiF_2) for all four plasma systems, Fig. 4.5b. As discussed below, these changes are likely the result of differences in the SiF_x thickness and adlayer. Finally, the data in Fig. 4.5b demonstrate that the SiF_2 scatter values are highly dependent on the plasma composition as well as T_S. Specifically, *S*(SiF_2) values measured in the SiF_4 system are consistently higher than those measured in the SiF_4/H_2 system under the same *P* and T_S. This suggests that the role of SiF_2 changes upon addition of H_2.

4.2.3. Determination of Θ_R. In addition to deriving Θ_R from rotational excitation spectra, an alternative method can be used involving analysis of the *J*-state

Reproduced with permission of the copyright owner. Further reproduction prohibited without permission.

dependence of the molecule's scattering ratio as a function of T_S.[37-39] In addition to kinetic energy differences between incident and scattered molecules, there can also be differences in rotational state populations for incident and scattered species based on the internal (rotational) temperature of the molecules. If Θ_R of the molecules in the molecular beam equals the T_S, the population of a specific rotational state in the incident beam will be the same as that for molecules in the same state emanating from the surface (assuming thermal accommodation on the surface). Thus, when $\Theta_R = T_S$, population state changes do not affect the measurement of *S*, and all rotational states will exhibit the same value for *S*. By examining the *S* values for different rotational states as a function of T_S, we can thus determine Θ_R. Note that this method for Θ_R determination assumes that changes in the scatter coefficient are due only to changing substrate temperature. We will explore the limitations to this assumption in the Section 4.2.4.

Figure 4.6a shows the scatter ratio of three rovibrational states from the SiF_2 $A^1B_1 - X^1A_1$ transition as a function of T_S. The T_S at which *S* values for all three *J* states intersect yields an estimate of Θ_R. From Fig. 4.6a, it appears that intersection of these scatter values occurs at $\Theta_R = 725 \pm 100$ K. Determination of Θ_R for SiF from T_S data is less straightforward. Figure 4.6b shows scatter coefficients of three rotational states from the Q_1 branch of SiF as a function of T_s. At 375 K, SiF modeled data yield $S = 0.69 \pm 0.10$, $S = 0.70 \pm 0.07$, and $S = 0.87 \pm 0.12$ for the J = 0.5, 4.5, and 9.5 states, respectively. Increases in T_S result in significant increases in scatter values for all three *J* states, but at different slopes. From Figure 4.6b, it is difficult to identify Θ_R for SiF since all three rotational lines yield nearly equivalent *S* for T_S between 400 and 700 K. For both SiF

Reproduced with permission of the copyright owner. Further reproduction prohibited without permission.

Reproduced with permission of the copyright owner. Further reproduction prohibited without permission.

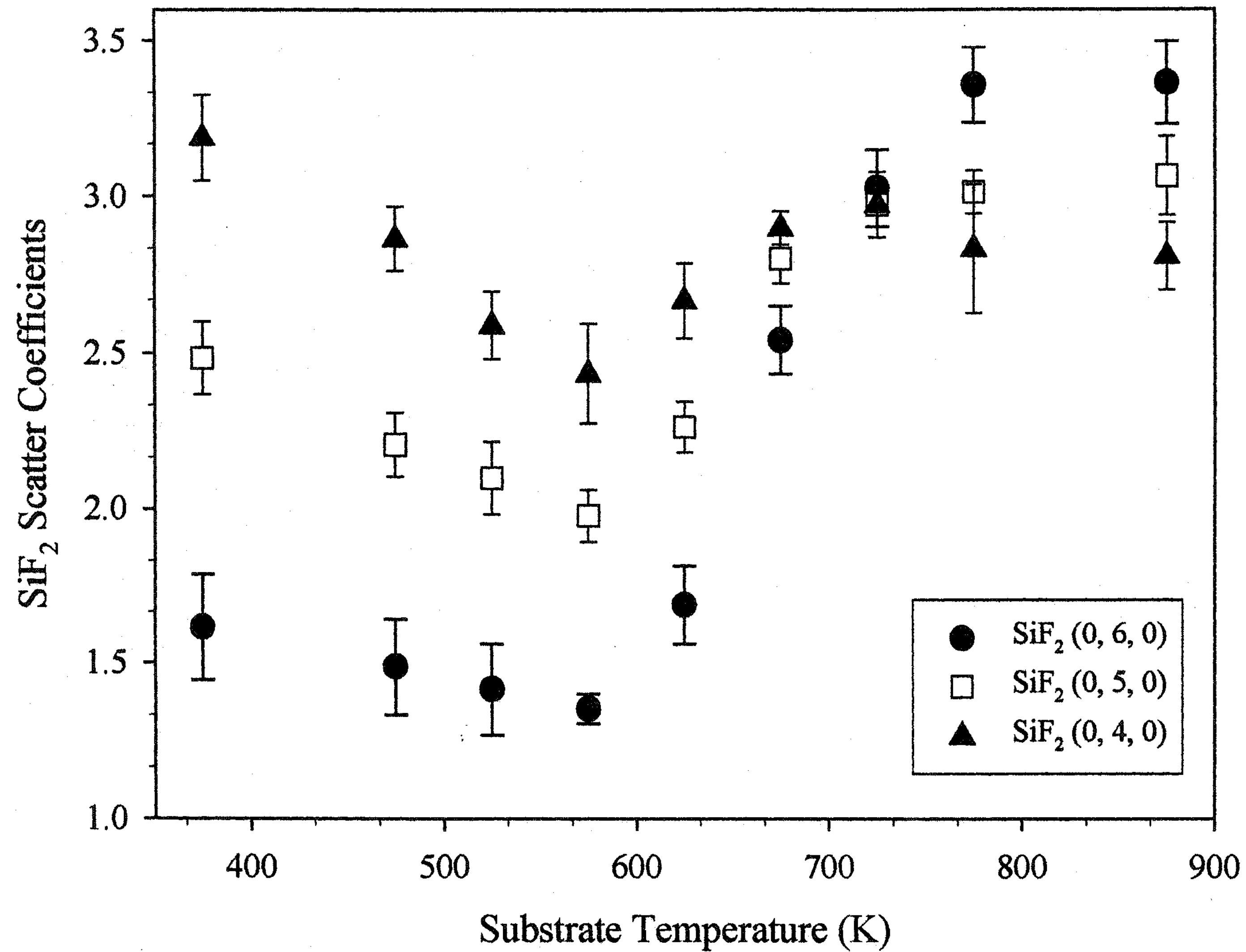

Figure 4.6. (A) Rotational state dependence of scatter ratios as a function of substrate temperature for 2^6_0 (●), 2^5_0 (□), and 2^4_0 (▲) SiF_2 rovibronic states.

Reproduced with permission of the copyright owner. Further reproduction prohibited without permission.

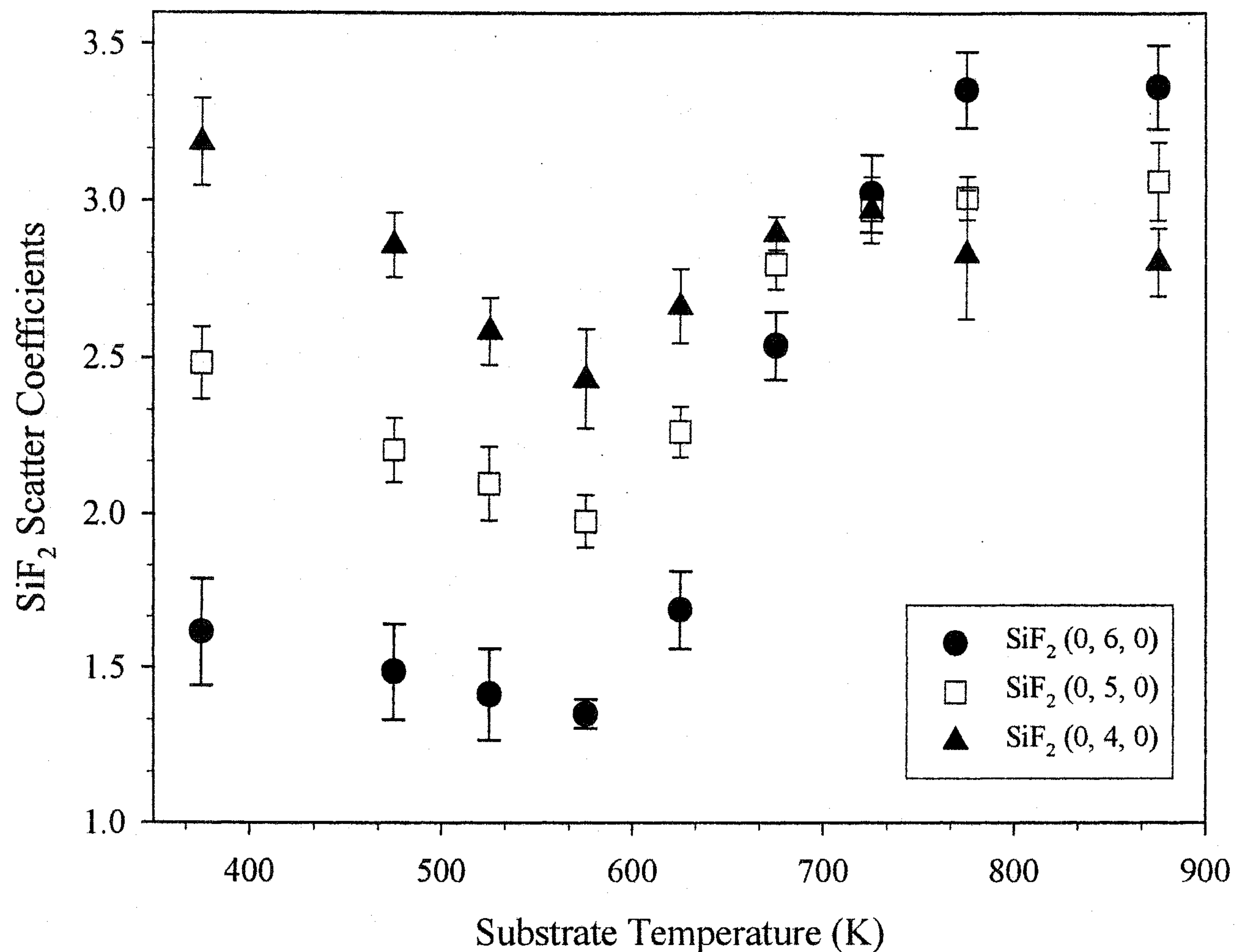

Figure 4.6. (A) Rotational state dependence of scatter ratios as a function of substrate temperature for 2^6_0 (●), 2^5_0 (□), and 2^4_0 (▲) SiF_2 rovibronic states.

and SiF_2, however, we would note that this analysis is at least consistent with results obtained from the excitation spectra.

4.3. Discussion

We have extensively studied the effects of plasma parameters such as rf power and gas ratios on the radical-surface interactions of SiF_x radicals.[32,33] These data, in conjunction with empirical studies of deposited films, allow for the formulation of possible mechanisms responsible for both film growth as well as Si etching. We have extended our investigation of SiF_4-containing plasmas to substrate temperature effects. Here, we discuss the mechanistic implications of changes in surface reactivity as a function of T_S.

Like many glow discharge systems, SiF_4 plasmas can either etch or deposit thin film materials. We have identified three main types of plasma conditions. SiF_4 plasma conditions that are principally etching (40 W and 170 W, 100% SiF_4) are categorized as Type 1, while those plasmas that result primarily in film deposition (40 W and 170 W, 10% H_2) are considered Type 3. Type 2 plasmas result in F atom implantation only and are discussed further in Chapter 5. Regardless of the plasma type, however, both SiF and SiF_2 show the same general scatter trends as a function of T_S; namely a significant increase in surface scatter at $T_S > 575$ K. These results are in good agreement with literature studies of F atom etching of Si using a XeF_2 source.[7,10,40] Winters first reported increased desorption of SiF_2 at $T_S \geq 600$ K using mass spectrometry to investigate both the desorbing species and the surface composition of Si after XeF_2 dosing.[6,11,12] A careful review of the literature data by Winters and Coburn demonstrated that SiF_2 desorption is

Reproduced with permission of the copyright owner. Further reproduction prohibited without permission.

low at $T_S < 600$ K, yet becomes the dominant etch product at $T_S > 600$ K.[6] Moreover, the quantity of SiF_2 in the etch product at $T_S = 300$ K was negligible. These studies, however, do not account for the effects of other energetic species present during plasma processing of a surface.

Sebel et al. recently conducted similar studies of T_S effects on SiF_2 desorption during Si etching,[7] including the effects of Ar^+ bombardment at different T_S. This work more closely resembles plasma conditions as energetic ion bombardment can significantly alter surface interactions of plasma species.[41] Under these conditions (i.e. with ion bombardment), SiF_2 production was non-negligible at $T_S < 600$ K, although SiF_4 was the major etch product. At $T_S > 600$ K, Sebel et al.[7] achieved similar results to those of Winters and coworkers,[6] with SiF_2 being the major etch product generated in this temperature regime. In these studies, it was suggested that SiF_2 desorption increases above $T_S = 600$ K because the thermal energy of the surface overcomes the energy required for desorption (260 meV).[7] The increases in SiF_2 scatter at $T_S > 600$ K that we observe in our experiments can also be attributed to surpassing the desorption energy for SiF_2.

We observe an increase in SiF_2 scatter at elevated substrate temperatures for all four plasma systems studied here, Fig. 4.4b. There are, however, some significant differences between the four systems. In 170 W plasmas, $S(SiF_2)$ increased by ~24%, regardless of feed gas composition. For 40 W plasmas, however, SiF_2 scatter increased more dramatically and was dependent upon feed gas composition with ~90% and ~160% increases observed for 100% SiF_4 and 90:10 SiF_4:H_2 plasmas, respectively. These differences are likely the result of differences in ion bombardment of the surface adlayer

Reproduced with permission of the copyright owner. Further reproduction prohibited without permission.

under different plasma conditions. At $P = 170$ W, there is a much greater flux of bombarding ions to the surface which serve to deplete the surface of SiF_2 moieties and may be volatilized only as they are produced. At $P = 40$ W, however, the surface adlayer is rich in SiF_2 species which can desorb from the surface as the substrate temperature increases above ~600 K. Previous work using Ar^+ ion beams showed that ion bombardment resulted in a decrease in the SiF_2 surface concentration and the formation of a reaction layer with submonolayer fluorine coverage.[6,7] In our work, SiF scatter also shows significant increases at $T_S > 600$ K. As the desorption energy for SiF should be only slightly higher than that for SiF_2, we also attribute this behavior to reaching a thermal energy greater than the desorption energy.

At $T_S < 600$ K, the SiF_x species display different scatter behavior. Specifically, SiF_2 scatter decreases by ~32% for 170 W plasmas and by ~24% for 40 W plasmas. Within experimental error, no changes in scatter are observed for SiF at $T_s < 575$ K within each system. Ibbotson and coworkers examined the dependence of Si etch rate on T_S under ion bombardment.[16] As T_S increased, the etch rate decreased until $T_S \sim 500$ K, at which point a sharp rise in etch with increasing T_S occurs. This effect is related to the change in surface adlayer concentrations and thickness with increasing substrate temperature. In those studies, SiF_3 was the most abundant species in the adlayer when $T_S = 300$ K, but the major species shift to SiF_2 and SiF functional groups as T_S is increased. The decrease in SiF_2 scatter we see between room temperature and 575 K is also likely related to the adlayer composition and thickness. The negligible changes in surface scatter we observe for the SiF radical may be the result of a combination of SiF(ads) stability[42,43] and its relatively low abundance in the surface adlayer at $T_S < 600$ K.

Reproduced with permission of the copyright owner. Further reproduction prohibited without permission.

Clearly, the very different roles of SiF (deposition precursor) and SiF_2 (etch product) in fluorosilane plasma processing become evident by examining their surface interactions under different plasma conditions.

It is interesting to compare our T_S dependence results for SiF and SiF_2 with past IRIS studies of other plasma species such as SiH, NH, and OH. We observed negligible SiH scatter at all substrate temperatures (T_S = 300-673 K) during a-Si:H deposition from SiH_4 plasmas.[44] Although it is non-zero, the amount of NH scatter in NH_3 plasmas also does not change appreciably with T_S.[45] Thus, SiH and NH represent a class of plasma species whose surface interactions are apparently unaffected by elevated T_S. This is similar to what we observe for SiF at T_S = 300-600 K. In both H_2O and tetraethoxysilane (TEOS)/O_2 plasmas, however, we found significantly greater amounts of OH radicals desorb from Si substrates at $T_S > 350$ K.[44] This increase in OH scatter was attributed primarily to a decrease in surface reactions accessible to the impinging OH radicals, suggesting that surface composition can significantly alter the production of desorbing species during plasma-surface interactions. SiF and SiF_2 scatter behavior is analogous to the OH results at $T_S > 600$ K. All of these studies demonstrate the importance of T_S investigations to understanding the plasma-surface interactions as well as the overall chemistry of etching and deposition in these systems.

4.4. Conclusions

Surface reactivities of SiF and SiF_2 in fluorosilane plasmas have been measured as a function of substrate temperature under a variety of plasma conditions including rf power and feed gas composition. Regardless of radical or plasma parameters, a

Reproduced with permission of the copyright owner. Further reproduction prohibited without permission.

significant increase in surface scatter was observed at $T_S \geq \sim 600$ K. This temperature corresponds to the energy for desorption of both SiF and SiF_2; thus, at higher T_S it is easier for desorption to occur. Correction of the observed scatter due to thermal equilibration at the substrate surface revealed small decreases in surface scatter of SiF and SiF_2 as T_S was increased from 300 to 600 K. These changes may be the result of changes in the SiF_x adlayer on the surface. In addition to surface reactivity measurements, rotational temperatures (θ_R) of 450 ± 50 K and 752 ± 100 K have been determined for SiF and SiF_2, respectively.

Reproduced with permission of the copyright owner. Further reproduction prohibited without permission.

References

1. M. Tsuji, Y. Nishimura *Jpn. J. Appl. Phys. Part 1* **36**, 6922 (1997).
2. M. Syed, T. Inokuma, Y. Kurata, S. Hasegawa *J. Appl. Phys., Part 1* **38**, 1303 (1999).
3. N. Sugiomoto, A. Hozumi, O. Takai *Han'guk Pyomyon Konghak Hoechi* **29**, 577 (1996).
4. J. Staffa, D. Hwang, B. Luther, J. Ruzyllo, R. Grant *Appl. Phys. Lett.* **67**, 1902 (1995).
5. G. Bruno, P. Capezzuto, G. Cicala *J. Appl. Phys.* **69**, 7256 (1991).
6. H. F. Winters, J. W. Coburn *Surf. Sci. Rep.* **14**, 161 (1992).
7. P. G. M. Sebel, L. J. F. Hermans, H. C. W. Beijerinck *J. Vac. Sci. Technol. A* **18**, 2759 (2000).
8. S. Vanhaelemeersch, J. Van Hoeymissen, D. Vermeylen, J. Peeters *J. Appl. Phys.* **70**, 3892 (1991).
9. J. S. Horwitz, J. A. Dagata, D. W. Shinn, M. C. Lin *AIP Conf. Proc.* **191**, 445 (1989).
10. J. W. Coburn, C. B. Mullins *Proc. - Electrochem. Soc.* **92**, 276 (1992).
11. H. F. Winters, I. C. Plumb *J. Vac. Sci. Technol. B* **9**, 197 (1991).
12. H. F. Winters *J. Vac. Sci. Technol. B* **1**, 927 (1983).
13. H. F. Winters *J. Appl. Phys.* **49**, 5165 (1978).
14. Y. Babanov, V. Svetovoy *Acta Phys. Pol. A* **A77**, 355 (1990).
15. M. Hiroi, T. Tatsumi *Jpn. J. Appl. Phys. Part 1* **33**, 2244 (1994).

Reproduced with permission of the copyright owner. Further reproduction prohibited without permission.

16. D. E. Ibbotson, D. L. Flamm, J. A. Mucha, V. M. Donnelly *Appl. Phys. Lett.* **44**, 1129 (1984).

17. V. M. Bermudez *J. Vac. Sci. Technol. A* **10**, 3478 (1992).

18. K. L. Williams, E. R. Fisher *J. Vac. Sci. Technol. A*, manuscript in preparation.

19. A. Madan, S. R. Ovshinsky, E. Benn *Philos. Mag. B* **40**, 259 (1979).

20. S. Zhang, D. E. Brodie *J. Appl. Phys.* **72**, 1446 (1992).

21. H. Matsumura, H. Ihara *J. Appl. Phys.* **64**, 6505 (1988).

22. J. J. Lim, B. Y. Ryu, J. I. Ryu, J. Jang *Thin Solid Films* **289**, 227 (1996).

23. S. Kasouit, S. Kumar, R. Vanderhaghen, I. Roca, P. Cabarrocas, I. French *J. Non-Crystalline Solids* **299-302**, 113 (2002).

24. J. Hanna, A. Kamo, M. Azuma, N. Shibata, H. Shirai, I. Shimizu *Mat. Res. Soc. Symp. Proc.* **118**, 79 (1988).

25. T. Gungor, H. Tolunay *Turk. J. Phys.* **26**, 269 (2002).

26. L. E. Carter, E. A. Carter *J. Phys. Chem.* **100**, 873 (1996).

27. D. L. Flamm, V. M. Donnelly, J. A. Mucha *J. Appl. Phys.* **52**, 3633 (1981).

28. K. P. Giapis, T. K. Minton *Mat. Res. Soc. Symp. Proc.* **406**, 33 (1996).

29. C. B. Mullins, J. W. Coburn *J. Appl. Phys.* **76**, 7562 (1994).

30. D. W. Squire, J. A. Dagata, D. S. Y. Hsu, C. S. Dulcey, M. C. Lin *J. Phys. Chem.* **92**, 2827 (1988).

31. A. C. Stanton, A. Freedman, J. Wormhoudt, P. P. Gaspar *Chem. Phys. Lett.* **122**, 190 (1985).

32. W. M. M. Kessels, P. R. McCurdy, K. L. Williams, G. R. Barker, V. A. Venturo, E. R. Fisher *Journal of Physical Chemistry B* **106**, 2680 (2002).

Reproduced with permission of the copyright owner. Further reproduction prohibited without permission.

33. K. L. Williams, E. R. Fisher *J. Vac. Sci. Technol. A*, submitted for publication. (2003).

34. Y. M. Khanna, G. Besenbruch, J. L. Margrave *J. Chem. Phys.* **46**, 2310 (1967).

35. S. J. Davis, S. G. Hadley *Phys. Rev. A* **14**, 1146 (1976).

36. J. Zhang, K. L. Williams, E. R. Fisher *J. Phys. Chem. A*, submitted for publication. (2002).

37. K. H. A. Bogart, J. P. Cushing, E. R. Fisher *377-383* **267**, 377 (1997).

38. E. R. Fisher, P. Ho, W. G. Breiland, R. J. Buss *J. Phys. Chem.* **97**, 10287 (1993).

39. C. I. Butoi, M. L. Steen, J. R. D. Peers, E. R. Fisher *J. Phys. Chem. B* **105**, 5957 (2001).

40. D. E. Ibbostson, D. L. Flamm, J. A. Mucha, V. M. Donnelly *Appl. Phys. Lett.* **44**, 1129 (1984).

41. K. L. Williams, I. T. Martin, E. R. Fisher *J. Am. Soc. Mass. Spectrom.* **13**, 518 (2002).

42. C. J. Wu, E. A. Carter *J. Am. Chem. Soc.* **113**, 9061 (1991).

43. C. J. Wu, E. A. Carter *Phys. Rev. B* **45**, 9065 (1992).

44. P. R. McCurdy, K. H. A. Bogart, N. F. Dalleska, E. R. Fisher *Rev. Sci. Instrum.* **68**, 1684 (1997).

45. P. R. McCurdy, C. I. Butoi, K. L. Williams, E. R. Fisher *J. Phys. Chem. B* **103**, 6919 (1999).

Reproduced with permission of the copyright owner. Further reproduction prohibited without permission.

CHAPTER 5

MECHANISMS FOR DEPOSITION AND ETCHING IN FLUOROSILANE PLASMA PROCESSING OF SILICON

Keri L. Williams, Carmen I. Butoi, and Ellen R. Fisher

This chapter has been submitted to *J. Vac. Sci. Technol. A*. Printed with permission from Keri L. Williams, Carmen I. Butoi, and Ellen R. Fisher.

This dissertation chapter contains results from a full paper submitted to the Journal of Vacuum Science and Technology A in February 2003. The manuscript was written by Keri L. Williams and edited by Ellen R. Fisher. Carmen I. Butoi was responsible for initially training Keri L. Williams on the IRIS technique. All data collection and analysis were performed by Keri L. Williams. This chapter describes the effect of rf power (*P*) and source gas ratios on film, plasma-surface, and gas-phase composition for SiF_4 and SiF_4/H_2 plasmas. Film characterization and gas phase analysis has been used to characterize material properties, the plasma-surface interface, and the gas phase. From these data, three SiF_4 plasma types have been defined.

Reproduced with permission of the copyright owner. Further reproduction prohibited without permission.

5.1. Introduction

As discussed in the previous chapter, fluorosilane plasmas have been widely studied because of their ability to deposit and etch Si-based materials. To deposit films, a suitable diluent is added to the silicon feed gas to create a wide range of fluorinated silicon alloys (F-SiO_2,[1-3] a-Si:H,F,[4,5] a-SiC:F,[6,7] and a-Si_xN_y:F[8-10]). Typically, fluorine incorporation results in significantly improved material properties over the traditional silicon alloy films.[11,12] Madan and Ovshinsky have reported that a-Si:H,F films prepared from SiF_4 and H_2 are thermally more stable than a-Si:H and have a considerably reduced density of localized states.[13] Consequently, these materials have been used in the fabrication of solar cells,[14-16] photoreceptors,[10] and thin film transistors.[17] These materials have been deposited using several feed gas compositions: SiF_4/H_2,[11,14,18-20] SiH_2F_2,[21] SiH_4/SiF_4,[12,22,23] and Si_2F_6.[16] Of these, SiF_4/H_2 plasmas have been the most often used.

Much of the research on fluorosilane plasmas has focused on the production of high quality fluorinated silicon materials (i.e. a-Si:H,F, F-SiO_2)[11,12,15,24] and understanding the role of individual species in SiF_4 and SiF_4/H_2 plasmas.[11,15,17,18,25-27] Optical emission spectroscopy (OES) and mass spectrometry (MS) measurements made by Bruno et al.[18] as well as laser induced fluorescence (LIF) studies by Lee and Deneufville[14,15] have offered insight into possible deposition precursors. In both cases, SiF radicals are suggested to have a significant role in the deposition of a-SiH,F films. Gas-phase measurements such as these are important steps to understanding the overall fluorosilane chemistry, but do not address chemistry occurring at the plasma-surface

Reproduced with permission of the copyright owner. Further reproduction prohibited without permission.

interface. Surface-reactivity measurements, however, can complement the current body of work and offer new insight to yet undetermined fluorosilane surface chemistry.

In the absence of diluent, SiF_4 plasmas selectively etch Si over SiO_2[28-30] and Si_3N_4.[31-33] Etching in these systems has been attributed to processes such as radical-surface reactions and ion bombardment.[34] Although there are several radical-surface reactions that may contribute to silicon etching, F atoms are considered to be the fundamental etchant.[35] Indeed, extensive investigations have elucidated many details of the mechanism of F atom etching. Seminal works by Mucha et al.[36,37] and Winters and Coburn[34] have reported F atom etch mechanisms showing Si-Si bond cleavage to form SiF_2 and SiF_4 which desorb from the surface. Both proposed etch products have been experimentally observed during F atom etching of Si, yet few studies have characterized SiF_2 and SiF_4 *during* fluorosilane plasma etching of silicon surfaces.

In addition to the contribution of radical reactions, ion bombardment significantly affects plasma-surface interactions.[38] High-energy ions are believed to considerably enhance etching by sputtering fragments such as SiF_2 from the silicon surface. Furthermore, ions may promote etching by transferring energy to the surface or reacting to produce additional sources for etching.[39] Investigations into the ion effects on Si etching have been performed,[39-41] yet most of these studies have examined only atomic or molecular beams containing a single species, not taking into account the effects of other important species present in plasma beams. Different mechanistic routes in the presence of the full range of plasmas species, however, assist silicon etching. We have recently investigated the effects of substrate temperature (T_S) and bombarding ions on SiF_2 surface scatter during plasma etching of silicon, Chapter 4.[42] Those studies clearly

Reproduced with permission of the copyright owner. Further reproduction prohibited without permission.

demonstrated that plasma-surface reactions are strongly affected by the flux of charged species to the surface.

To gain a more detailed understanding of etching and deposition reactions in fluorosilane plasmas, it is important to have knowledge of gas-phase and surface reactions of plasma species, both ionic and neutral, as well as characterization of the overall surface modification that occurs during either material removal or film formation. It is often difficult, however, to characterize the role of individual plasma species, especially radicals, without perturbing the plasma environment. Our IRIS technique directly measures the steady-state surface loss coefficients of gas-phase species *during* plasma processing of a substrate. IRIS combines molecular beam and plasma technologies with LIF to provide spatially resolved two-dimensional (2D) images of molecules involved in film formation and substrate etching.[43] To date, a wide range of scatter coefficients (*S*) have been measured for several different molecules[38,44-47] in a variety of plasma systems. In the present work, we extend our IRIS studies to SiF_2 and SiF in both SiF_4 and SiF_4/H_2 plasmas.

The IRIS study of SiF_2 and SiF radicals in SiF_4-based plasmas was undertaken for a variety of reasons. First, as noted above, fluorosilane plasmas are technologically relevant for both Si etching and deposition of fluorinated silicon alloys. Second, SiF_4 offers a good model system for examining SiF_2, a known Si etch product in all fluorinated plasma systems. Third, plasma-surface measurements of multiple plasma species in a single system provide the opportunity to better understand primary mechanisms responsible for etching and deposition. Finally, since the etching and deposition regimes of fluorosilane plasmas behave similarly to those of fluorocarbon

Reproduced with permission of the copyright owner. Further reproduction prohibited without permission.

plasmas, we have measured scatter coefficients for SiF_2 and SiF in SiF_4 and SiF_4/H_2 plasmas for comparison to our work with fluorocarbon systems. Analogous to CF_2 in C_2F_6 and C_2F_6/H_2 plasmas, SiF_2 surface reactivity appears to be directly related to the degree of etching or deposition taking place as an overall plasma process.[48-50] Similarly, SiF and CF molecules are responsible for promoting film growth in their respective systems.[51,52] The current study provides a description of the plasma-surface interface by correlating direct measurement of SiF_2 and SiF radical-surface interactions, relative gas phase density measurements, and a-Si:H,F film analysis.

5.2. Results

5.2.1. Plasma Regime Determined by Film Characterization. In general, plasmas can affect surfaces in one of three ways: etching, surface modification with no net deposition or etching, or deposition. For ease of discussion, we classify these as Type 1, Type 2, and Type 3 plasmas, respectively. No film deposition is observed in the 100% SiF_4 plasmas and, overall, etching occurs at $P > 20$ W. Indeed, we have measured an etch rate of ~12 Å/min for an 80 W, 100% SiF_4 plasma. Thus, this is a Type 1 system. Analysis of substrates exposed to a 100% SiF_4 plasma with $P = 20$ W, showed no net etching or deposition. XPS analysis revealed, however, F incorporation at the substrate surface (~30% F); this system is thus defined as a Type 2 plasma. Similar results were observed for the 50% H_2 plasma system at $P > 40$ W (~4% F). In contrast, all other SiF_4/H_2 systems, both 10% and 50% H_2, resulted in net deposition of a-Si:H,F films, defining these systems as Type 3 plasmas. For Type 3 systems, films were characterized by SEM, FTIR, XPS, and ellipsometry as discussed in Chapter 2.

Reproduced with permission of the copyright owner. Further reproduction prohibited without permission.

All depositing plasmas produced smooth, conformal films as shown in Figure 5.1. FTIR spectra of a-Si:H,F films deposited on Si substrates using 10% H_2 plasmas at different *P*, Figure 5.2, display similar absorption bands between 600 and 1000 cm^{-1} making it difficult to identify bonding structure. Some distinct absorption peaks, however, have been identified from literature assignments: SiH_2 stretching and bending bands (~2100, ~900, ~842, and ~650 cm^{-1}); SiF_2 stretches (~983 and ~935 cm^{-1}); and an SiF stretch at ~857 cm^{-1}.[19,53-55] SiO stretching at ~1100 cm^{-1} is likely the result of deposition of etch products from the glass reactor. Several of these functional groups are affected by increasing *P*. Specifically, SiF_2 and SiH_2 absorption bands show significant decreases at $P > 45$ W, whereas SiH (2000 cm^{-1}) and HSiF (1000 cm^{-1}) groups begin to appear at $P > 45$ W.

XPS analysis was used to quantify the amount of fluorine incorporation in films deposited in 10% H_2 plasmas. Elemental composition analyses revealed that the fluorine concentration in our a-Si:H,F materials is strongly affected by *P*. Films deposited at $P =$ 20 W showed ~25% fluorine, whereas films deposited at $P = 80$ W had ~15% fluorine incorporation. This suggests that these materials may not be very robust because F incorporation > 1% produces poor electronic properties due to easy hydrolysis forming Si-OH and HF.[17,20] Under hermetically sealed conditions or with an appropriate barrier film, however, these films may perform comparably to other fluorinated Si materials.

Another factor in producing high quality a-Si:H,F films is the concentration of SiF_2 and SiH_2 in the materials as these moieties lead to easy oxidation.[17] To investigate the effect of H_2 addition on SiF_2 and SiH_2 content in these materials, the amount of H_2 in the feed gas was varied for films deposited at $P = 20$ W. Figure 5.3 shows FTIR spectra

Reproduced with permission of the copyright owner. Further reproduction prohibited without permission.

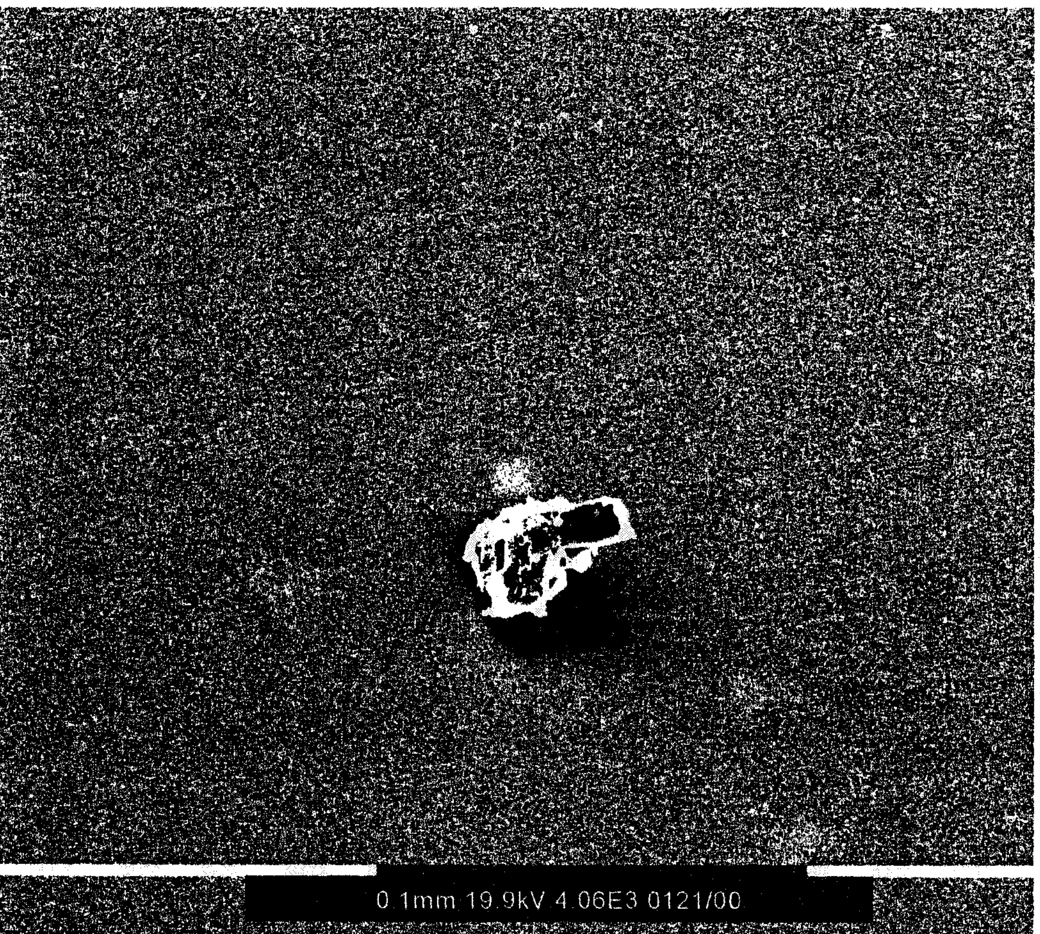

Figure 5.1. Scanning electron micrograph of an a-Si:H,F film deposited in a 90:10 SiF_4/H_2, 20 W plasma. The SEM image is shown at 4.06×10^3 magnification.

Reproduced with permission of the copyright owner. Further reproduction prohibited without permission.

Reproduced with permission of the copyright owner. Further reproduction prohibited without permission.

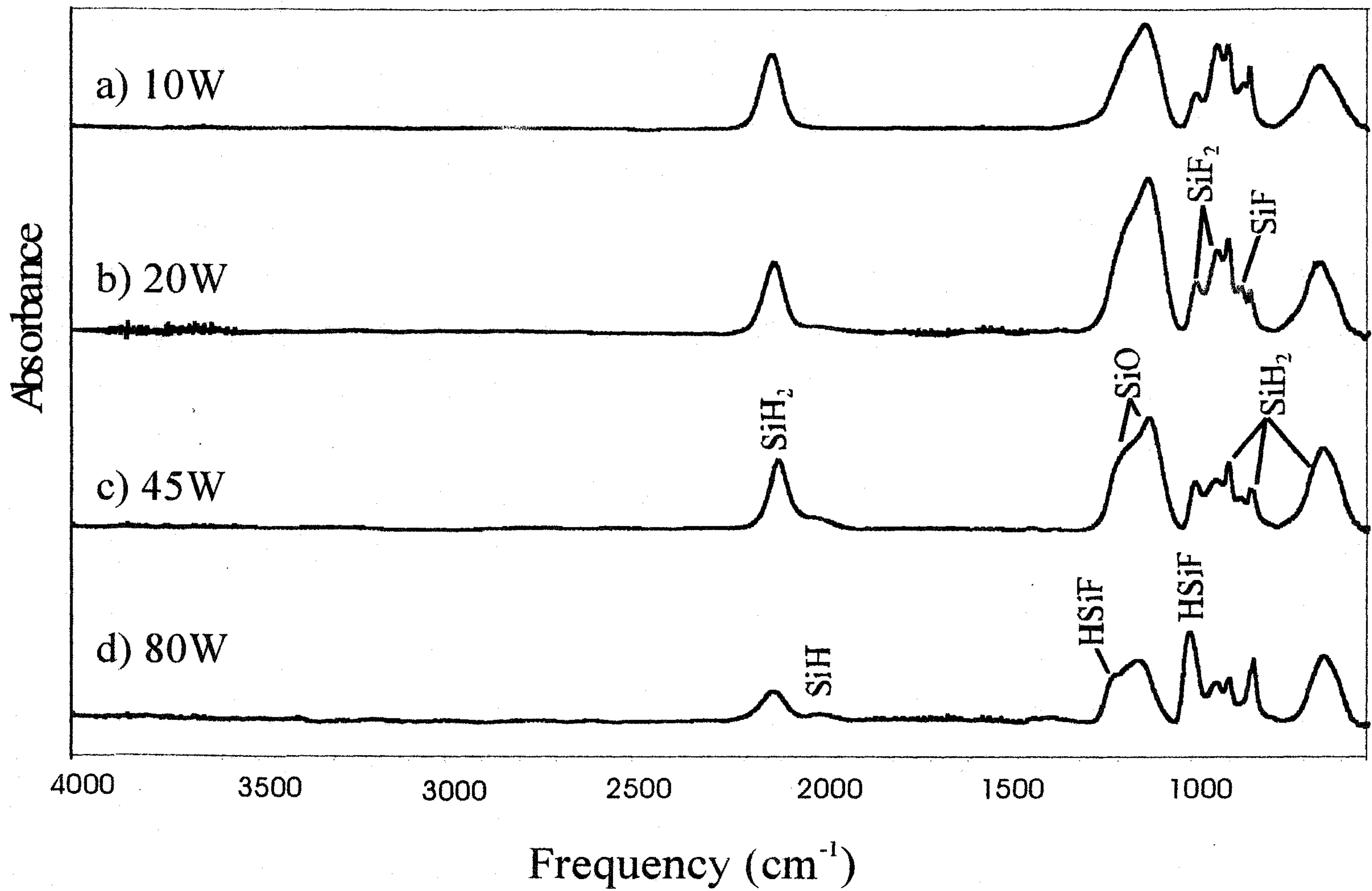

Figure 5.2. FTIR transmission spectra of amorphous fluorinated, hydrogenated silicon (a-Si:H,F) films deposited from SiF_4 plasmas with 10% H_2 addition in an inductively coupled rf plasma at a) 10 W, b) 20 W, c) 45 W, and d) 80 W.

Reproduced with permission of the copyright owner. Further reproduction prohibited without permission.

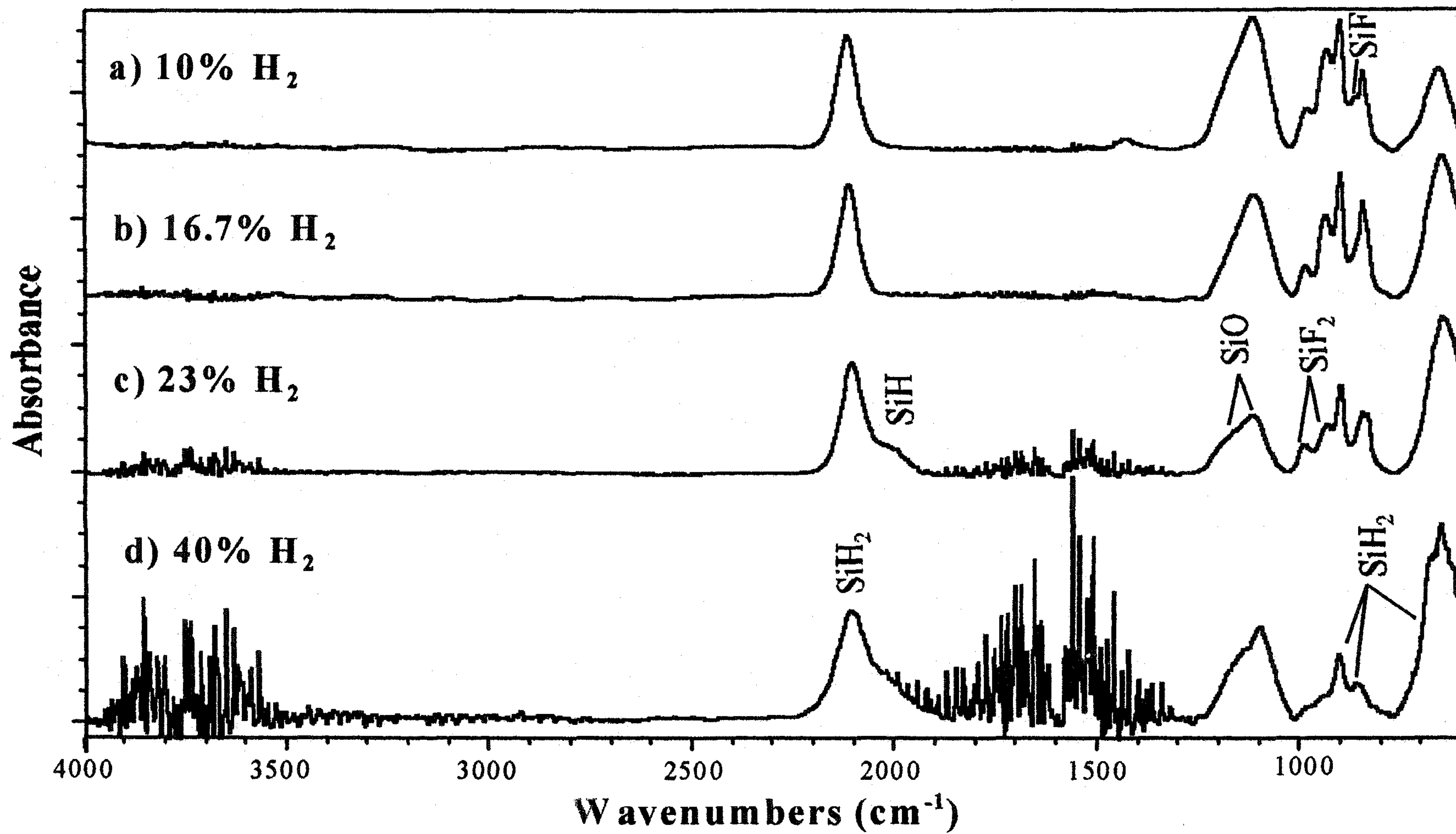

Figure 5.3. FTIR transmission spectra of amorphous fluorinated, hydrogenated silicon (a-Si:H,F) films deposited from SiF_4 plasmas in an inductively coupled rf plasma at 20 W applied power with a) 10%, b) 16.7%, c) 23%, and d) 40% H_2 addition.

of a-Si:H,F films deposited from SiF_4 plasmas with 10-40% H_2 content. These materials also contain several SiH_x and SiF_x absorption bands between 600 and 1000 cm^{-1}. SiH_2 incorporation is observed in all of these spectra, whereas only small amounts of SiH are observed for 23% H_2 addition. In contrast, SiF_x incorporation appears to be indirectly proportional to %H_2 added. This is confirmed by XPS analysis, which shows ~25% F using 10% H_2 addition, and ~15% F with 50% H_2 addition.

Figure 5.4 shows FTIR spectra of films deposited with 10% H_2 addition as a function of *P*, using the biased plates described in Chapter 2 to limit ion bombardment of the Si substrate. The SiH absorption at ~2000 cm^{-1} is observed at all *P*,[19,56] along with the SiH_2 absorption band at 2095 cm^{-1}. At the lowest applied rf power, $P = 20$ W, the SiH group dominates over SiH_2. This strongly contrasts with what was observed without the biased plates, Fig. 5.2, where there was virtually no SiH incorporation at the lowest *P*.

In addition to compositional changes, removal of charged species significantly affects film deposition rates, as shown in Figure 5.5 for films deposited with and without the biased deflector plates. At $P < 50$ W, deposition rates for films produced under both conditions increase with *P*. At $P > 60$ W, however, film deposition rate in the presence of charged species levels off at ~2400 Å/min while deposition rates in the absence of charged species increase linearly ($r^2 = 0.948$) with *P*. This behavior suggests that ion bombardment at higher *P* may serve to remove the a-Si:H,F film as it deposits. Deposition rate data for 10%H_2 plasmas are given in Table 5.1.

5.2.2. Gas-phase production of plasma species. Along with complete film analysis, gas phase composition is extremely important for understanding plasma chemistry and may be useful in determining specific reaction mechanisms responsible for

Reproduced with permission of the copyright owner. Further reproduction prohibited without permission.

Reproduced with permission of the copyright owner. Further reproduction prohibited without permission.

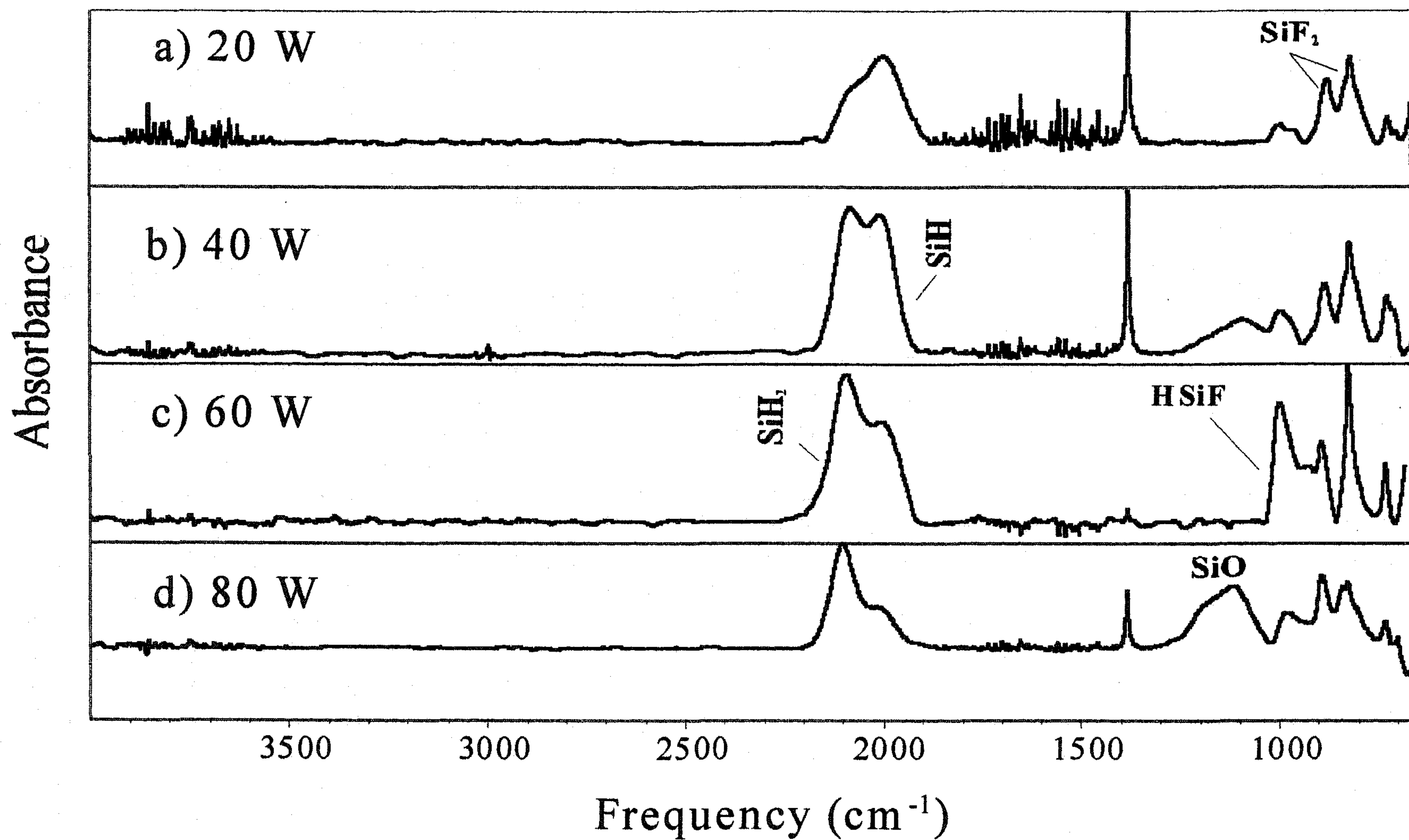

Figure 5.4. FTIR transmission spectra of amorphous fluorinated, hydrogenated silicon (a-Si:H,F) films deposited in the absence of charged species from SiF_4/H_2 plasmas with 10% H_2 addition at a) 20 W, b) 40 W, c) 60 W, and d) 80 W. Charged species were removed using a pair of copper plates biased to +200 V_{dc}.

Reproduced with permission of the copyright owner. Further reproduction prohibited without permission.

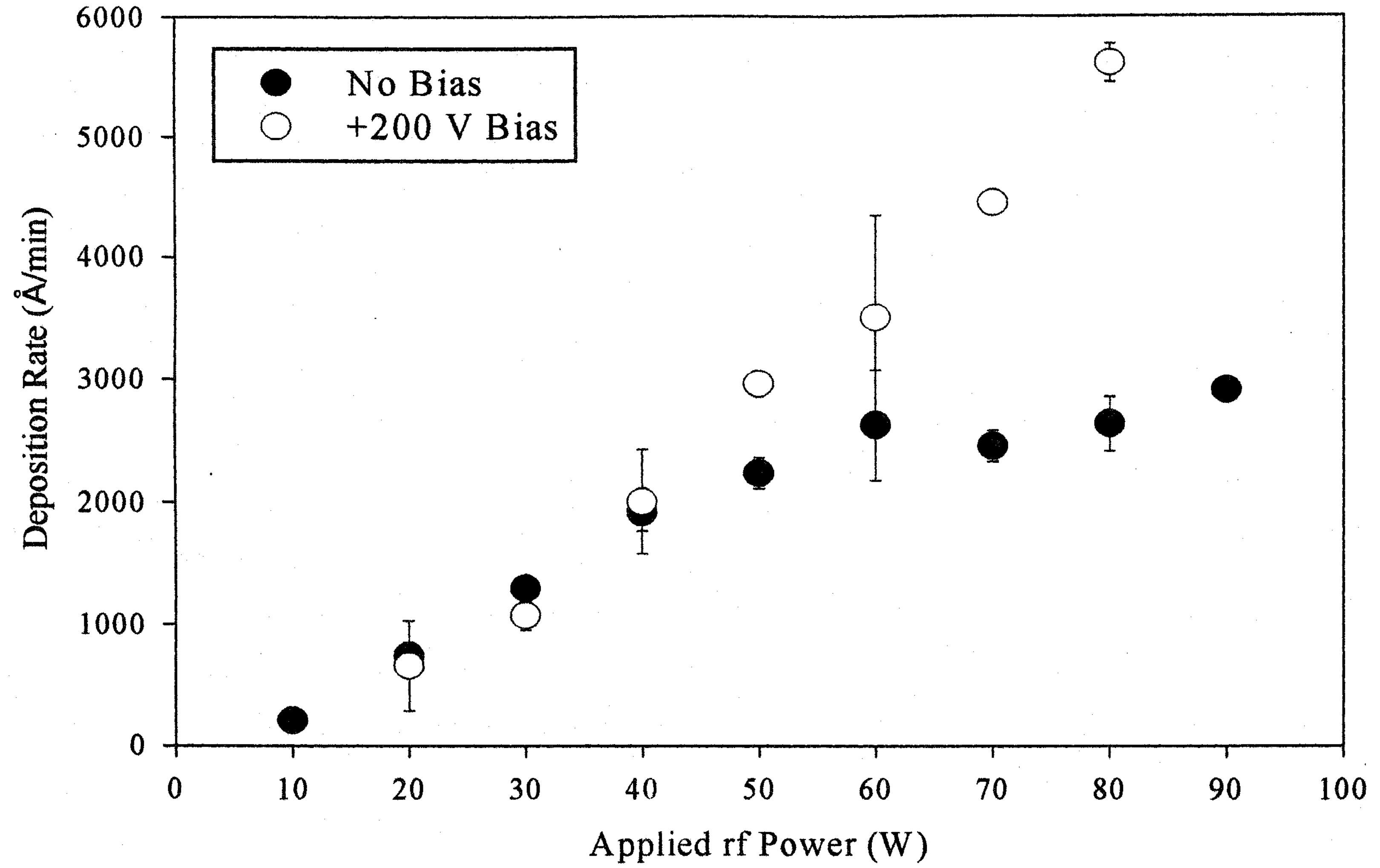

Figure 5.5. Deposition rates for films deposited as a function of applied rf power in the presence of charged species (●) and with charged species removed (○) using a pair of copper plates biased to +200 V_{dc}. Films deposited in the absence of charged species show a linear increase in deposition rate with plasma power ($r^2 = 0.948$).

Table 5.1: Deposition rate data for a-Si:H,F films produced as a function of P^a and $\%H_2{}^b$.

P	Deposition Rate-No Bias	Deposition Rate-Bias	% H_2 Addition	Deposition Rate-No Bias
20	744 ± 109	659 ± 54	0	0
30	1293 ± 85	1072 ± 12	5	2272 ± 4
40	1918 ± 155	2004 ± 280	6	2448 ± 43
50	2237 ± 125	2957 ± 98	8	2915 ± 22
60	2624 ± 233	3986 ± 45	10	2637 ± 79
70	2456 ± 124	4444 ± 3	15	2214 ± 19
80	2637 ± 220	5610 ± 159	20	2480 ± 188
-----	-----	-----	25	2021 ± 2
-----	-----	-----	30	1514 ± 24
-----	-----	-----	40	1073 ± 181
-----	-----	-----	50	628 ± 250

[a]All data measured on films deposited from 10% H_2 plasmas.
[b]All data measured on films deposited from 40 W plasmas.

Reproduced with permission of the copyright owner. Further reproduction prohibited without permission.

the three types of plasmas. Initial identification of plasma species was performed using optical emission spectroscopy. A typical spectrum for a SiF_4/H_2 plasma at 170 W is shown in Figure 5.6. From this spectrum, it is clear that SiF_x (x = 1 – 3) and H are present in these plasmas. As OES measures only excited state species and the amount of information for these data is limited, additional measurements were made using MS. Relative densities for a variety of neutral species (Si_xF_y, H_xSiF_y, F_2, and HF) have been measured as a function of *P* and % H_2 addition using MS.

Figure 5.7 shows a mass spectrum of molecules produced in a 170 W, 90:10 SiF_4/H_2 plasma molecular beam.

Normalized bar graphs in Figure 5.8a shows the effect of *P* on gas-phase production of F_2, SiF_x (x = 1 - 3), and Si_2F_5 in SiF_4 plasmas. The effect of *P* on SiF(g) has also been measured with LIF, yielding similar results, indicating that the observed MS signal is indeed attributable primarily to plasma radicals rather than cracking of stable gas molecules. All species studied (SiF_x (x = 1 - 3), F_2, and Si_2F_5) show similar increases with *P*. Radical production increases slowly with *P* up to *P* = ~100 W and then increases significantly at $P \geq 100$ W. With the addition of H_2, H_xSiF_y and HF are formed in addition to SiF_x (x = 1-3), Figure 5.8b. No measurable signal for Si_2F_5 could be found with the addition of any H_2 to the feed gas. Similarly, SiF and SiF_3 also showed significant depletion from the gas-phase with H_2 addition. In contrast, F_2, HF, HSiF, and $HSiF_2$ all increased with %H_2. Nearly linear increases are observed for all but $HSiF_2$, which increases rapidly before leveling off above 20% H_2.

For the H_2 addition data, it is instructive to directly compare trends observed in the MS results with LIF density measurements for SiF and SiF_2, Figure 5.9. SiF

Reproduced with permission of the copyright owner. Further reproduction prohibited without permission.

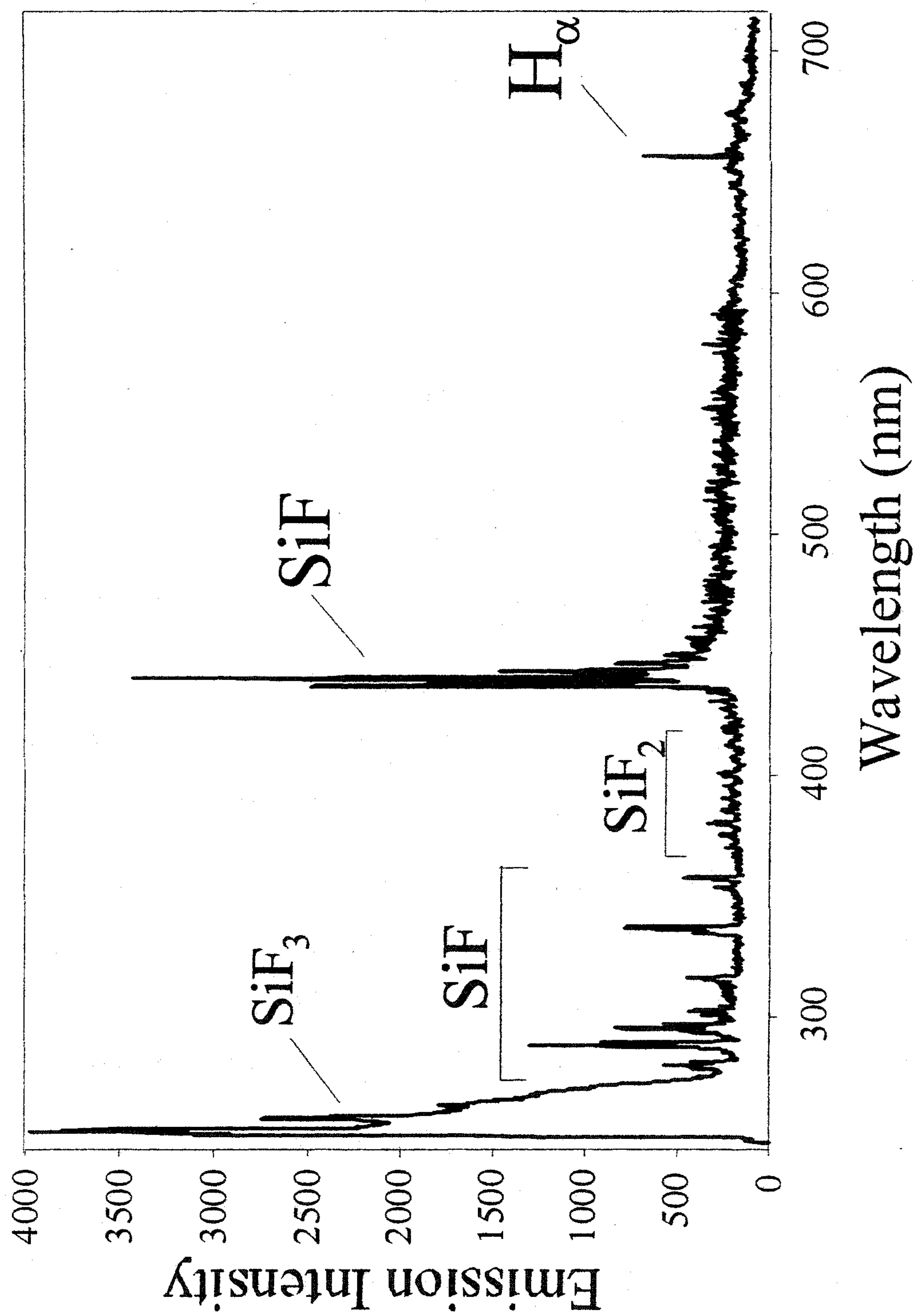

Figure 5.6. Optical emission spectrum of 170 W SiF_4/H_2 plasma with 10% H_2 addition.

Reproduced with permission of the copyright owner. Further reproduction prohibited without permission.

Reproduced with permission of the copyright owner. Further reproduction prohibited without permission.

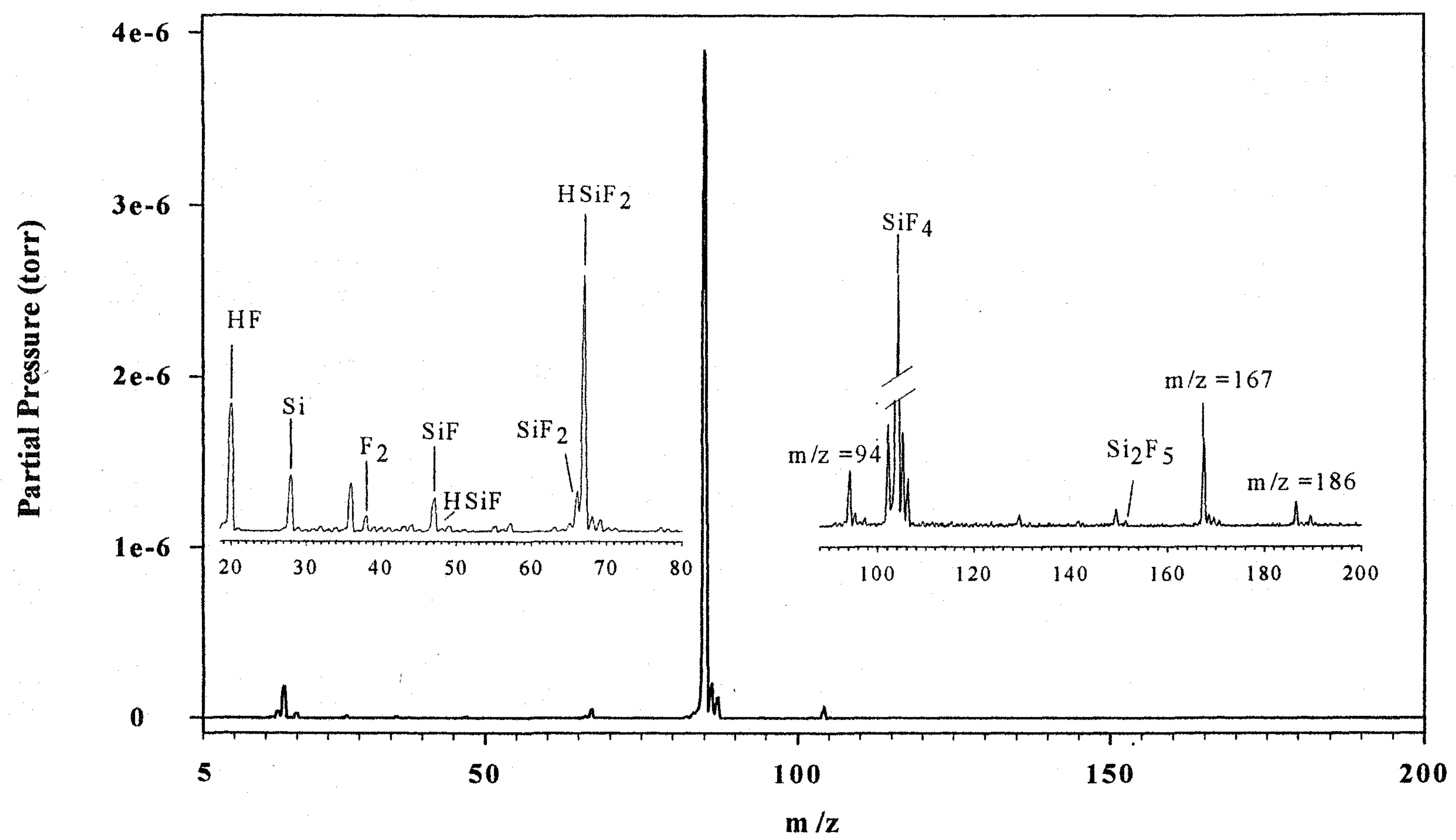

Figure 5.7. Experimental mass spectrum of neutral species from 5 to 200 amu in an 80 W, 90:10 SiF_4/H_2 plasma molecular beam (15 sccm total gas flow). The observed spectrum is obtained by setting the ionization voltage to 30 eV and subtracting a background spectrum of 90:10 SiF_4/H_2 gas. All unlabeled mass lines can be attributed to signals from residual H_2O or hydrocarbons.

Reproduced with permission of the copyright owner. Further reproduction prohibited without permission.

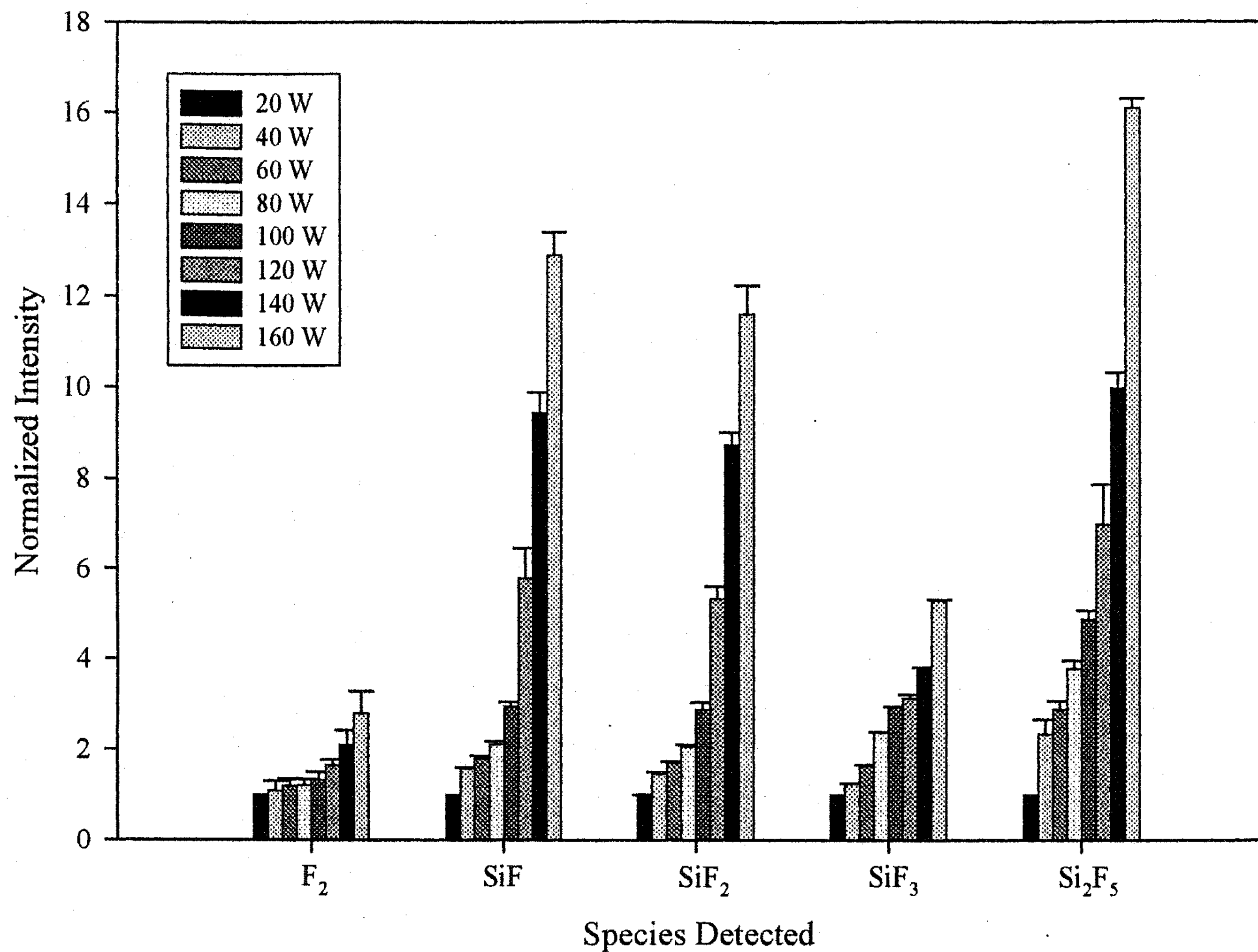

Figure 5.8. (A) Bar graphs representing the effect of applied rf power (20 to 160 W) on relative gas-phase densities of plasma species in pure SiF_4 plasmas using MS.

Reproduced with permission of the copyright owner. Further reproduction prohibited without permission.

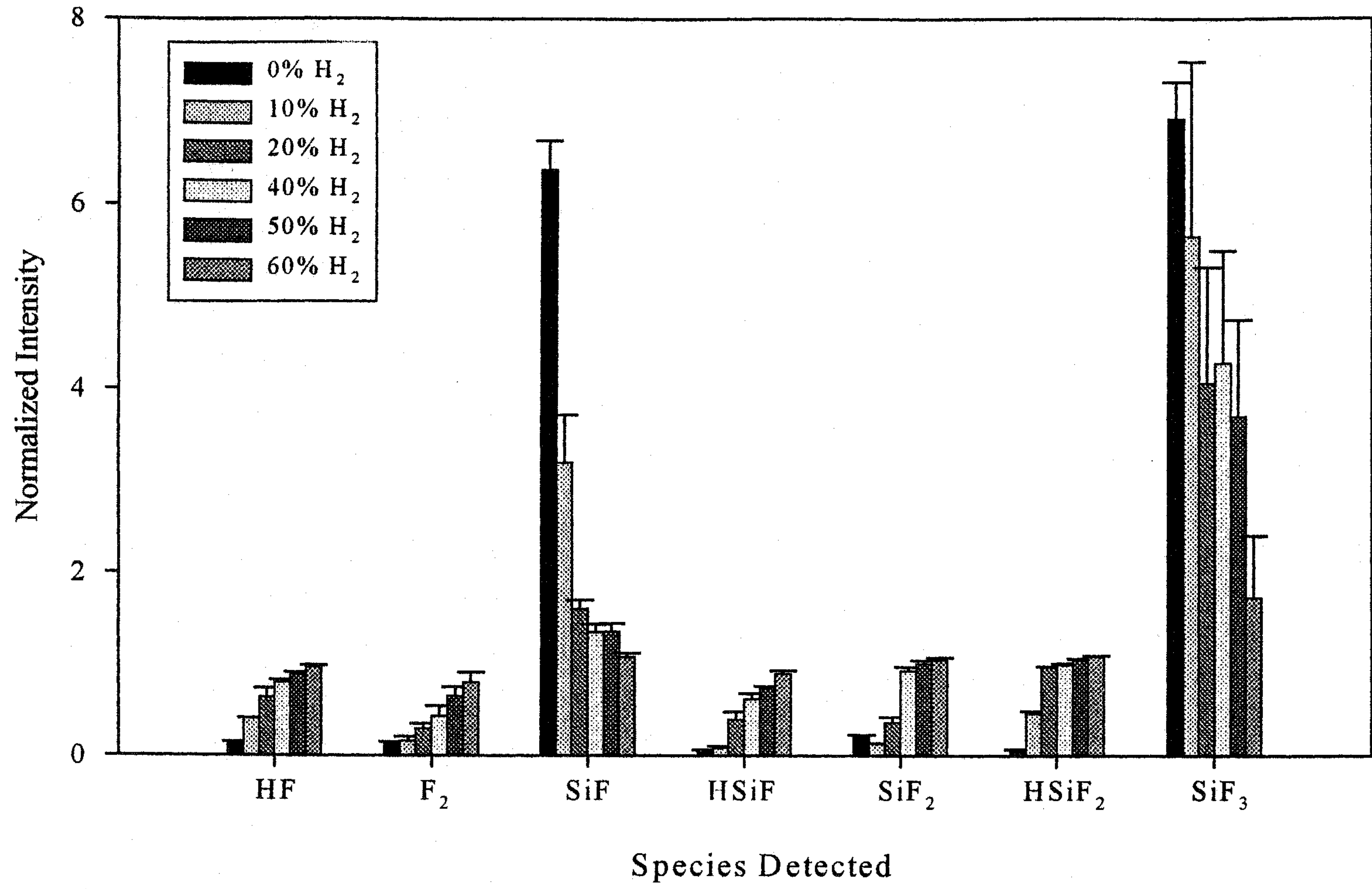

Figure 5.8. (B) Bar graphs representing the effect of H_2 dilution (0 to 70 % H_2) on relative gas-phase densities of plasma species in 170 W SiF_4/H_2 plasmas using MS.

Reproduced with permission of the copyright owner. Further reproduction prohibited without permission.

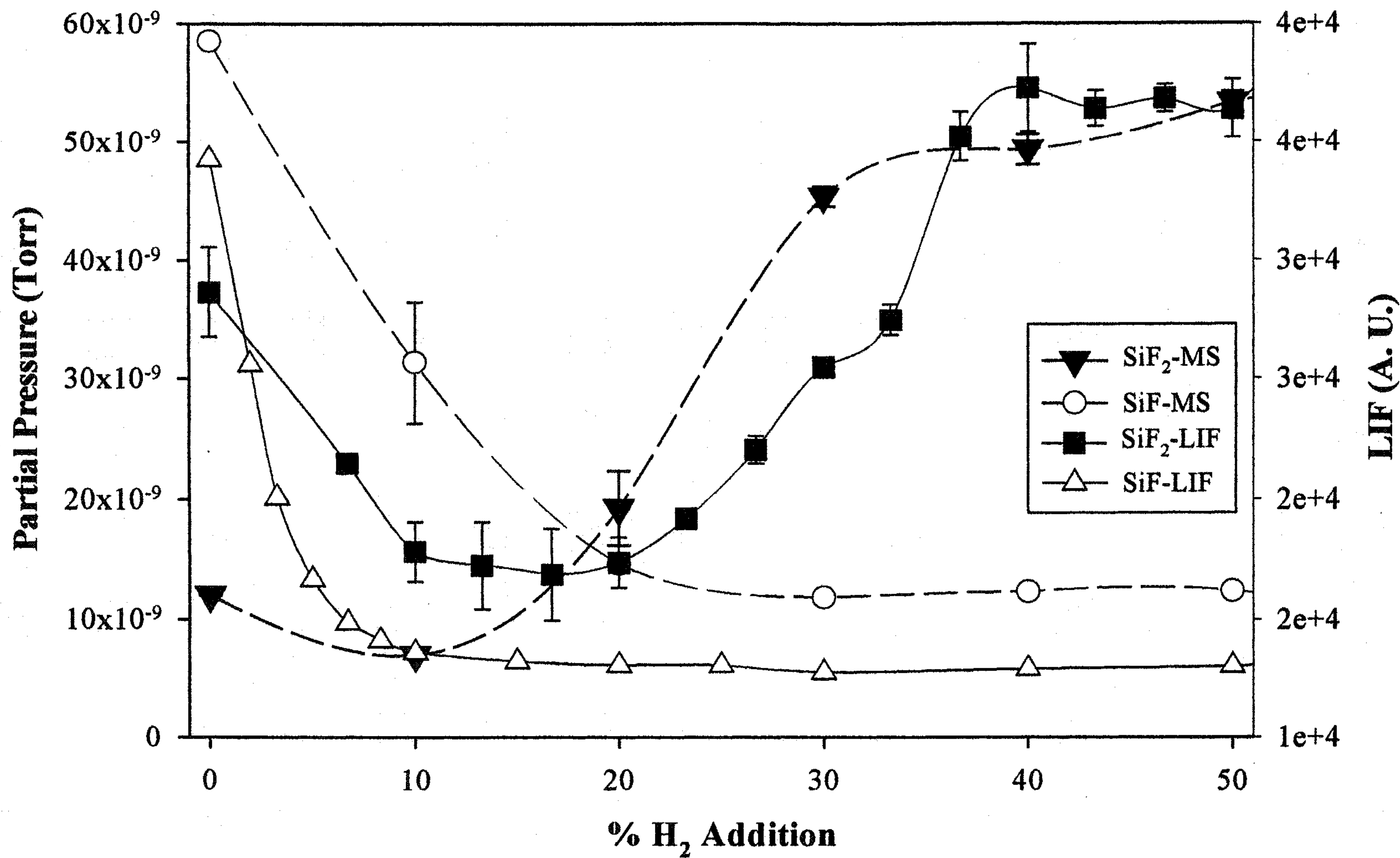

Figure 5.9. Comparison of relative gas phase densities of SiF (open symbols) and SiF_2 (closed symbols) measured using LIF and MS to characterize the effects of % H_2 addition.

decreases rapidly with H_2 addition, being essentially eliminated from the gas phase above ~20% H_2. SiF_2 initially decreases with H_2 addition, up to ~10%, and then rapidly increases before leveling off above ~30-40% H_2 addition. Our gas phase studies using LIF of SiF_2 show an equivalent trend. This may suggest a correlation between the depletion of SiF_2 and the production of $HSiF_2$ at low H_2 addition (≤20%). Several gas phase reactions, discussed below, may be responsible for such significant changes in gas phase concentrations of each of these species.

Just as changing gas phase composition of species strongly affects the type of surface processing that occurs, ion density and energy also play an important role in both etching and deposition. As described in Chapter 2, nascent ions were characterized in SiF_4/H_2 plasmas under a variety of plasma conditions. Both *P* and ion perturbation studies have been performed to more fully characterize nascent ions in SiF_4/H_2 system. Figure 5.10 shows a typical nascent ions spectrum. Only four ions, SiF_x ($x = 0$ –3) were present for all plasmas studied. The effect of *P* on the total nascent ion concentration is shown in Figure 5.11. Additionally, the effect of placing a grounded mesh in the path of the molecular beam is also shown. Increases in *P* result in concomitant increases in nascent ion density. This agrees with previously reported results of *P* effects on nascent ions.[57,58] However, previous studies in the Fisher group characterizing nascent ion perturbation by the grounded mesh have resulted in complete removal of nascent ions.[57,58] For SiF_4/H_2 plasma systems, only partial removal of nascent ions was observed. Although, a small percentage of ions remain, ion bombardment is greatly reduced in systems where a grounded mesh is present. This is evident in both FTIR and deposition rate data of films deposited with reduced ion bombardment, Figures 5.3 and 5.4.

Reproduced with permission of the copyright owner. Further reproduction prohibited without permission.

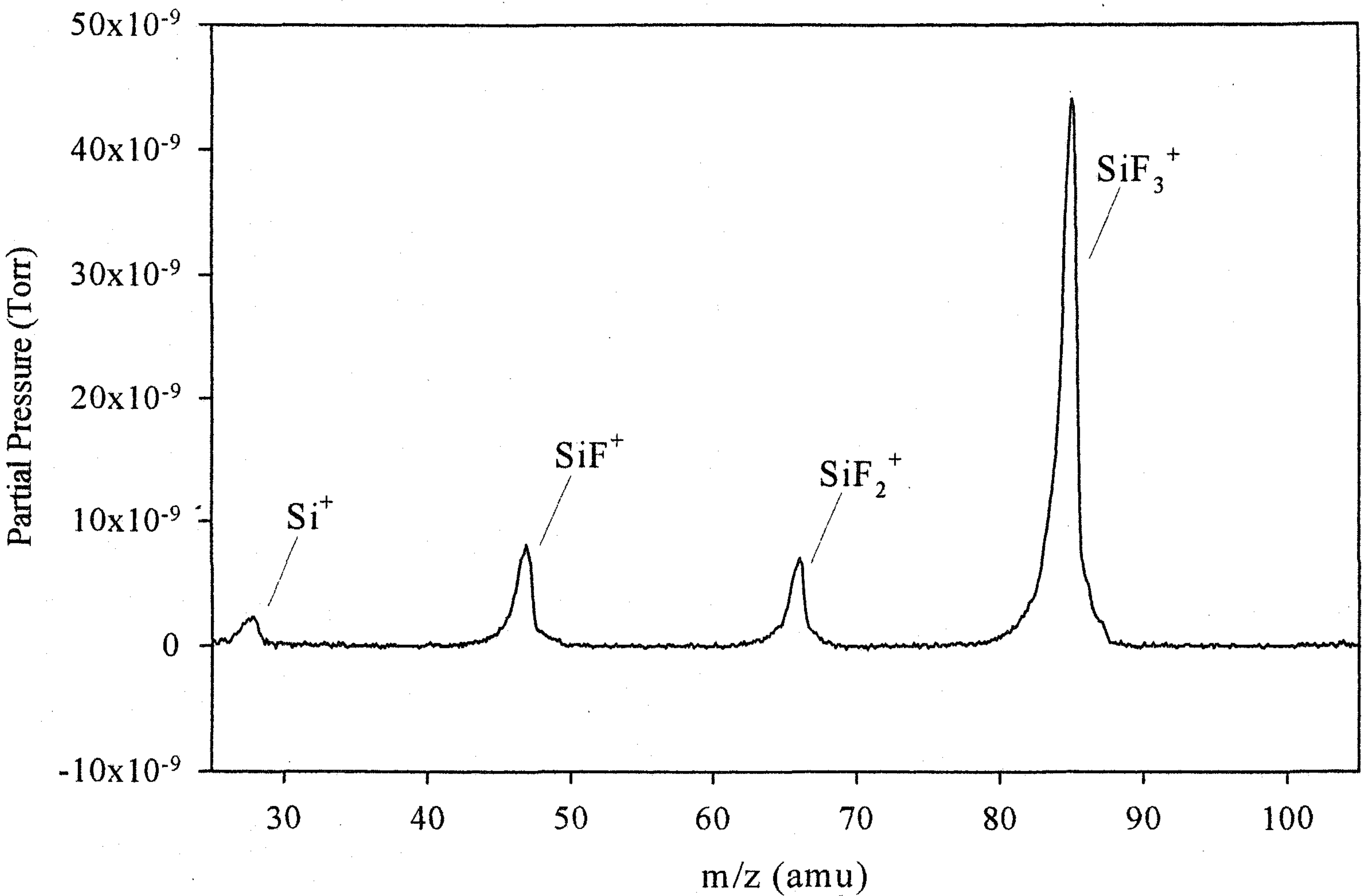

Figure 5.10. Typical nascent ion mass spectrum from a 90:10 SiF_4/H_2 plasma at 170 W.

Reproduced with permission of the copyright owner. Further reproduction prohibited without permission.

Reproduced with permission of the copyright owner. Further reproduction prohibited without permission.

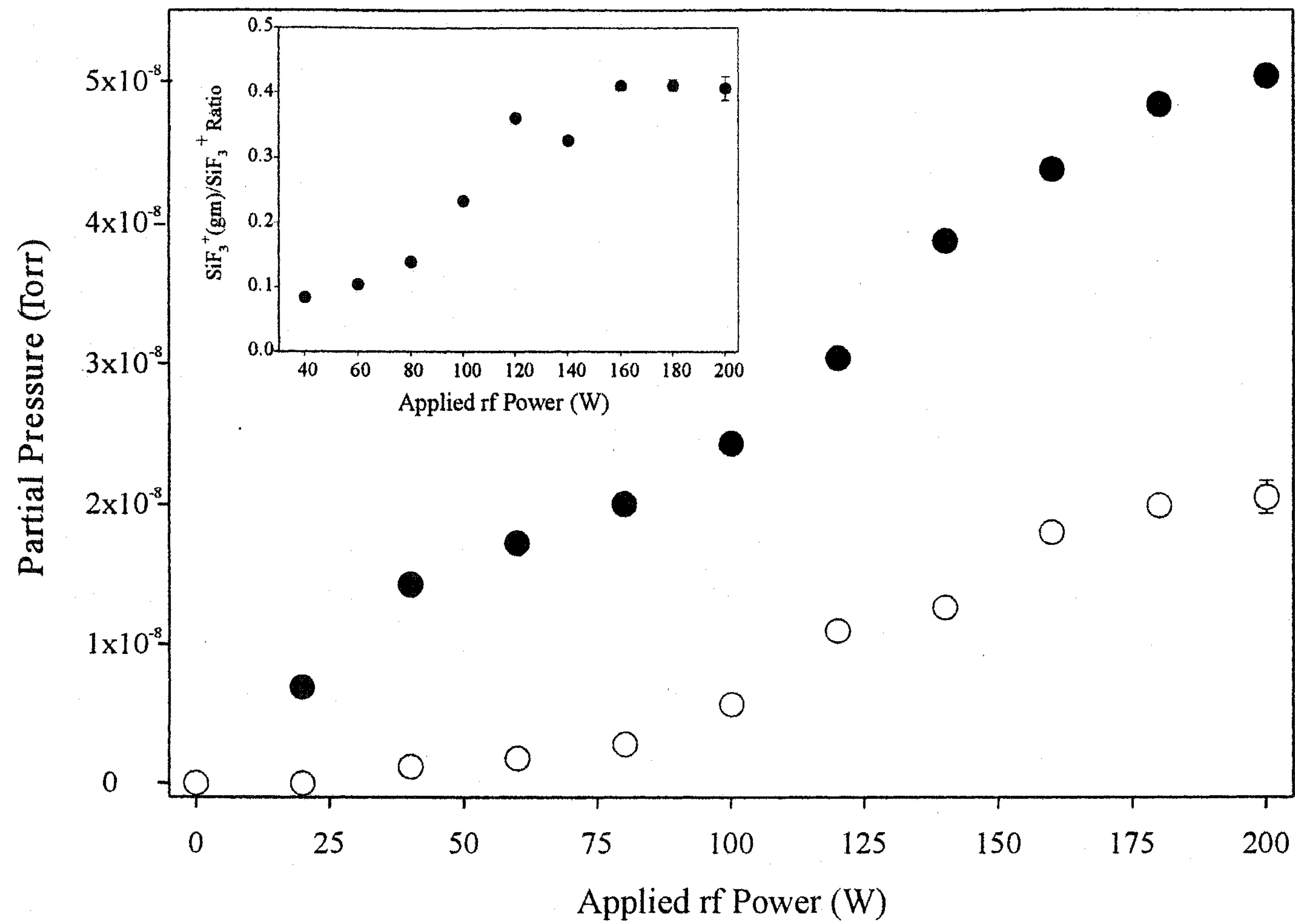

Figure 5.11. The effect of plasma power on total nascent ion concentration (•) and ions present with a grounded mesh placed into the path of the molecular beam (○). The ratio of ions with perturbation to ions without perturbation is show in the inset.

5.2.3. Gas-Surface Interactions of SiF_x Radicals in SiF_4 Plasmas. To gain a more complete understanding of the chemistry that contributes to the resulting materials produced in fluorosilane plasmas, it is also important to examine the plasma-surface interface where the growing material is being formed. LIF offers a non-intrusive and highly selective study of one type of radical in a molecular beam populated by a variety of different species. Accurate analysis of specific species begins with spectroscopically verifying the presence of the molecule of interest. We have previously reported excitation spectra for the A^1B_1 - X^1A_1 electronic transition for SiF_2 and the $A^2\Sigma^+ \sim X^2\Pi$ transition for SiF in Chapter 4.[25] A comparison to literature spectra verified that the fluorescing species are indeed SiF_2 and SiF.[14,15,35,59,60] It should be noted that no additional signal from other fluorescing species occurred in the spectral ranges for either molecule.

Surface reactivities for the SiF and SiF_2 species have been measured by tuning the laser output to a single rotational line for each molecule of interest and collecting a series of ICCD images, Fig. 5.12. These images show fluorescence from SiF radicals in a 100% SiF_4 plasma molecular beam at P = 170 W, a Type 1 system. Figure 5.12a corresponds to SiF LIF signal in the incident molecular beam only. Signals from both incident and scattered SiF molecules are imaged in Fig. 5.12b, taken with a Si substrate in the path of the molecular beam. Figure 5.12c is the difference between Fig. 5.12b and Fig. 5.12a, representing only signal from SiF leaving the surface. Relatively little SiF scatter is observed. One dimensional (1-D) cross sections corresponding to the images in Figs. 5.12a (incident SiF) and 5.12c (scattered SiF), are shown in Fig. 5.13 along with

Reproduced with permission of the copyright owner. Further reproduction prohibited without permission.

Reproduced with permission of the copyright owner. Further reproduction prohibited without permission.

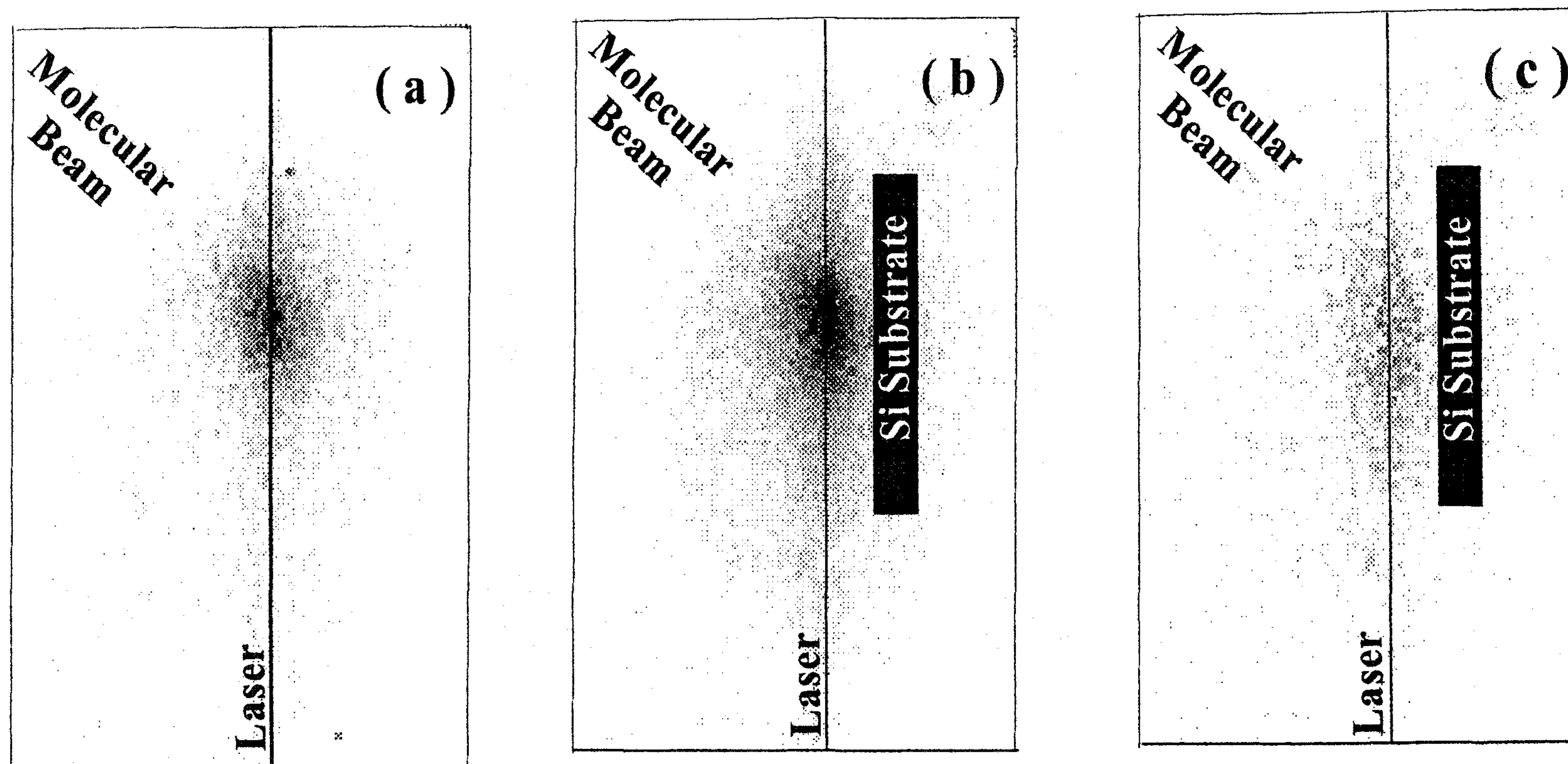

Figure 5.12. Spatially resolved two-dimensional ICCD images of the LIF signal for the SiF 5.5 rotational line (a) in the 100% SiF_4 plasma molecular beam (no substrate) and (b) with a 300 K Si (100) substrate rotated into the path of the molecular beam at a laser surface distance of 3 mm. (c) The difference between the images shown in (a) and (b), corresponding to SiF radicals scattering from the surface. LIF signals with the highest intensity appear as the darkest regions in the images. The solid lines indicate the location of the laser beam.

Reproduced with permission of the copyright owner. Further reproduction prohibited without permission.

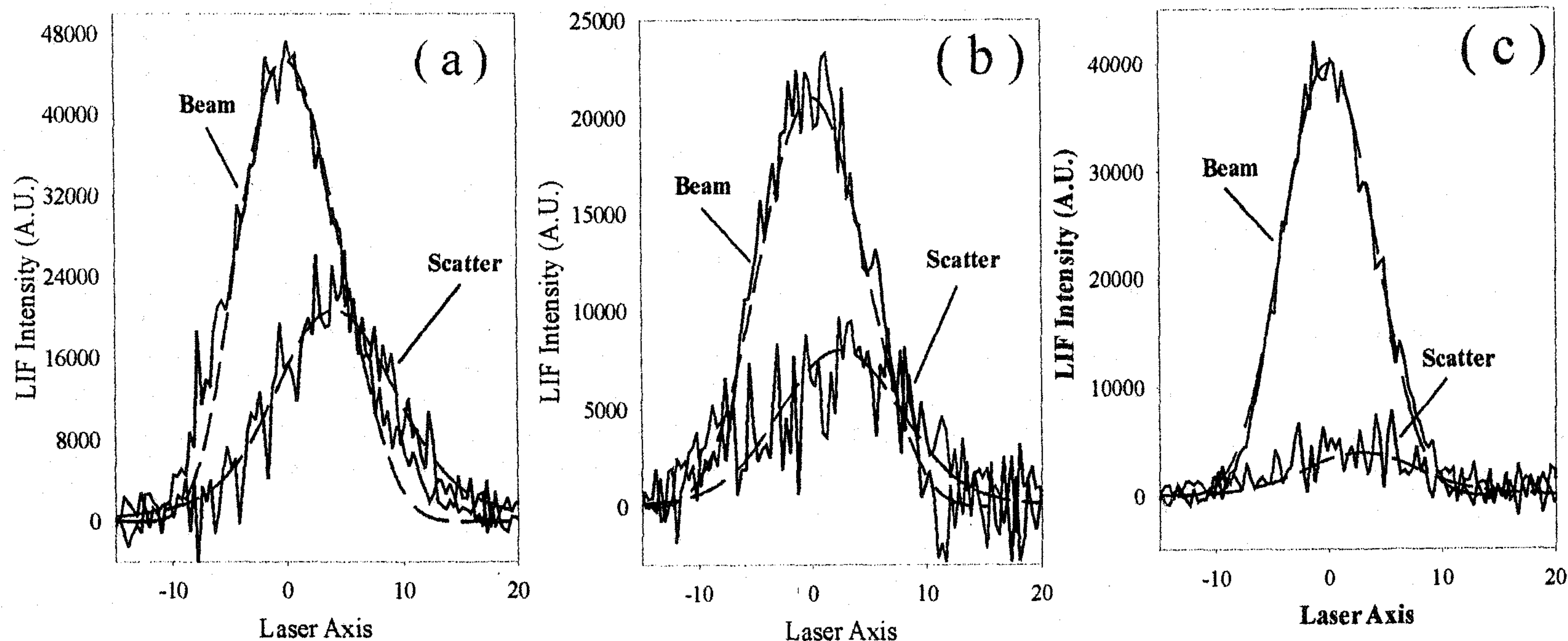

Figure 5.13. Cross-sectional data for the LIF of SiF in the incident molecular beam and scattered from the Si (100) substrate using a 100% SiF_4 plasma molecular beam at a) 170 W, b) 80 W, and c) 20 W. The laser-surface distance is 3 mm. Dashed lines represent the simulated curves from the geometric model, assuming adsorption-desorption scattering and $S = 0.73 \pm 0.08$, 0.48 ± 0.08, and 0.15 ± 0.10 respectively.

similar data from plasmas with lower P. The broad spatial distribution and the shift of the scattered signal peak maximum away from the molecular beam peak maximum indicate SiF radicals scatter with a cosine angular distribution. Dashed lines represent the simulated curves from the geometric model, assuming adsorption-desorption scattering and $S = 0.73 \pm 0.08$, 0.48 ± 0.08, and 0.15 ± 0.10 for Figures 5.13a-c, respectively.

Similar surface scatter measurements were made for both SiF and SiF_2 using a variety of plasma parameters, Tables 5.2 and 5.3. SiF_2 scatter varies greatly from $S \sim 0.26$ to 4.0 depending upon plasma conditions, Figure 5.14. This suggests SiF_2 surface interactions are sensitive to the three different plasma types. The surface interactions of SiF, however, are less sensitive, changing only from $S \sim 0.21$ to $S \sim 1.28$ with changing plasma parameters. We measure the most significant dependence of SiF scatter on P, with S increasing by ~50% when P is increased from 20 to 170 W. In contrast, SiF S values show no significant difference with the addition of either 10% or 50% H_2. These values contrast with those for the SiF_2 molecule, which show surface production ($S > 1$) at $P > 40$ W. SiF_2 scatter also exhibits a significant decrease with the addition of H_2.

5.2.4. Effect of plasma ions on SiF_x reactivity. Considering the significant changes that occur for a-Si:H,F films when bombarding ions are removed, it is important to characterize surface reactivity of SiF and SiF_2 as a function of ion bombardment. Previous studies of CF_2,[61] NH_2,[38] and NH[62] species in a variety of plasma systems have shown that ions play an important role in surface reactivity and in the overall film composition. We have examined the effects of ions on surface interactions of both SiF

Reproduced with permission of the copyright owner. Further reproduction prohibited without permission.

Reproduced with permission of the copyright owner. Further reproduction prohibited without permission.

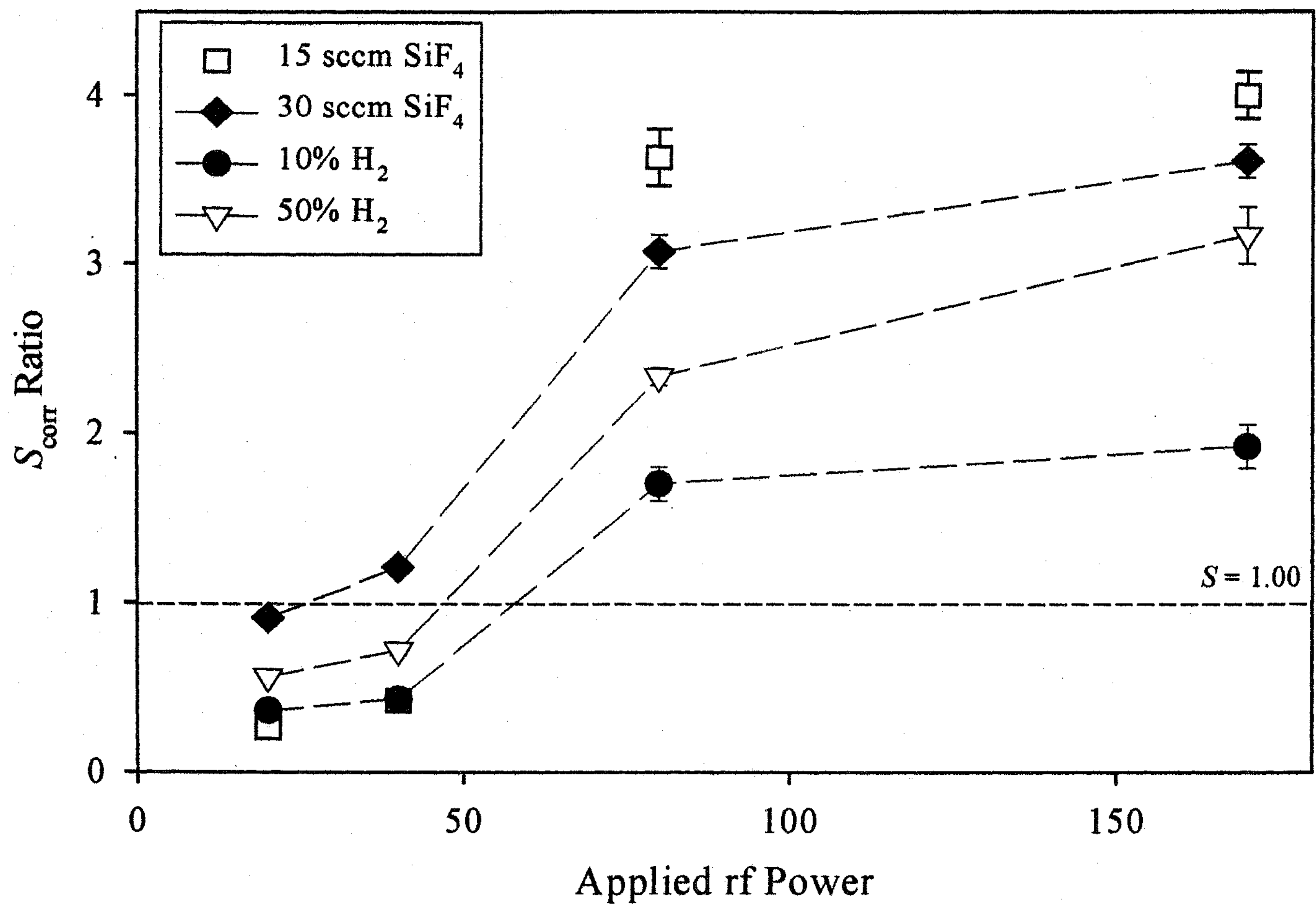

Figure 5.14. The effect of applied rf power on scatter ratios (S) for 15 sccm SiF_4 (□), 30 sccm SiF_4 (▼), 90:10 SiF_4/H_2 (●), and 50:50 SiF_4/H_2 (Δ) plasma systems.

and SiF_2 in 170 W SiF_4 and SiF_4/H_2 plasmas by measuring S values with either ± 200 V_{dc} substrate biasing or with a grounded mesh (g.m.) in the path of the molecular beam, Tables 5.2 and 5.3. With +200 V_{dc} biasing, positively charged species are repelled as they approach the substrate, making ion bombardment of the surface negligible. In contrast, -200 V_{dc} biasing effectively increases SiF_2 scatter by accelerating positively charged species toward the substrate. The g.m. removes the majority (> 75%) of charged species prior to interaction with the substrate.[42]

For systems in which we have perturbed the ions, we define δSc as the difference between S measured with no perturbation of the charged species and S measured with either biased Si (S_{bias}) or with the g.m. (S_{gm}). Thus, $\delta Sc = S - S_{bias}$ or $\delta Sc = S - S_{g.m.}$ S values for SiF_2 in the SiF_4/H_2 systems are listed in Table 5.3. Under all feed gas conditions, +200V_{dc} substrate biasing yields a decrease in S values for SiF_2, resulting in positive δSc, with values ranging from δSc = +0.19 ± 0.11 for a 10% H_2 plasma to δSc = +0.53 ± 0.13 for a 50% H_2 plasma. Similar positive δSc values were obtained with the g.m. studies. δSc = +0.84 ± 0.16 for the 50% H_2 system, but was only δSc = 0.18 ± 0.11 for the 10% H_2 system. In contrast, with the -200 V_{dc} biased Si, δSc values were all negative, ranging from δSc = -0.19 ± 0.13 for a 50% H_2 plasma to δSc = -0.84 ± 0.11 for a 10% H_2 plasma. This same trend was also observed for the previously reported[42] S values for SiF_2 in 100% SiF_4 systems, Table 5.3. Thus, changes in SiF_2 scatter with ion perturbation behave as expected if ion bombardment enhanced desorption of SiF_2. Similar ion effects have also been observed for CF_2 in fluorocarbon-based systems and NH_2 in NH_3 plasmas.[38,61]

Reproduced with permission of the copyright owner. Further reproduction prohibited without permission.

Table 5.2: Reactivity data for SiF using SiF_4 Plasmas.

Flow Conditions	Type	*P* (W)	Ion Perturbation	*S* Value	*Corrected S* Value[a]
15 sccm SiF_4	2	20	None	0.18 ± 0.05	0.26 ± 0.07
	1	40	None	0.30 ± 0.05	0.43 ± 0.07
	1	80	None	0.42 ± 0.05	0.69 ± 0.08
	1	170	None	0.50 ± 0.07	0.82 ± 0.11
30 sccm SiF_4	2	20	None	0.15 ± 0.10	0.21 ± 0.14
	1	40	None	0.30 ± 0.10	0.43 ± 0.14
	1	80	None	0.48 ± 0.08	0.79 ± 0.13
	1	170	None	0.73 ± 0.08	1.20 ± 0.13
90:10 SiF_4:H_2	3	20	None	0.23 ± 0.08	0.33 ± 0.11
	3	40	None	0.15 ± 0.10	0.21 ± 0.14
	3	80	None	0.45 ± 0.10	0.74 ± 0.16
	3	170	None	0.78 ± 0.15	1.28 ± 0.25
50:50 SiF_4:H_2	3	20	None	0.30 ± 0.05	0.43 ± 0.07
	3	40	None	0.40 ± 0.05	0.57 ± 0.07
	2	80	None	0.55 ± 0.05	0.90 ± 0.08
	2	170	None	0.62 ± 0.06	1.02 ± 0.10
15 sccm SiF_4	1	170	g.m.[b]	0.45 ± 0.05	0.74 ± 0.08
	1	170	+200 V_{dc}	0.58 ± 0.05	0.95 ± 0.08
	1	170	-200 V_{dc}	0.68 ± 0.05	1.12 ± 0.08
30 sccm SiF_4	1	170	g.m.[b]	0.78 ± 0.05	1.28 ± 0.08
	1	170	+200 V_{dc}	0.65 ± 0.07	1.07 ± 0.11
	1	170	-200 V_{dc}	0.60 ± 0.05	0.98 ± 0.08
90:10 SiF_4:H_2	3	170	g.m.[b]	0.70 ± 0.09	1.15 ± 0.15
	3	170	+200 V_{dc}	0.70 ± 0.09	1.15 ± 0.15
	3	170	-200 V_{dc}	0.58 ± 0.07	0.95 ± 0.11
50:50 SiF_4:H_2	2	170	g.m.[b]	0.60 ± 0.05	0.98 ± 0.08
	2	170	+200 V_{dc}	0.52 ± 0.06	0.85 ± 0.10
	2	170	-200 V_{dc}	0.62 ± 0.06	1.02 ± 0.10

[a]All corrected scatter values calculated using previously measured SiF velocities.[63] The correction factor for P = 20 W and 40 W scatter values is 1.42, and for P = 80 W and 170 W it is 1.64. [b]g.m. designates measurements performed with a grounded mesh screen in the path of the molecular beam.

Reproduced with permission of the copyright owner. Further reproduction prohibited without permission.

Table 5.3: Scatter Coefficient data for SiF_2 using SiF_4 Plasmas.

Flow Conditions	Type	*P* (W)	Ion Perturbation	*S* Value	*Corrected S* Value[a]
15 sccm SiF_4[42]	2	20	None	0.20 ± 0.02	0.26 ± 0.03
	1	40	None	0.32 ± 0.01	0.42 ± 0.01
	1	80	None	2.79 ± 0.13	3.63 ± 0.17
	1	170	None	3.08 ± 0.11	4.00 ± 0.14
30 sccm SiF_4[42]	2	20	None	0.70 ± 0.03	0.91 ± 0.04
	1	40	None	0.93 ± 0.01	1.21 ± 0.01
	1	80	None	2.36 ± 0.08	3.07 ± 0.10
	1	170	None	2.78 ± 0.08	3.61 ± 0.10
90:10 SiF_4:H_2	3	20	None	0.28 ± 0.01	0.36 ± 0.01
	3	40	None	0.33 ± 0.01	0.43 ± 0.01
	3	80	None	1.31 ± 0.08	1.70 ± 0.10
	3	170	None	1.48 ± 0.10	1.92 ± 0.13
50:50 SiF_4:H_2	3	20	None	0.43 ± 0.01	0.56 ± 0.01
	3	40	None	0.55 ± 0.02	0.72 ± 0.03
	2	80	None	1.79 ± 0.04	2.33 ± 0.05
	2	170	None	2.44 ± 0.13	3.17 ± 0.17
15 sccm SiF_4[42]	1	170	g.m.[b]	2.25 ± 0.09	2.93 ± 0.11
	1	170	+200 V_{dc}	2.63 ± 0.02	3.42 ± 0.03
	1	170	-200 V_{dc}	3.78 ± 0.04	4.91 ± 0.05
30 sccm SiF_4[42]	1	170	g.m.[b]	2.00 ± 0.14	2.60 ± 0.18
	1	170	+200 V_{dc}	2.43 ± 0.04	3.15 ± 0.18
	1	170	-200 V_{dc}	3.03 ± 0.04	3.94 ± 0.05
90:10 SiF_4:H_2	3	170	g.m.[b]	1.30 ± 0.20	1.69 ± 0.03
	3	170	+200 V_{dc}	1.31 ± 0.05	1.70 ± 0.07
	3	170	-200 V_{dc}	2.32 ± 0.04	3.02 ± 0.05
50:50 SiF_4:H_2	2	170	g.m.[b]	1.60 ± 0.09	2.08 ± 0.12
	2	170	+200 V_{dc}	1.91 ± 0.03	2.48 ± 0.04
	2	170	-200 V_{dc}	2.63 ± 0.03	3.42 ± 0.04

[a]All corrected scatter values calculated using previously measured SiF_2 velocities.[63] The correction factor for $P = 20$ W, 40 W, 80 W, and 170 W scatter values is 1.30. [b]g.m. designates measurements performed with a grounded mesh screen in the path of the molecular beam.

Reproduced with permission of the copyright owner. Further reproduction prohibited without permission.

Scatter coefficients for SiF, Table 5.2, are not significantly altered by perturbing the charged species in the plasma. Given that the g.m. removes >75% of the charged species, these results indicate that SiF surface scatter is not enhanced by ion bombardment in contrast to the SiF_2 results. This is also in contrast with results of our previous IRIS studies, wherein ions have clearly participated in the desorption of plasma species (CF_2, NH_2, and NH).[45,58,64] As an additional note, it is well established that ion bombardment also significantly affects the composition of the SiF_x adlayer in silicon etching systems.[34] Our results would suggest, therefore, that SiF scatter is independent of surface adlayer composition.

5.3. Discussion

In fluorosilane plasmas, the balance between film growth and substrate etching depends on the interactions of plasma species with the substrate being processed. As in many fluorine-containing systems, the plasma regime can be shifted between deposition and etching by varying feed gas composition, pressure, and P. F atom etching of Si and film deposition has been studied extensively in F-based systems.[11,12,18,20-23,28-33] Likewise, gas-phase plasma species thought to be important in these processes have often been identified and measured as a function of different plasma parameters; yet surface interactions of these molecules are not fully understood. We discuss here how correlating plasma type with SiF_x surface interactions along with gas phase densities offers insight into plausible surface and gas-phase mechanisms.

A wide variety of experiments have been employed to fully study the three plasma types discussed in Section 5.1: etching, surface modification, and deposition.

Reproduced with permission of the copyright owner. Further reproduction prohibited without permission.

Insight into the reactions of gas-phase radicals with a surface *during* plasma processing can be obtained with the IRIS technique, which has been used to measure S for several different radicals including SiH,[43] NH,[58] NH_2,[46] CF,[51] CF_2,[61] OH,[44] SiF, and SiF_2 in a variety of plasma systems. IRIS measurements for most of these species have assigned S values with very small ranges as a function of plasma parameters. Furthermore, previously investigated species rarely have $S > 1.5$ regardless of the overall plasma regime. One notable exception is CF_2 in a 50 W C_2F_6 plasma at a photoresist surface, where $S > 1.5$ was reported.[61] SiF_2 reactivity data are the first IRIS results where varying plasma parameters yields extremely high scatter coefficients and a wide S value range ($0.26 < S < 4.0$), demonstrating that SiF_2 scatter is extremely sensitive to changes in plasma chemistry.

5.3.1. Type 1 Plasmas. Surface production of SiF_2 is observed for all Type 1 systems, Table 5.2. There are several physical and chemical surface reactions that can account for the observed $S > 1$, including reactions 5.1-5.3.

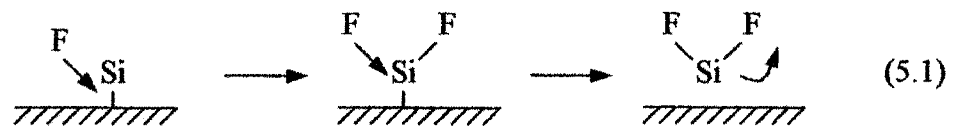

(5.1)

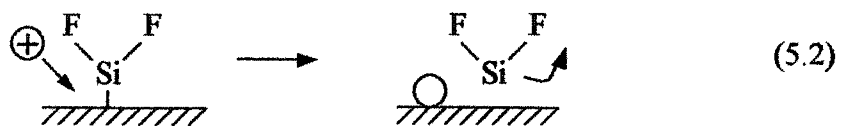

(5.2)

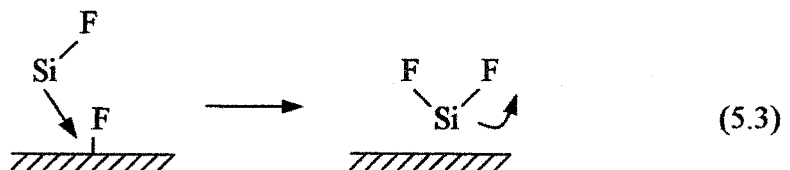

(5.3)

Reproduced with permission of the copyright owner. Further reproduction prohibited without permission.

Reaction 1 represents SiF_2 as a product of F atom etching. However, it is well established in the literature that both SiF_2 and SiF_4 are volatile products of Si etching by F atoms.[34,37] Regardless of which etch product is dominant, Reaction 1 is undoubtedly a large contributor to the surface generation of SiF_2 in Type 1 systems. One explanation for the observed increase in SiF_2 scatter with P is the concomitant increase in F atom density as a result of increased fragmentation of the source gas. This ultimately increases etching and, thus, surface production of SiF_2.

A secondary enhancement of SiF_2 scatter by ion sputtering is portrayed in Reaction 5.2. Ion effects on SiF_2 desorption and specific ion-induced mechanisms have been discussed previously,[42,65] and are supported by additional observations that ion bombardment enhances the silicon etching process at high P. Radical-ion beam experiments also indicate a number of radicals chemically sputtered by ions in the presence of F atoms can be much greater than unity.[66,67]

A third potentially important contribution is the evolution of SiF_2 through surface reactions of other plasma species. Although many species may contribute in such a manner, Reaction 5.3 depicts only one possibility, SiF abstraction of adsorbed F to form SiF_2, which can then desorb from the surface. IRIS measurements of SiF yield $S < 1$ (i.e. surface loss) for the same plasma conditions reported for SiF_2 scatter. Thus, it is possible that SiF_2 surface scatter is enhanced by the reaction of SiF radicals at the surface to produce SiF_2. This is discussed further in Section 5.3.3.

5.3.2. Type 2 Systems. At $P < 40$ W in 100% SiF_4 plasmas, Type 2 conditions become dominant as a function of the feed gas composition, resulting in only F atom

Reproduced with permission of the copyright owner. Further reproduction prohibited without permission.

implantation. Interestingly, IRIS measurements under these conditions indicate SiF_2 is lost at the surface. There are several plasma surface interactions that may account for this phenomenon. Using a XeF_2 molecular beam, Coburn and Winters[34] have identified SiF_4 as the primary etch product of F atom etching on Si at $T_S < 600$ K, whereas SiF_2 dominates at $T_S > 600$ K. Localized heating of the Si substrate during plasma processing could result in desorption similar to those observed by Coburn and Winters.[68] At low *P*, there may not be enough energy to desorb significant amounts of SiF_2. The effect of Ar^+ bombardment on the SiF_x adlayer has also been measured.[34] SiF_3 was the major adlayer species in the absence of ions, whereas SiF_2 becomes the dominant adlayer moiety under 450 eV Ar^+ bombardment. Our ion perturbation studies show SiF_2 desorption is significantly enhanced by energetic ions, consistent with a higher SiF_2 adlayer density. Moreover, relative ion densities measured in the IRIS instrument show an ~5 fold decrease from $P = 170$ W to $P = 25$ W, indicating that ion sputtering of SiF_2 should be greatly diminished at low *P*. One additional note is that an increase in SiF_4 flow rate also results in increased SiF_2 scatter for Type 2 systems, Table 5.3. This increase in SiF_2 scatter, indicative of a shift toward etching, may also be correlated to the F atom density in the plasma.

Addition of H_2 to the feed gas shifts the plasma regime away from Type 1. At low powers ($P = 20$, 40 W), Type 3 conditions exist, whereas at higher *P* (80 and 170 W), Type 2 conditions are prevalent, Tables 5.2 and 5.3. One possible explanation for this difference is the increased ion bombardment in higher power plasmas. As discussed in Section 5.3.1, ions also contribute to the observed increases in surface scatter in Type 2 systems.[42] Furthermore, increased ion bombardment can prevent film formation through

Reproduced with permission of the copyright owner. Further reproduction prohibited without permission.

sputtering of deposited materials. If the balance between film growth and film sputtering has reached equilibrium, then only F atom implantation is observed.

5.3.3. Type 3 Systems. Both 10% and 50% H_2 addition to the feed gas result in low SiF_2 scatter values, Table 5.3, as well as formation of a-Si:H,F film. In addition to H atom scavenging of F atoms, new deposition precursors are formed, significantly altering both the gas-phase and surface chemistry, resulting in Type 3 systems. Several surface reactions may be responsible for film deposition and the resulting low SiF_2 scatter values observed. Mechanisms for SiF_2 surface loss, as well as the role of SiF in film deposition and the production of $HSiF_x$ deposition are discussed in the following sections.

5.3.3.1. Role of SiF_2 in Film Deposition. The equilibrium between etching and deposition processes can be monitored by film deposition rate, which is inversely mirrored by SiF_2 gas-phase density. Minimal $SiF_2(g)$ is produced under the highest deposition rate conditions (10% H_2), Table 5.1, whereas considerable increases in $SiF_2(g)$ arise under etching conditions (H_2 < 10% or H_2 > 20%). Several possible mechanisms may explain $SiF_2(g)$ depletion with the introduction of H_2 including Processes 4 and 5.

Mass spectrometry studies have identified HSiF, $HSiF_2$, and HF in SiF_4/H_2 plasmas, suggesting both of these reactions are plausible.[42] Reaction 5.4a has also been proposed by Shimizu et al.[69] and by Bruno et al.[18] as an important pathway to formation of $HSiF_2$ (g). Reaction 5.4b also contributes to the loss of $SiF_2(g)$, and produces HF(g). The majority of HF is, however, formed by gas phase reactions such as process 5.6. Considering slow reaction kinetics[69] and the stability of both SiF_2 and H_2, depletion of gas-phase SiF_2 is not likely a result of reaction 5.5. Rather, SiF_2 consumption may be more directly related to the loss of gas phase F atoms by reaction 5.6. As F atom etching

Reproduced with permission of the copyright owner. Further reproduction prohibited without permission.

of Si produces SiF_2, the depletion of F(g) would result in a concomitant decrease in etch products desorbed from reactor walls. Inhibition of F atom etching would also affect the observed deposition rate, linking SiF_2(g) density and deposition rate.

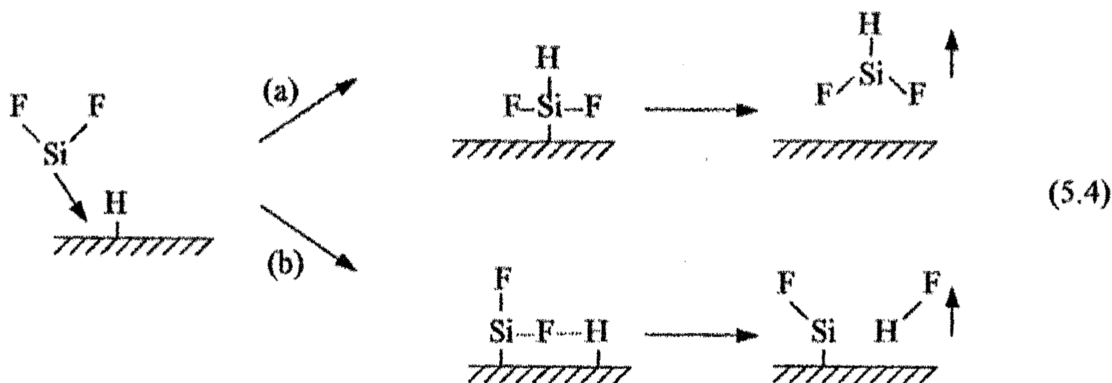

(5.4)

$$SiF_2(g) + H_2(g) \rightarrow HSiF(g) + HF(g) \quad (5.5)$$

$$F(g) + H_2(g) \rightarrow HF(g) + H(g) \quad (5.6)$$

With < 10% H_2, reaction 5.6 is limited by the H_2 concentration. An excess of H_2 (> 20%) results in depletion of F(g) by Reaction 5.6, yet SiF_2 density is elevated and deposition rate decreases. Thus, it is likely that additional gas-phase processes producing SiF_2 may be activated under these conditions, including process 5.7.

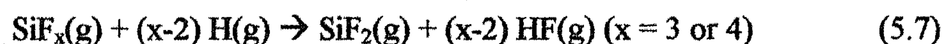

$$SiF_x(g) + (x-2)\,H(g) \rightarrow SiF_2(g) + (x-2)\,HF(g) \; (x = 3 \text{ or } 4) \quad (5.7)$$

Furthermore, it has been suggested[17] that H atoms can act as an etchant by abstracting surface F atoms as in reaction 5.8.

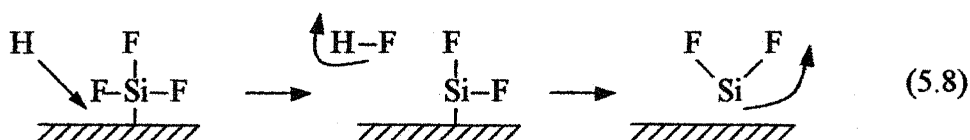

(5.8)

Reproduced with permission of the copyright owner. Further reproduction prohibited without permission.

This could result in an additional enhancement of SiF_2 desorption from the reactor walls, increasing the overall density of SiF_2 in the plasma.

5.3.3.2. SiF as a Deposition Precursor. Relatively little emphasis has been given to the role of SiF in fluorine-containing plasmas, despite it being a proposed film deposition precursor. In etching systems, most research has focused on SiF_2, SiF_4, and CF_2 as the major etch products, leaving the role of SiF poorly characterized. During a-Si:H,F film deposition, however, SiF gas density and reactivity measurements offer insight into the surface chemistry responsible for film growth.

LIF and MS measurements both indicate that SiF density decreases significantly under deposition conditions, Fig. 5.9. An ~6 fold decrease is observed from 100% SiF_4 to 80:20 SiF_4/H_2. Such large decreases in the gas phase densities could result from increases in SiF surface reactivity or gas phase reactions of SiF. Contribution to film growth is related to both gas phase density and to sticking probability. A small gas phase density could suggest that SiF contributions to film deposition may be small. A high sticking probability, however, could partially compensate for a low density. Indeed, studies of deposition precursors in similar plasma systems such as SiH in SiH_4 plasmas have demonstrated analogous behavior, exhibiting high reactivity with low gas-phase densities. [70] Near unity reactivity has been measured for SiH regardless of plasma conditions, yet it is not considered to be the largest contributor to high quality film growth. With the combination of moderately high surface reactivity and relatively low gas phase density, it is possible that SiF is not the largest contributor to F incorporation in a-Si:H,F films. Nevertheless, SiF may still be important to overall film production both

Reproduced with permission of the copyright owner. Further reproduction prohibited without permission.

as a precursor to film growth and in the gas phase formation of other H_xSiF_y deposition precursors, discussed below.

From our IRIS measurements, it is clear that SiF is consumed at the surface even under etching conditions. The simplest mechanism to explain this high reactivity is a direct adsorption-desorption process, Reaction 5.9, where * represents a surface site.

$$SiF(g) + * \rightleftharpoons SiF(ads) \qquad (5.9)$$

When the forward reaction is dominant, S should be <0.5. Additional surface chemistry such as Reactions 5.3, and 5.10 – 5.12 can, however, obscure the true contribution of Reaction 5.9.

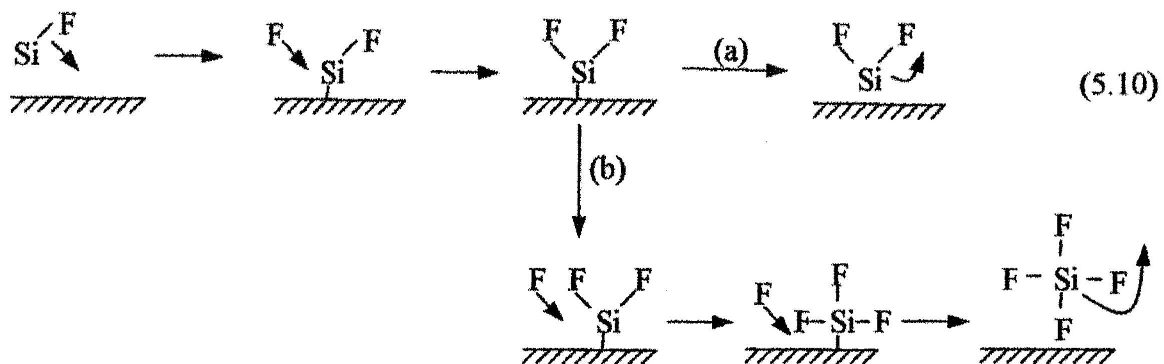

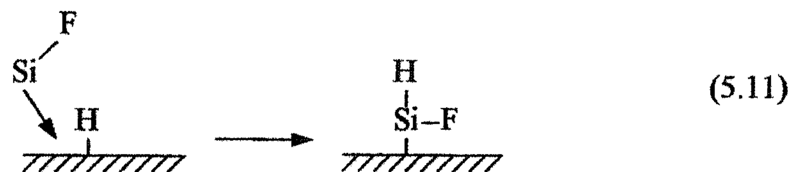

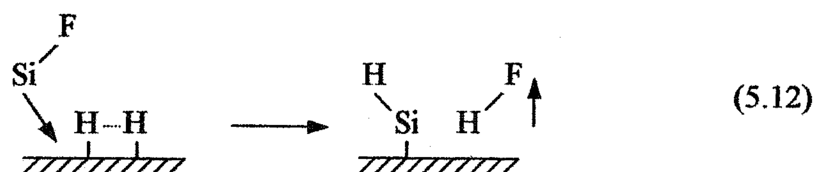

Reproduced with permission of the copyright owner. Further reproduction prohibited without permission.

Although, IRIS measurements cannot monitor individual reactions, contributions by some pathways can be ruled out. SiF_2 reactivity and gas-phase measurements show a strong dependence upon plasma parameters. SiF_2 is lost to the surface at $P < 80$ W, whereas surface production occurs at $P \geq 80$ W. Reactions 5.3 and 5.10a are, therefore, possible contributors to the extremely large SiF_2 scatter values observed at high P. If these reactions play a significant role in SiF_2 surface production, however, then we would expect to see SiF scatter diminish when SiF_2 scatter increases. Perusal of Tables 5.2 and 5.3 indicate that this is not the case. For example, SiF scatter increases by ~0.50 from P = 20 W to P = 170 W (15 sccm SiF_4), and SiF_2 scatter increases by ~3.7 over this same power range. Although Reactions 5.3 and 5.10a could still be minor contributors to SiF_2 surface production, this could be masked by additional reactions that produce SiF at the surface. These processes, such as reactions 5.13 – 5.15, likely occur with higher probability as P increases.

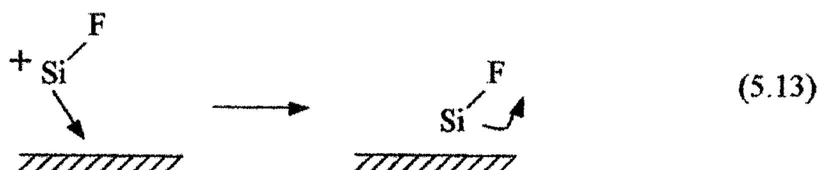

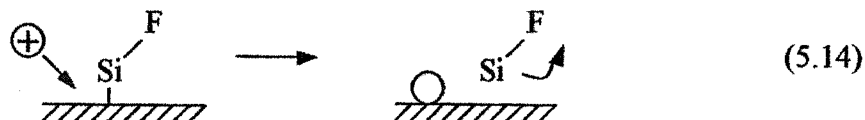

$$SiF_x(x=2\text{-}4)(g) + 2^* \rightarrow SiF_{x-1}\,(ads) + F(ads) \quad (5.15)$$

Additionally, localized heating of the substrate can occur at higher P, which would result in a shift in the Reaction 5.9 equilibrium, towards desorption of SiF.

Reproduced with permission of the copyright owner. Further reproduction prohibited without permission.

We can also examine the likelihood that these reactions contribute to the increase in SiF surface scatter observed under different plasma conditions. For example, Coburn and Winters showed there is a significant amount of SiF and SiF_2 in the SiF_x adlayer under ion bombardment conditions.[71] With more SiF present in the adlayer, more SiF(g) could desorb from the surface. Our results, however, show that whereas ions are important in the surface generation of other plasma species, SiF exhibits no change in scatter with increased ion bombardment or with ion-depleted conditions. Thus, reactions 5.13 and 5.14 are not likely contributors to the observed changes in SiF surface interactions. Localized substrate heating, however, could still be a contributing process as neutral species become more energetic at high *P*.[63] Computer simulations of CF_3^+ show surface dissociation of higher order CF_x species, analogous to process 5.15, becomes more likely when the incident neutrals are more energetic.[39,72] Previous studies in our laboratories demonstrated that the kinetic energy of both SiF and SiF_2 increases substantially with *P*.[63] Thus, the increase in SiF scatter at high *P* is most likely the result of localized substrate heating and surface dissociation of higher energy SiF_x molecules.

5.3.3.3. Formation of $HSiF_x$ During Film Deposition. SiF may also play a key role in the formation of HSiF, which is considered a deposition precursor along with $HSiF_2$.[69] As discussed above, both SiF(g) and SiF_3(g) decrease significantly with increasing H_2 addition. In contrast, HF(g), HSiF(g), and $HSiF_2$(g) densities increase rapidly in the presence of H_2, Fig. 5.8. Several reactions may be responsible for these trends, including processes 5.16 – 5.19.

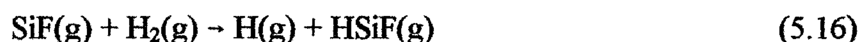

$$SiF(g) + H_2(g) \rightarrow H(g) + HSiF(g) \quad (5.16)$$

$$SiF_2(g) + H_2(g) \rightarrow HSiF(g) + HF(g) \quad (5.17)$$

Reproduced with permission of the copyright owner. Further reproduction prohibited without permission.

$$SiF_3(g) + H_2(g) \rightarrow HSiF_2(g) + HF(g) \quad (5.18)$$

Although reactions 5.16 and 5.17 are both reasonable pathways to explain increases in HSiF with H_2 addition, SiF_2 exhibits low gas-phase reactivity with H_2,[60] indicating that reaction 5.17 may not be a major contributor to HSiF production.[69] Depletion of SiF_3 with H_2 addition can be described by reaction 5.18, which produces HF and $HSiF_2$. This reaction accounts for both an increase in gas-phase HF and $HSiF_2$ with H_2 addition, and the observed decrease in SiF_3. An additional route to formation of $HSiF_2(g)$ proposed by Shimizu[69] and Bruno et al.[18] is shown in Reaction 5.19

$$SiF_2(g) + H(g) \rightarrow HSiF_2(g) \quad (5.19).$$

This reaction has previously been cited as the major route to formation of $HSiF_2$,[18,27] and directly links the decrease in SiF_2 with the increase in $HSiF_2$ occurring below ~20% H_2.

Regardless of the gas-phase mechanisms for production of HSiF and $HSiF_2$, these species are considered important deposition precursors. Both molecules show large increases in relative gas-phase density with the addition of H_2 suggesting that they may be important contributors to film formation, but $HSiF_2$ in particular, demonstrates a rapid 10 fold increase with the addition of 20% H_2, which directly correlates to an increased deposition rate, Table 5.1. This suggests that species like $HSiF_2$ are important in the deposition process. Unfortunately, no surface reactivity measurements have been made for either $HSiF_2$ or HSiF. Studies of $HSiF_x$ surface interactions are needed for a more complete understanding of their role in film growth as well as additional insight into SiF and H surface chemistry.

5.3.4. Predicting Plasma Chemistry from SiF_2 and SiF. It is evident from our studies that SiF and SiF_2 have very different roles in fluorosilane plasmas. SiF_2 is highly

Reproduced with permission of the copyright owner. Further reproduction prohibited without permission.

sensitive to changes in feed gas composition that result in the overall shift from etching to deposition. This demonstrates the typical behavior of an etch product. In contrast, SiF seems relatively insensitive to modifications in feed gas mixture, even when the process changes from etching to deposition. SiF_2 and SiF surface reactivities are also affected quite differently by ion bombardment. Once again the SiF_2 surface interactions are extremely sensitive to the presence of ions, whereas SiF surface reactivity remains unaffected by charged species. These data establish SiF_2 as an etch product and suggest that SiF is not central to the etch process. Some similarities do exist, however, between these two molecules. For example, the reactivity of both species is significantly decreased (i.e. increased scatter) with increasing P, although the trends are not likely the result of the same mechanisms.

Some additional observations can be made about the reactivity trends observed for SiF_2 with respect to plasma chemistry. Regardless of plasma parameters, no film formation (Type 1 plasma) was observed when $S(SiF_2) > 1.5$. The range between $S(SiF_2) = 0.2 - 1.5$ represents the regime where either F implantation (Type 2) or film formation (Type 3) dominates the plasma process. Note that scatter values on the low end of this range represent significant surface loss (high reactivity) for SiF_2. These changes are inversely proportional to film deposition rate, with the lowest SiF_2 scatter occurring under conditions that result in the highest deposition rate. Moreover, low SiF_2 scatter values are directly correlated with increased incorporation of SiF_2 moieties in a-Si:H,F materials, Figs. 5.2 and 5.3. These trends suggest SiF_2 scatter coefficients may be used as a measure of the overall process in SiF_4 and SiF_4/H_2 plasmas.

Reproduced with permission of the copyright owner. Further reproduction prohibited without permission.

5.4. Summary

This work explored the roles of SiF and SiF_2 in SiF_4 and SiF_4/H_2 systems through film characterization, gas-phase density measurements, and surface interaction studies. Plasma types have been identified by the overall processing of the Si substrate: etching (Type 1), F-atom implantation (Type 2), and film deposition (Type 3). In Type 3 plasmas, film composition and deposition rates were measured for a-Si:H,F films deposited from SiF_4/H_2 plasmas with various feed ratios. FTIR spectra compare well with those previously reported for similar films. As *P* is increased, SiF_2 and SiH_2 functional group incorporation decreases, whereas SiH and HSiF concentrations increase. Significant decreases in SiF_2 and SiF incorporation in the films are observed with increasing H_2. Furthermore, deposition rate is not linearly dependent upon applied rf power or H_2 addition.

Gas-phase measurements of plasma-produced radicals have also been characterized as a function of plasma power and feed gas composition. These LIF and MS measurements indicate that SiF is a likely deposition precursor and may be important to the formation of HSiF(g), which is also a deposition precursor. Both HSiF and $HSiF_2$ densities show substantial increases as the plasma is shifted from etching to deposition, indicating that surface reactivity of H_xSiF_y species would be valuable. Interestingly, the gas-phase density of SiF_2 is sensitive to the overall plasma chemistry. For example, SiF_2(g) is inversely correlated with film deposition rates in the SiF_4/H_2 plasmas. In Type I plasmas, SiF_2 is also strongly correlated with the plasma power.

Film properties, gas-phase densities, and measured scatter coefficients for SiF_2 and SiF have been correlated, along with the overall plasma type. Specifically, SiF_2

Reproduced with permission of the copyright owner. Further reproduction prohibited without permission.

surface scatter can be used as an indicator of plasma type. In Type 1 systems, SiF_2 displays the highest surface scatter (S >1). This complements previous work in the literature indicating SiF_2 as a major Si etch product. In Type 3 systems, SiF_2 has the lowest measured surface scatter (highest reactivity), indicative of incorporation into the growing film. In contrast, SiF surface interactions appear to be only mildly influenced by plasma parameters such as applied rf power and ion bombardment. Moreover, SiF does not display significantly different behavior as a function of plasma type. Clearly, the use of multiple analysis techniques to characterize the overall plasma as well as studying several species in a single plasma system offers increased insight into the chemistry responsible for etching and deposition.

Reproduced with permission of the copyright owner. Further reproduction prohibited without permission.

References

1. F. Iacona, G. Casella, F. La Via, S. Lombardo, V. Raineri, G. Spoto *Microelectron. Eng.* **50**, 67 (2000).
2. V. Pankov, J. C. Alonso, A. Ortiz *J. Appl. Phys.* **86**, 275 (1999).
3. Y. Uchida, K. Taguchi, S. Sugahara, M. Matsummura *Jpn. J. Appl. Phys.* **38**, (1999).
4. K.-Y. Choi, C. W. Lee, C. Lee *Jpn. J. Appl. Phys.* **34**, 4673 (1995).
5. T. Wadayama, Y. Maiwa, A. Hatta *Vibrational Spectroscopy* **13**, 107 (1996).
6. D. S. Kim, Y. H. Lee *J. Electrochem. Soc.* **141**, 3562 (1994).
7. G. Cicala, G. Bruno, P. Capezzuto *J. Vac. Sci. Technol. A* **16**, 2762 (1998).
8. I. Khan, H. A. Naseem, S. S. Ang, W. D. Brown *Mat. Res. Soc. Symp. Proc.* **219**, 757 (1991).
9. C. Gomez-Aleixandre, O. Sanchez, J. Albella *Mat. Res. Soc. Symp. Proc.* **190**, 107 (1991).
10. T. Nakanishi, Y. Marukawa, S. Takahashi *Electrophotography* **28**, 274 (1989).
11. A. Madan, S. R. Ovshinsky, E. Benn *Philos. Mag. B* **40**, 259 (1979).
12. S. K. Kim, K. C. Park, J. Jang *J. Appl. Phys.* 77, 5115 (1995).
13. A. Madan, S. R. Ovshinsky *J. Non-Crystalline Solids* **35-36**, 731 (1980).
14. H. Lee, J. P. Deneufville, S. R. Ovshinsky *J. Non-Crystalline Solids* **59 - 60**, 671 (1983).
15. H. Lee, J. P. Deneufville *J. Non-Crystalline Solids* **66**, 39 (1984).
16. H. Koinuma, T. Manako, H. Natsuaki, H. Fujioka, K. Fueki *J. Non-Crystalline Solids* **77 - 78**, 801 (1985).

Reproduced with permission of the copyright owner. Further reproduction prohibited without permission.

17. G. Cicala, G. Bruno, P. Capezzuto *Pure & Appl. Chem.* **68**, 1143 (1996).

18. G. Bruno, P. Capezzuto, G. Cicala *J. Appl. Phys.* **69**, 7256 (1991).

19. A. A. Langford, B. P. Nelson, M. L. Fleet, R. S. Crandall *Phys. Rev. B* **42**, 7245 (1990).

20. A. A. Langford, A. H. Mahan, M. L. Fleet, J. Bender *Phys. Rev. B* **41**, 8359 (1990).

21. A. Matsuda, K. Yagii, T. Kaga, K. Tanaka *Jpn. J. Appl. Phys.* **23**, L576 (1984).

22. M. Syed, T. Inokuma, Y. Kurata, S. Hasegawa *Jpn. J. Appl. Phys.* **36**, 6625 (1997).

23. H. J. Lim, B. Y. Ryu, J. I. Ryu, J. Jang *Thin Solid Films* **289**, 227 (1996).

24. S. M. Han, E. S. Aydil *J. Vac. Sci. Technol. A* **15**, 996 (1997).

25. K. L. Williams, E. R. Fisher *J. Vac. Sci. Technol. A*, submitted for publication (2003).

26. S. Ray, S. C. De, G. Ganguly, A. K. Barua *J. Appl. Phys.* **65**, 4024 (1989).

27. S. Oda, S. Ishihara, N. Shibata, H. Shirai, A. Miyauchi, K. Fukuda, A. Tanabe, H. Ohtoshi, J. Hanna, I. Shimizu *Jpn. J. Appl. Phys.* **25**, L188 (1986).

28. Y. Okada, S. Wagner *Mat. Res. Soc. Symp. Proc.* **192**, 541 (1990).

29. A. Darcy, A. Galijatovic, R. Barth, T. Kenny, K. D. Krantzman, T. A. Schoolcraft *J. Mol. Graphics* **14**, 260 (1996).

30. P. J. van den Hoek, W. Ravenek, E. J. Baerends *Phys. Rev. B* **38**, 12508 (1988).

31. D. R. Sparks *J. Electrochem. Soc.* **139**, 1736 (1992).

32. H. Boyd, M. S. Tang *Solid State Technol.* **22**, 133 (1979).

33. H. Hayashi, K. Kurihsen, M. Sekine *Jpn. J. Appl. Phys.* **35**, 2188 (1996).

Reproduced with permission of the copyright owner. Further reproduction prohibited without permission.

34. H. F. Winters, J. W. Coburn *Surf. Sci. Rep.* **14**, 161 (1992).

35. Y. Matsumi, S. Toyoda, Y. Hayashi, M. Miyamura, H. Yoshikawa, S. Komiya *J. Appl. Phys.* **60**, 4102 (1986).

36. J. A. Mucha, V. M. Donnelly, D. L. Flamm, L. M. Webb *J. Phys. Chem.* **85**, 3529 (1981).

37. J. A. Mucha, D. W. Hess; ACS Symposium, 1983; Vol. 219, pp 215.

38. C. I. Butoi, N. M. Mackie, P. R. McCurdy, J. R. D. Peers, E. R. Fisher *Plasmas Polym.* **40**, 77 (1999).

39. C. F. Abrams, D. B. Graves *J. Appl. Phys.* **86**, 5938 (1999).

40. G. S. Oehrlein *J. Vac. Sci. Technol. A* **11**, 34 (1993).

41. R. Murri, L. Schiavulli, G. Bruno, P. Capezzuto, G. Grillo *Thin Solid Films* **182**, 105 (1989).

42. K. L. Williams, I. T. Martin, E. R. Fisher *J. Am. Soc. Mass. Spectrom.* **13**, 518 (2002).

43. P. R. McCurdy, K. H. A. Bogart, N. F. Dalleska, E. R. Fisher *Rev. Sci. Instrum.* **68**, 1684 (1997).

44. K. H. A. Bogart, J. P. Cushing, E. R. Fisher *Chem. Phys. Lett.* **267**, 377 (1997).

45. C. I. Butoi, M. L. Steen, J. H. D. Peers, E. R. Fisher *Journal of Physical Chemistry B* **105**, 5957 (2001).

46. P. R. McCurdy, V. A. Venturo, E. R. Fisher *Chem. Phys. Lett.* **274**, 120 (1997).

47. K. H. A. B. P. R. McCurdy, N. F. Dalleska, and E. R. Fisher *Rev. Sci. Instrum.* **68**, 1684 (1997).

Reproduced with permission of the copyright owner. Further reproduction prohibited without permission.

48. N. M. Mackie, N. E. Capps, C. I. Butoi, E. R. Fisher *ACS Symposium Series* **787**, 168 (2001).

49. N. M. Mackie, N. E. Capps, E. R. Fisher *Polym. Prepr. (Am. Chem. Soc., Div. Polym. Chem.)* **39**, 924 (1998).

50. N. M. Mackie, E. R. Fisher *Polym. Prepr. (Am. Chem. Soc., Div. Polym. Chem.)* **38**, 1059 (1997).

51. I. T. Martin, E. R. Fisher, work in progress.

52. N. E. Capps, N. M. Mackie, E. R. Fisher *J. Appl. Phys.* **84**, 4736 (1998).

53. N. Mutsukura, M. Ohuchi, S. Satoh, Y. Machi *Thin Solid Films* **109**, 47 (1983).

54. T. Shimada, Y. Katayama *J. Phys. Soc. Japan* **49**, 1245 (1980).

55. C. J. Fang, L. Ley, H. R. Shanks, K. J. Gruntz, M. Cardona *Phys. Rev. B* **22**, 6140 (1980).

56. S. Re, S. C. De, G. Ganguly, A. K. Barua, A. J. Mascarenhas, M. M. Al-Jassin, S. K. Def *J. Appl. Phys.* **65**, 4024 (1989).

57. C. I. Butoi, M. L. Steen, J. R. D. Peers, E. R. Fisher *J. Phys. Chem. B* **105**, 5957 (2001).

58. M. L. Steen, K. R. Kull, E. R. Fisher *J. Appl. Phys.* **92**, 55 (2002).

59. J. W. C. Johns, R. F. Barrow *Proc. Roy. Soc. (London)* **71**, 476 (1958).

60. A. C. Stanton, A. Freedman, J. Wormhoudt, P. P. Gaspar *Chem. Phys. Lett.* **122**, 190 (1985).

61. N. M. Mackie, V. A. Venturo, E. R. Fisher *J. Phys. Chem.* **101**, 9425 (1997).

62. K. R. Kull, M. L. Steen, E. R. Fisher *J. Membr. Sci.*, manuscript in preparation.

63. J. Zhang, K. L. Williams, E. R. Fisher *J. Phys. Chem. A*, **107**, 593 (2003).

Reproduced with permission of the copyright owner. Further reproduction prohibited without permission.

64. C. I. Butoi, N. M. Mackie, K. L. Williams, N. E. Capps, E. R. Fisher *J. Vac. Sci. Technol. A* **18**, 2685 (2000).

65. E. R. Fisher *Plasma Sources Sci. Technol.* **11**, A105 (2002).

66. K. Miyata, M. Hori, T. Goto *J. Vac. Sci. Technol. A* **15**, 568 (1997).

67. A. D. Tserepi, J. Derouard, J. P. Booth, N. Sadeghi *J. Appl. Phys.* **81**, 2124 (1997).

68. H. F. Winters, J. W. Coburn *Surf. Sci. Rep.* **14**, 161 (1992).

69. I. Shimizu *J. Non-Crystalline Solids* **97 - 98**, 257 (1987).

70. W. M. M. Kessels, P. R. McCurdy, K. L. Williams, G. R. Barker, V. A. Venturo, E. R. Fisher *J. Phys. Chem. B* **106**, 2680 (2002).

71. P. G. M. Sebel, L. J. F. Hermans, H. C. W. Beijerinck *J. Vac. Sci. Technol. A* **18**, 2759 (2000).

72. C. F. Abrams, D. B. Graves *Thin Solid Films* **374**, 150 (2000).

Reproduced with permission of the copyright owner. Further reproduction prohibited without permission.

CHAPTER 6

Comparison of Silicon and Fluorine Sources in SiO:F,C Thin Film Deposition

Submitted to the *J. Electrochem. Soc.* and Printed with permission from Keri L. Williams and Ellen R. Fisher.

This dissertation chapter contains results from a full paper submitted to the Journal of the Electrochemical Society in August 2002. The manuscript was written by Keri L. Williams and edited by Ellen R. Fisher. This chapter describes a comparison study of fluorine and carbon-doped silicon dioxide (SiO:F,C) materials prepared by plasma-enhanced chemical vapor deposition using an inductively coupled rf plasma reactor. Hexamethyldisiloxane (HMDSO) and tetraethoxysilane (TEOS) were used as the silicon precursors with O_2 as the oxidant. With both silicon sources, three different fluorocarbon (FC) gases were studied: CF_4, C_2F_6, and hexafluoropropylene oxide (HFPO). FTIR, XPS, and ellipsometry are used to characterize films as a function of O_2 and FC source concentrations.

Reproduced with permission of the copyright owner. Further reproduction prohibited without permission.

6.1. Introduction

The increasing importance of multilevel metallization and, ultimately, shrinking device dimensions in ultra large scale integrated circuits (ULSI) has spawned volumes of research in an effort to reduce parasitic capacitance through intermetal dielectric layers (IMDs).[1,2] Currently, SiO_2 is used as the industry standard for IMD because of its low dielectric constant as well as robust physical properties.[3] Although a variety of low-*k* materials exist, including fluorinated SiO_2 (SiO:F)[4-7] and carbon doped SiO_2 (SiO:C),[8,9] F- and C-doped SiO_2 (SiO:F,C) films exhibit lower dielectric constant, while maintaining desired physical properties.[10] A further advantage of SiO:F materials over pure SiO_2 is the improved gap fill coverage attained because of simultaneous F etching of the growing SiO_2 film.[11]

Introduction of F and C into the bulk film composition can be achieved using fluorinated silicon or fluorocarbon (FC) precursors.[7-9,12-14] Unfortunately, F doping alone often results in hygroscopic materials, making the dielectric constant unstable upon exposure to air.[15] Although moisture sensitivity has been minimized by use of high density plasmas, high rf power, and high substrate temperature,[15,16] these changes in film processing can produce negative physical properties such as high thermal stress.[17] Chemical doping with nitrogen also improves water resistivity, but results in increased dielectric constant.[18] Whereas SiO:C is quite robust and does not change appreciably upon exposure to air, SiO:F,C materials typically have lower dielectric constants and more stable physical properties.[7,13,14,19] Thus, SiO:F,C films are well suited for applications that could be improved by the use of lower-*k* materials such as IMDs in ULSI fabrication.

Reproduced with permission of the copyright owner. Further reproduction prohibited without permission.

Much of the research investigating SiO:F,C materials has focused on parameteric studies of plasma enhanced chemical vapor deposition (PECVD) systems utilizing a single set of precursors.[7,9,12-14] From these, a great deal of empirical understanding of film composition and properties has been obtained. For example, the combination of F and C incorporation provides improved thermal and mechanical properties with moisture resistant films that typically have dielectric constants lower than that of SiO_2 (< 3.9).[7] Recent studies have identified Si-CH_3 as the species primarily responsible for moisture resistance, whereas decreasing dielectric constant has been directly correlated to increasing amounts of fluorine in the materials,[20] presumably as a result of a decrease in ionic polarization.[21] SiO:F films usually contain 2-14 % at. fluorine with dielectric constants as low as ~3.0.[22] Interestingly, it has also been shown that the amount of fluorine is not the only factor affecting the dielectric constant, but that the bonding environment of the F atoms also contributes to film properties.[21]

To further explore the effects of precursor chemistry on film properties, we have investigated a variety of plasma systems using hexamethyldisiloxane (HMDSO) and tetraethoxysilane (TEOS) as silicon precursors. Whereas both compounds have been used to produce high quality SiO_2 materials, the different structure of these molecules should allow different plasma chemistries to be exploited. Although both silicon sources contain Si-O bonding, the relative bond strengths are significantly different. Theoretical calculations by Ho and Melius suggest that the Si-O bond strength in TEOS is significantly weaker (~131 kcal/mol) than that in HMDSO (~147 kcal/mol).[23] This suggests that the retention of Si-O moieties from the siloxane precursor is much more probable with HMDSO. Additional evidence for this comes from TEOS/O_2[18] studies

Reproduced with permission of the copyright owner. Further reproduction prohibited without permission.

showing that a significant amount of the oxygen incorporated into the growing SiO_2 film arises from the gas-phase oxidant.[24,25]

In addition to different silicon precursors, we have also employed three different FC gases as C and F sources: CF_4, C_2F_6, and hexafluoropropylene oxide (HFPO). Both CF_4 and C_2F_6 have been used previously to dope SiO_2 materials.[12,13] Comparison of these two fluorocarbon sources should offer insight into the importance of the F/C ratio in FC sources. In addition, C_2F_6 has demonstrably different gas phase chemistry and etch capabilities than CF_4,[26,27] which may directly influence the growing SiO:F,C film. HFPO offers an additional source of oxygen and provides significantly different chemistry from both CF_4 and C_2F_6. Whereas the saturated fluorocarbon precursors typically produce only amorphous FC materials,[28,29] HFPO can produce highly ordered, CF_2-rich materials.[30] Furthermore film deposition rate is significantly slower in HFPO plasmas. Thus, one hypothesis for this work is that altering the combination of silicon and FC precursors will directly affect the amount of fluorine incorporation as well as the film deposition rate and the fluorocarbon environment in the resulting SiO:F,C materials. Details of growth rate and composition were obtained using ellipsometry, Fourier transform infrared (FTIR) spectroscopy and X-ray photoelectron spectroscopy (XPS). As O_2 selectively volatilizes carbon-containing moieties at the surface,[31] deeper insight into the growth mechanism of SiO:F,C was obtained by varying the oxidant concentration.

6.2. Results

In general, all six systems studied behaved similarly with respect to overall film

Reproduced with permission of the copyright owner. Further reproduction prohibited without permission.

deposition parameters. For this reason, we have elected to show typical spectra and other results depicting particular aspects of the deposition process, rather than spectra for all systems under all conditions. Exceptions to these typical deposition or film composition trends are also presented.

6.2.1. Film Composition. Figure 6.1 shows a series of transmission FTIR spectra for films deposited as a function of O_2 concentration and with constant pressures of 75 mtorr HMDSO and ~20 mtorr HFPO. The largest absorption band in the spectrum of the film deposited without O_2 arises from the Si-O-Si stretches at ~1060 cm^{-1}. The spectrum also contains absorption bands at ~2957, 2916, and 2865 cm^{-1}, corresponding to asymmetric and symmetric C-H stretches from $-CH_3$ and CH_2 groups. An additional absorption band at 1257 cm^{-1} is assigned to the $Si-CH_3$ stretch. With the addition of O_2, the hydrocarbon incorporation decreases and is nearly eliminated at 90% O_2. The Si-O-Si and Si-O-C stretches at ~1056 cm^{-1} are present in all spectra, but show significant changes in shape with the addition of O_2. The Si-O band around 1060 cm^{-1} narrows and develops a high frequency shoulder for films deposited with ≥890 mtorr O_2 (90%) in the feed. Similar spectral changes are observed for O_2 addition in the TEOS:HFPO, TEOS:CF_4, HMDSO:CF_4, and HMDSO:C_2F_6 feed gas combinations.

The SiO_2 films also exhibit strong dependence on the FC feed concentration. Figure 6.2 demonstrates the effect of changing the HFPO concentration for films deposited with constant pressures of 75 mtorr HMDSO and ~738 mtorr O_2. In each spectrum the Si-O absorbance peak at ~1060 cm^{-1} is present. However, increasing the amount of FC present in the feed significantly broadens this peak, suggesting a less

Reproduced with permission of the copyright owner. Further reproduction prohibited without permission.

Reproduced with permission of the copyright owner. Further reproduction prohibited without permission.

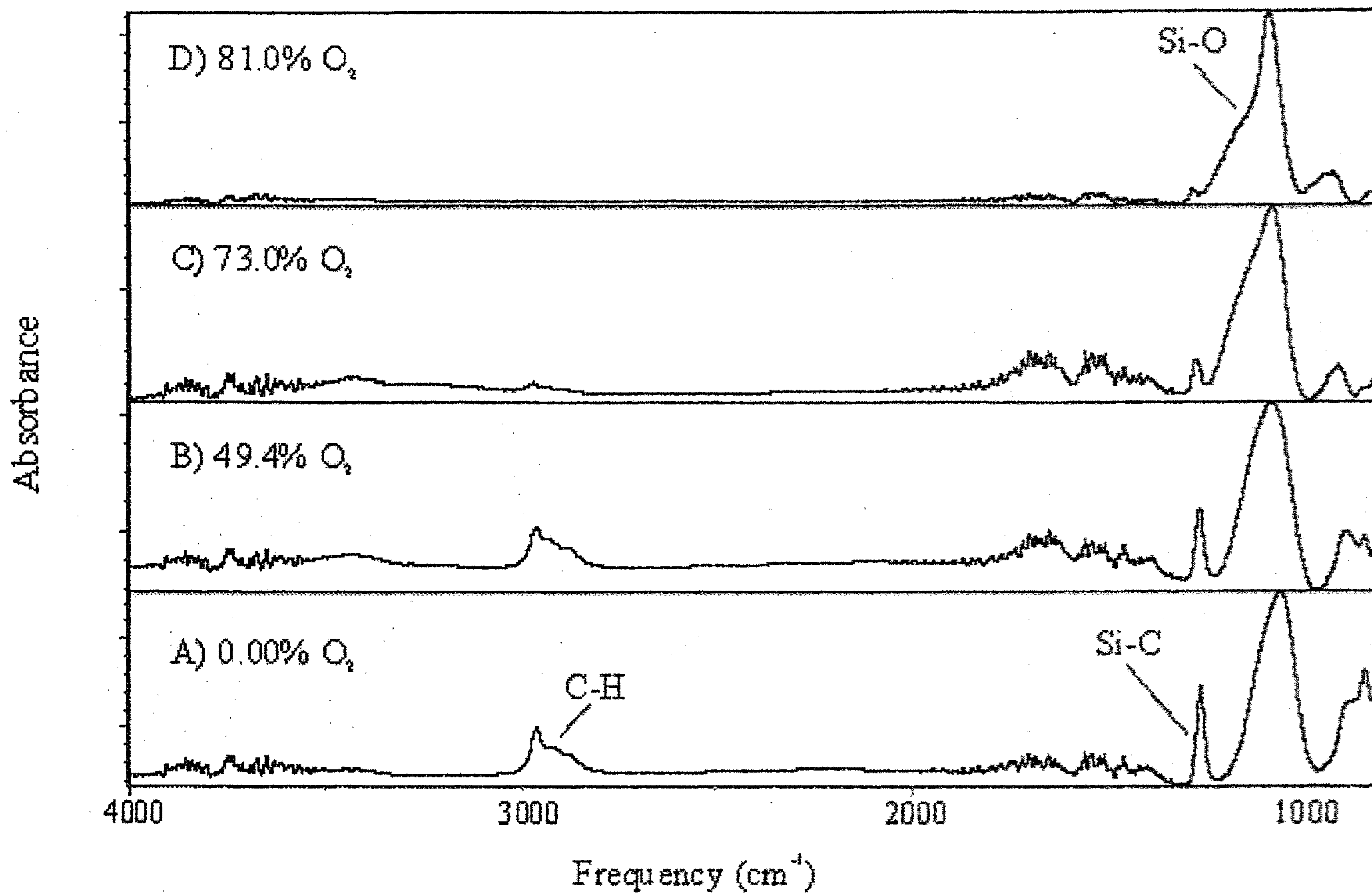

Figure 6.1. FTIR transmission spectra of SiO_2 films deposited at $P = 80$ W on KBr pellets from 75 mtorr HMDSO, 21 mtorr HFPO, and a) 0%, b) 160 mtorr (56%), c) 373 mtorr (78%), and d) 890 mtorr (90%) O_2.

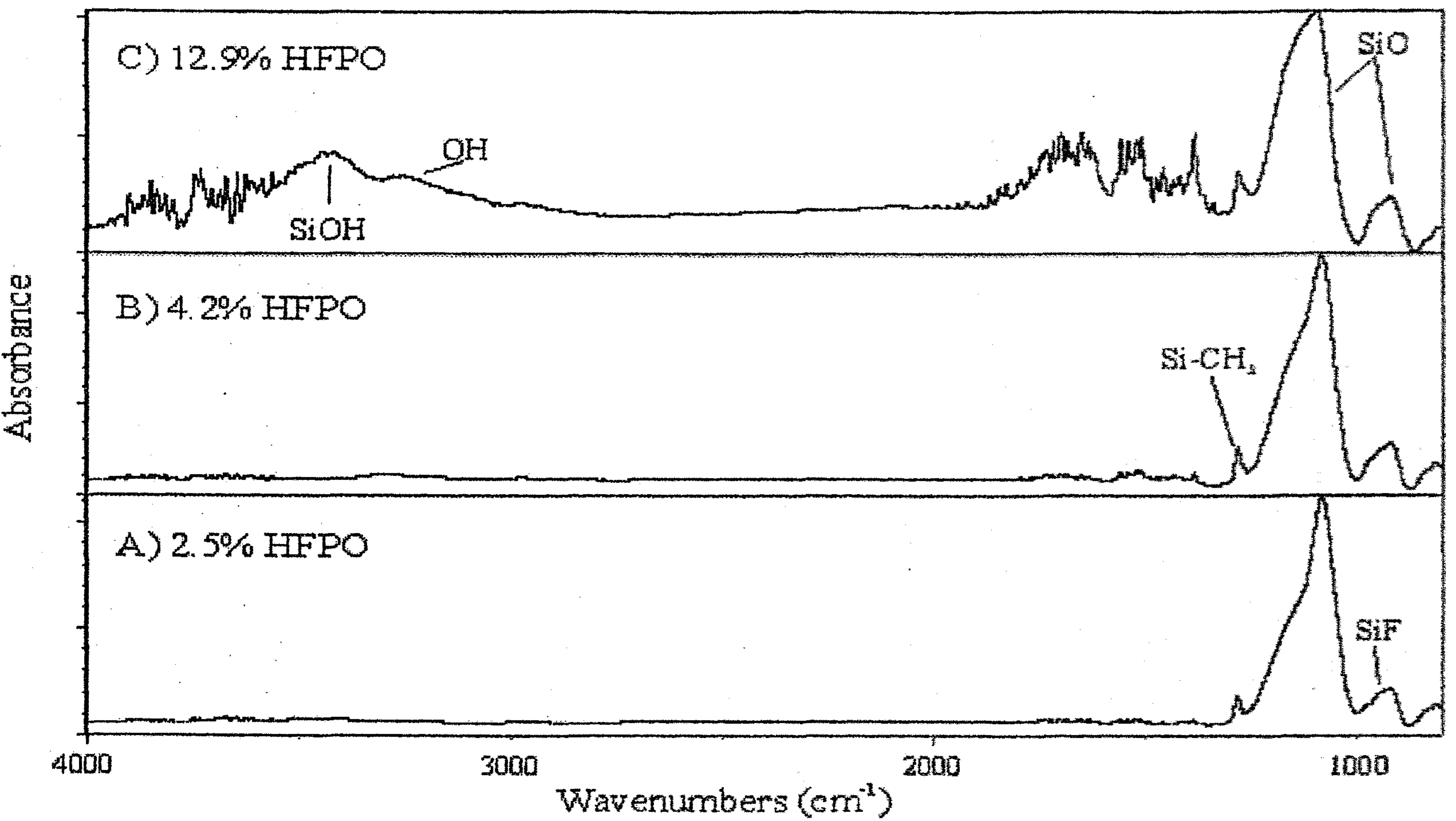

Figure 6.2. FTIR transmission spectra of SiO_2 films deposited at P = 80 W on KBr pellets from 75 mtorr HMDSO, 738 mtorr O_2, a) 21 mtorr (2.5%), b) 36 mtorr (4.3%), and c) 120 mtorr (12.7%) HFPO.

Reproduced with permission of the copyright owner. Further reproduction prohibited without permission.

ordered environment and incorporation of fluorocarbon in the film. A similar broadening of the Si-O peak upon increasing FC concentrations was seen for all FCs studied. Furthermore, a significant concentration of Si-OH is present in films deposited with P_{HFPO} > 120 mtorr (>12.7%) in the feed, indicating incorporation of water. Similar silanol incorporation was not, however, observed in films deposited with CF_4 and C_2F_6 precursors.

As noted in the Section 6.1, carbon and fluorine can significantly alter the dielectric constant of SiO_2 films. XPS survey spectra were used to generate atomic concentrations for films deposited under different feed gas conditions, Fig. 6.3. XPS atomic % values for carbon and fluorine as a function of O_2 in the feed for HMDSO:O_2:CF_4 plasmas are shown in Fig. 6.3a. A steady decrease in carbon content is observed, with the %C ranging from ~65% with no O_2 in the feed, to <10% at the highest O_2 conditions. Fluorine incorporation also decreases, albeit more modestly, ranging from ~10% to ~6.5 %. In contrast, both O and Si content in the films increase with increasing O_2 in the feed, Fig. 6.3b, with the Si:O ratio increasing from essentially 1:1 to nearly the stoichiometric ratio of 1:2. Trends similar to these were observed for O_2 addition in the other systems studied. Figure 6.4 shows the XPS C, F, Si, and O atomic concentrations in deposited films as a function of %CF_4 in the feed in the HMDSO system. Interestingly, all four elements display little change in atomic percent as a function of increasing FC content. This trend demonstrates the typical elemental dependence observed for all three FC feed gases in the HMDSO and TEOS systems.

Reproduced with permission of the copyright owner. Further reproduction prohibited without permission.

Reproduced with permission of the copyright owner. Further reproduction prohibited without permission.

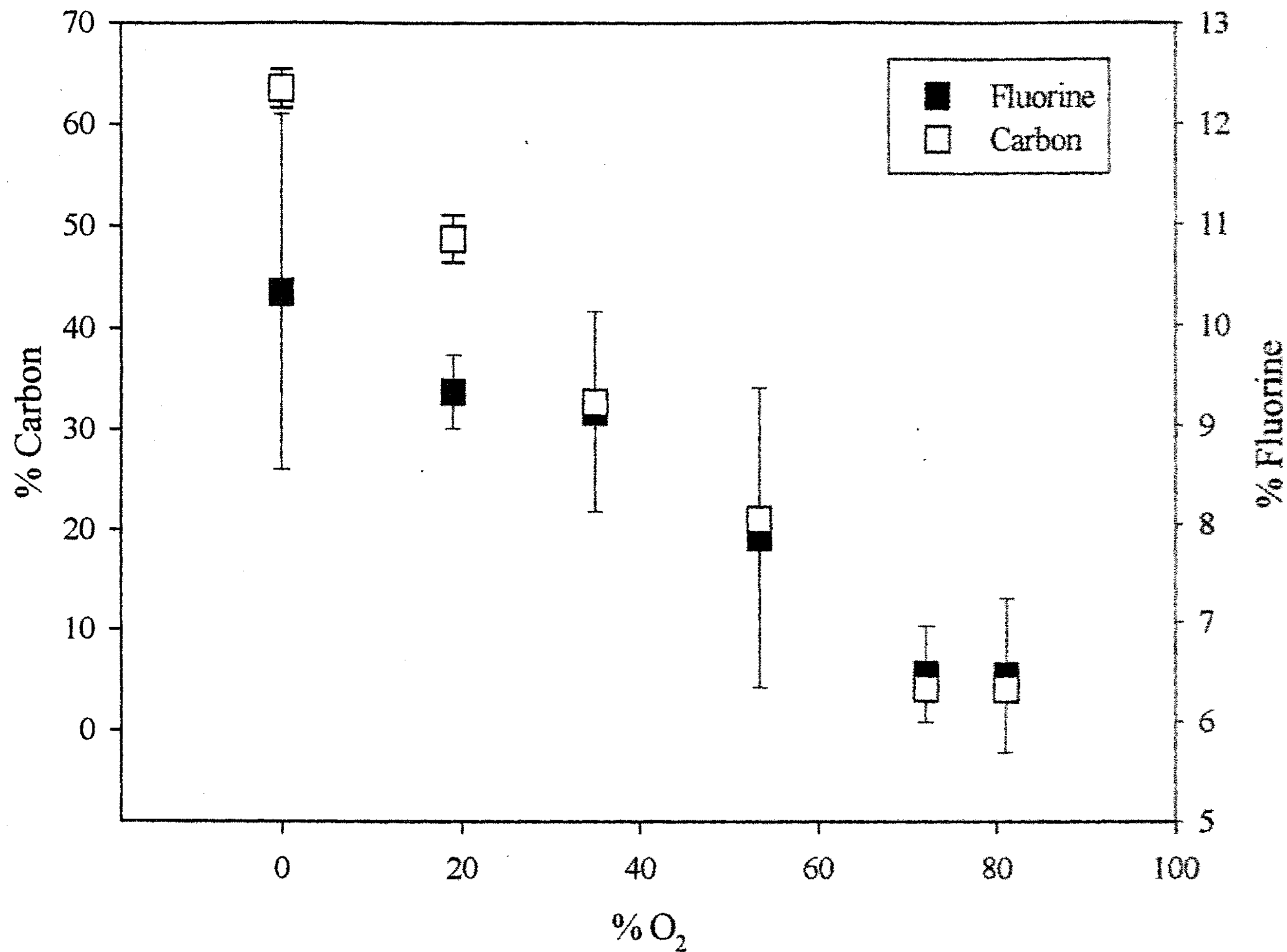

Figure 6.3. (A) Atomic concentrations taken from XPS analysis of films deposited from HMDSO:O_2:CF_4 plasmas as a function of % O_2 in the feed gas for C and F atoms.

Reproduced with permission of the copyright owner. Further reproduction prohibited without permission.

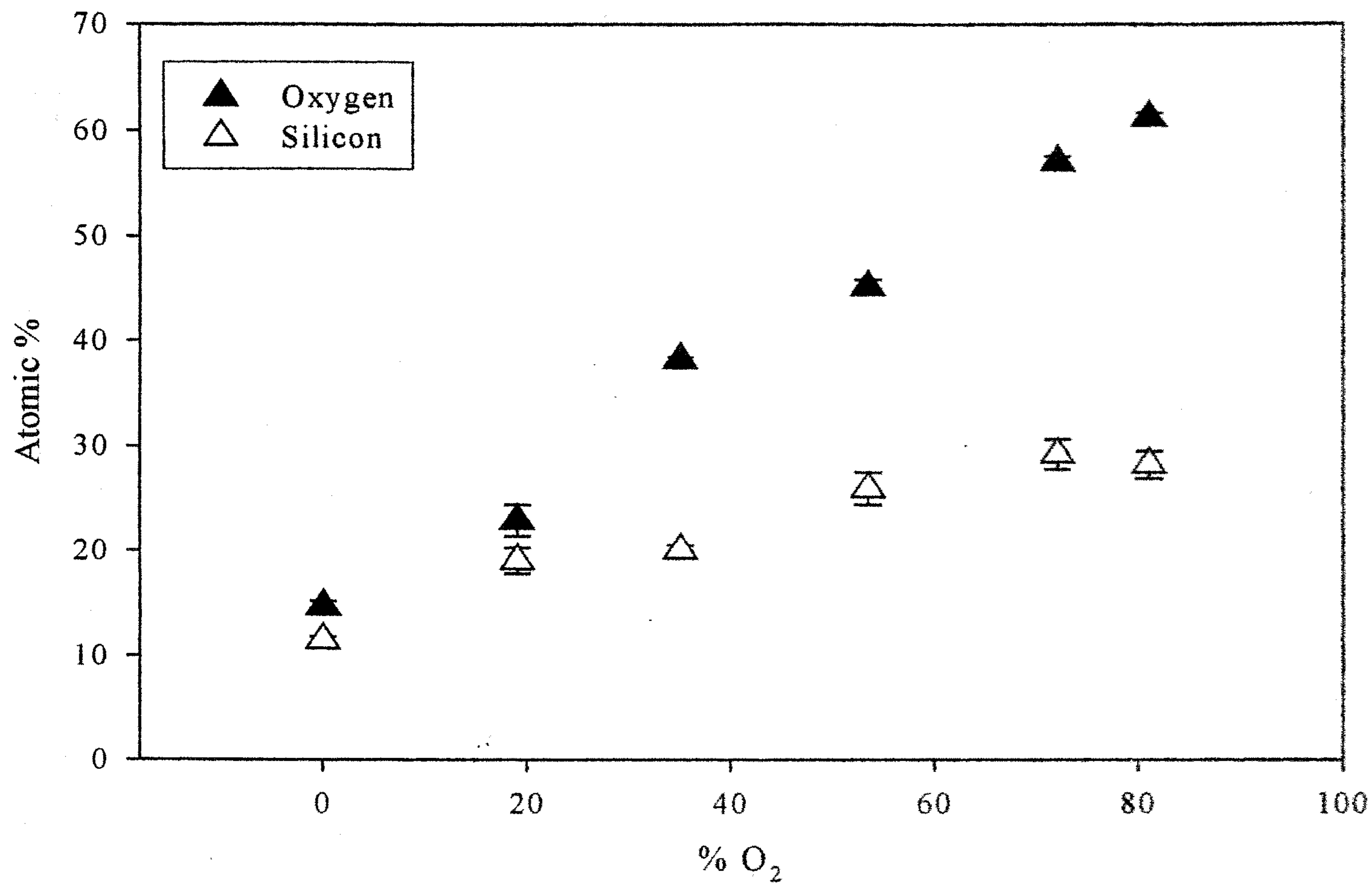

Figure 6.3. (B) Atomic concentrations taken from XPS analysis of films deposited from HMDSO:O_2:CF_4 plasmas as a function of % O_2 in the feed gas for Si and O atoms.

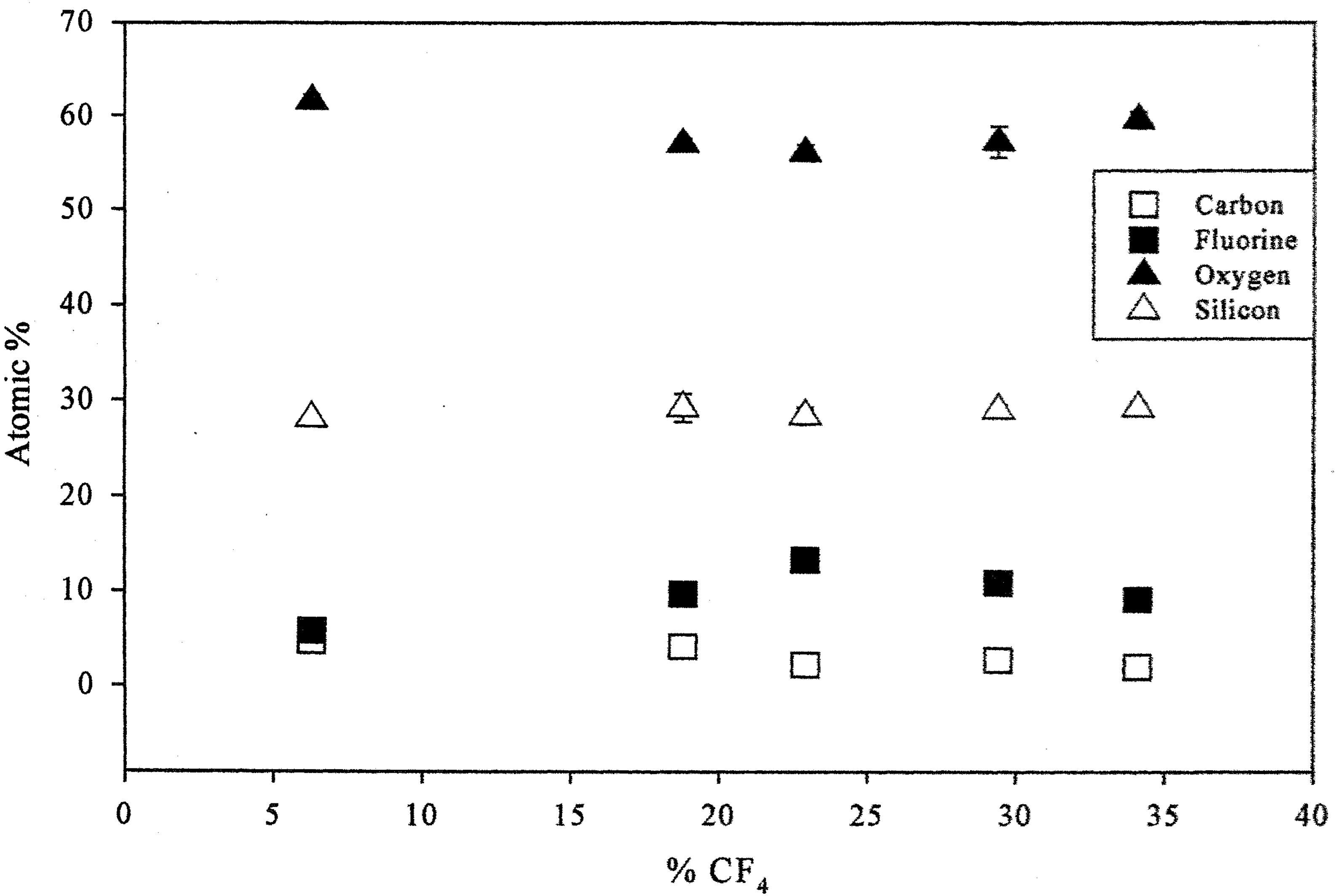

Figure 6.4. Atomic concentrations of C, F, Si, and O taken from XPS analysis of films deposited from HMDSO:O_2:CF_4 plasmas as a function of % CF_4 in the feed gas.

Reproduced with permission of the copyright owner. Further reproduction prohibited without permission.

6.2.2. Deposition Rates. The efficacy of a PECVD process is highly dependent on the gas-phase composition as well as the flux of reactive species to the surface of the depositing film. As plasma parameters can result in significant changes in the flux of fast depositing moieties, the rate of film growth can also be affected. Thus, deposition rate can be used in conjunction with elemental composition of a deposited material to gain insight into the consequences of different feed gases on the overall film. Note that the substrates were placed 10 cm downstream from the coil, which significantly reduces the deposition rate from what is expected directly in the coil region of the plasma.[32]

The effect of O_2 addition on deposition rates with constant FC concentration (~130 mtorr for CF_4, ~100 mtorr for C_2F_6, and ~20 mtorr for HFPO) is shown in Fig. 6.5 for both TEOS and HMDSO. In all systems, film deposition rates decreased as O_2 concentrations in the feed increased. Deposition rates measured for systems with CF_4 show a steady decrease with increasing O_2 concentrations in both Si systems, whereas with C_2F_6, the deposition rate drops dramatically with just a small amount of O_2 in the feed. In contrast, the HFPO systems yielded only a slight decrease in deposition rate with small amounts of O_2 in the feed (~10 Å/min), but decreased much more rapidly at higher O_2 concentrations. In all cases, the deposition rates in the HMDSO systems were significantly higher than the TEOS systems. This is consistent with previous studies of SiO_2 deposition from TEOS and HMDSO dielectric barrier discharges.[33,34]

Deposition rates were also measured as a function of FC concentration, Fig. 6.6. In all systems, the deposition rate trend is unique to the FC gas used and is dependent on the Si source only in the HFPO system. CF_4 addition initially increases the deposition rate, reaching a maximum at ~20-25% CF_4 before dropping off rapidly at higher

Reproduced with permission of the copyright owner. Further reproduction prohibited without permission.

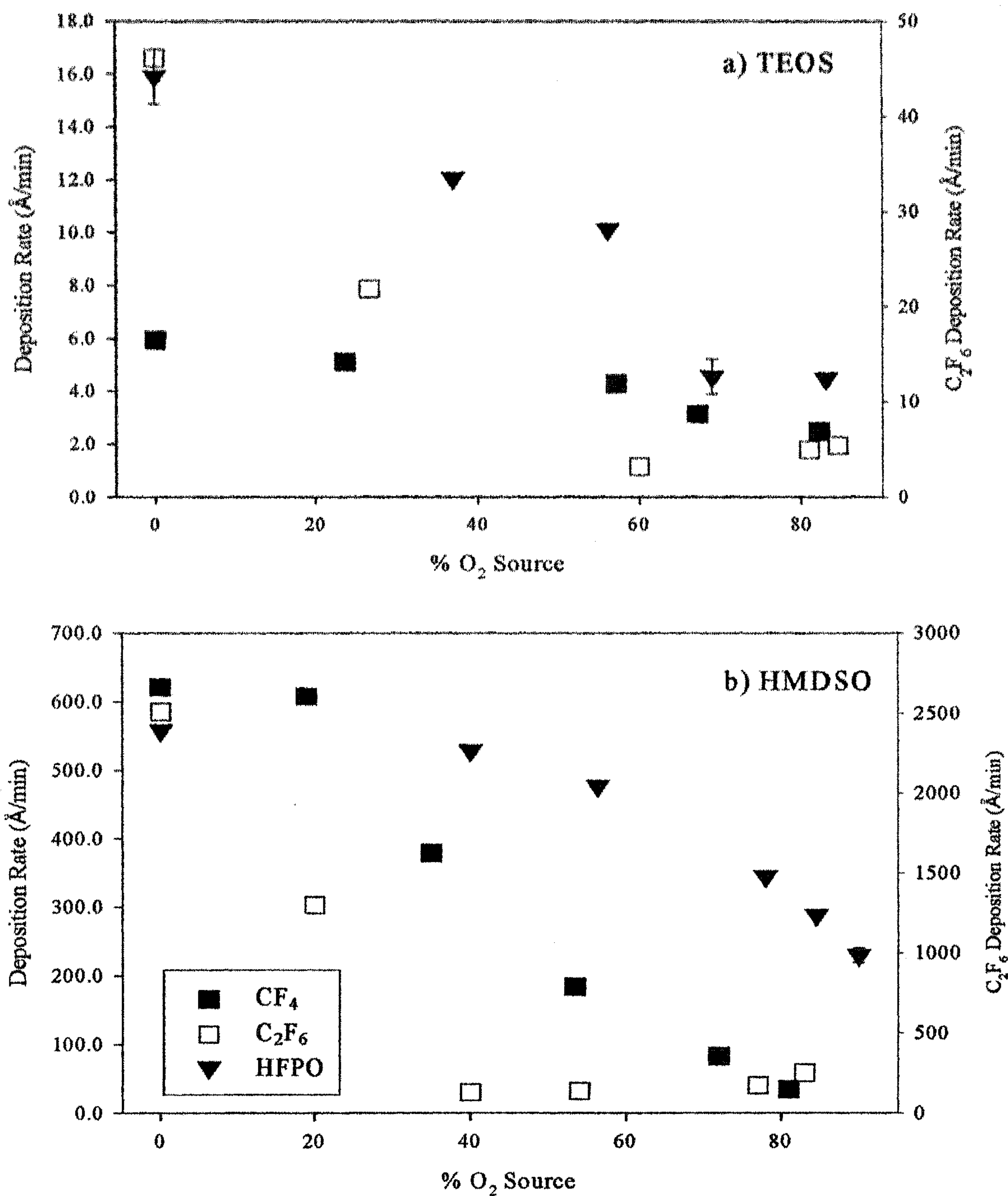

Figure 6.5. Dependence of SiO_2 film deposition rate on % O_2 added to the plasma gas feed for a) TEOS and b) HMDSO plasma systems: CF_4 (■), C_2F_6 (□), and HFPO (▼). Error bars indicate standard deviation of the average values. The FC concentrations were held constant at ~130 mtorr for CF_4, ~100 mtorr for C_2F_6, and ~20 mtorr for HFPO.

Reproduced with permission of the copyright owner. Further reproduction prohibited without permission.

Reproduced with permission of the copyright owner. Further reproduction prohibited without permission.

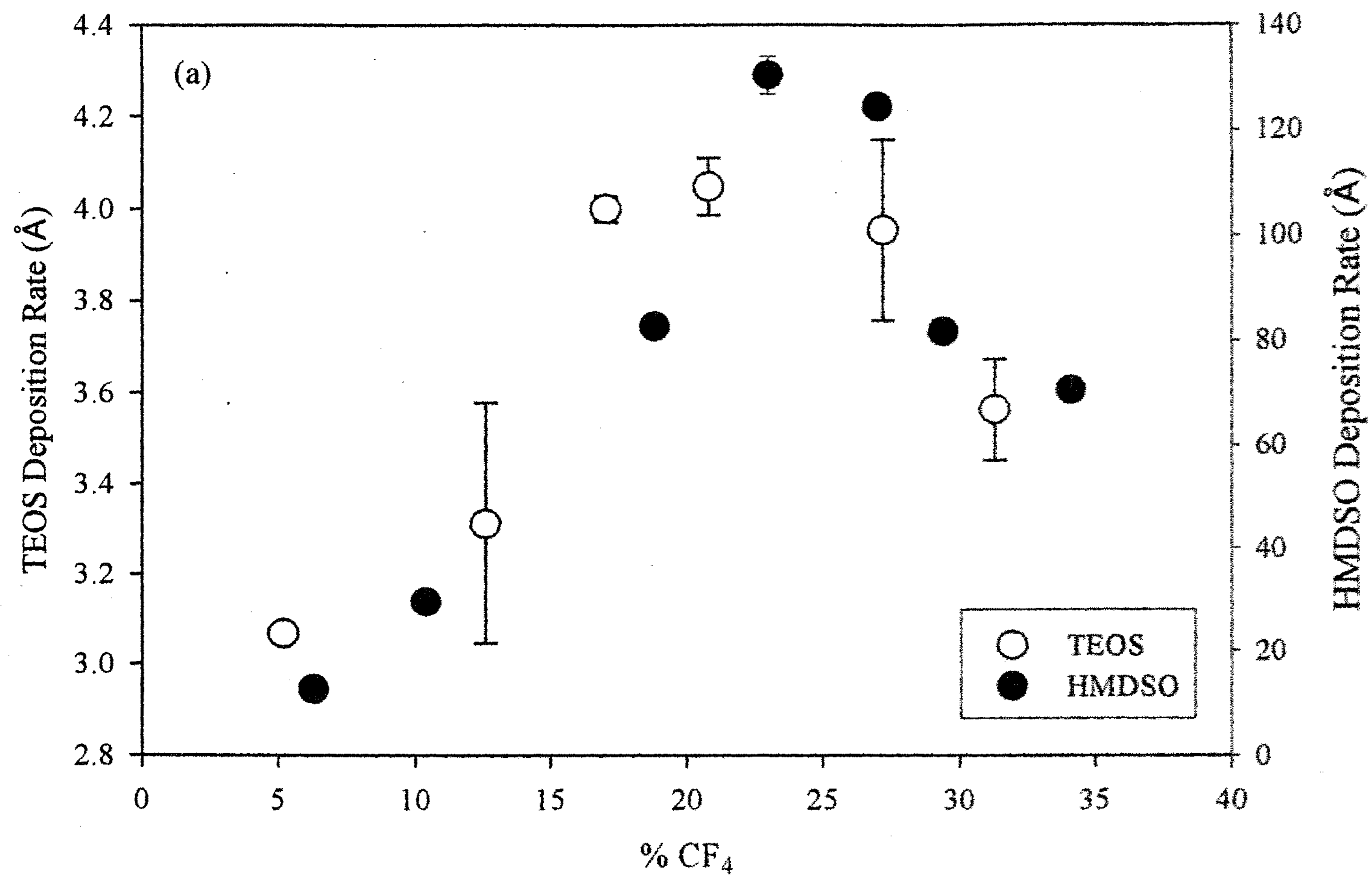

Figure 6.6. (A) Dependence of SiO_2 film deposition rate on CF_4 for TOES (○) and HMDSO (●) plasma systems. Error bars indicate standard deviation of the average values. The oxygen content was held constant at ~500-750 mtorr, depending on the system.

Reproduced with permission of the copyright owner. Further reproduction prohibited without permission.

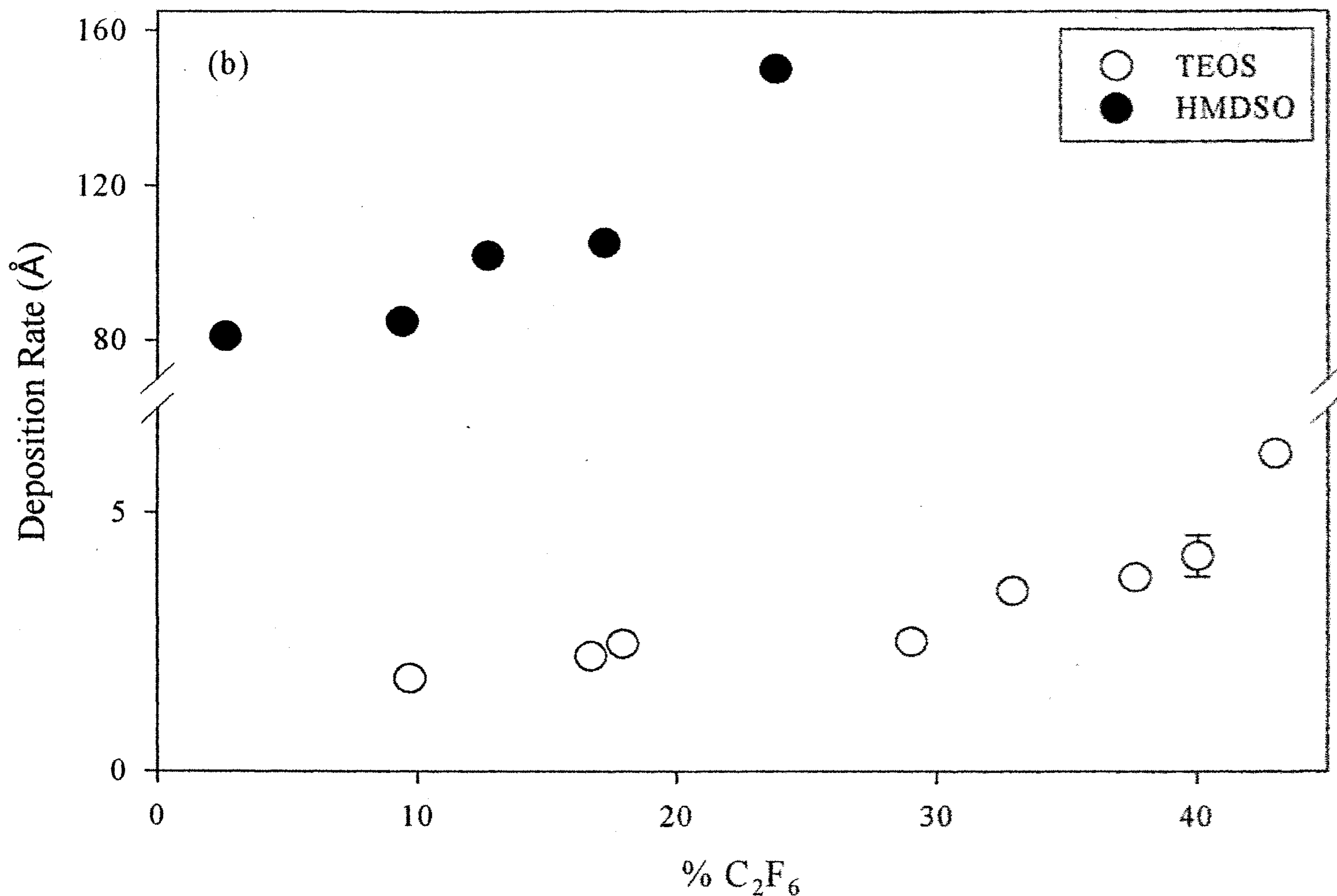

Figure 6.6. (B) Dependence of SiO_2 film deposition rate on C_2F_6 TOES (○) and HMDSO (●) plasma systems. Error bars indicate standard deviation of the average values. The oxygen content was held constant at ~500-750 mtorr, depending on the system.

Reproduced with permission of the copyright owner. Further reproduction prohibited without permission.

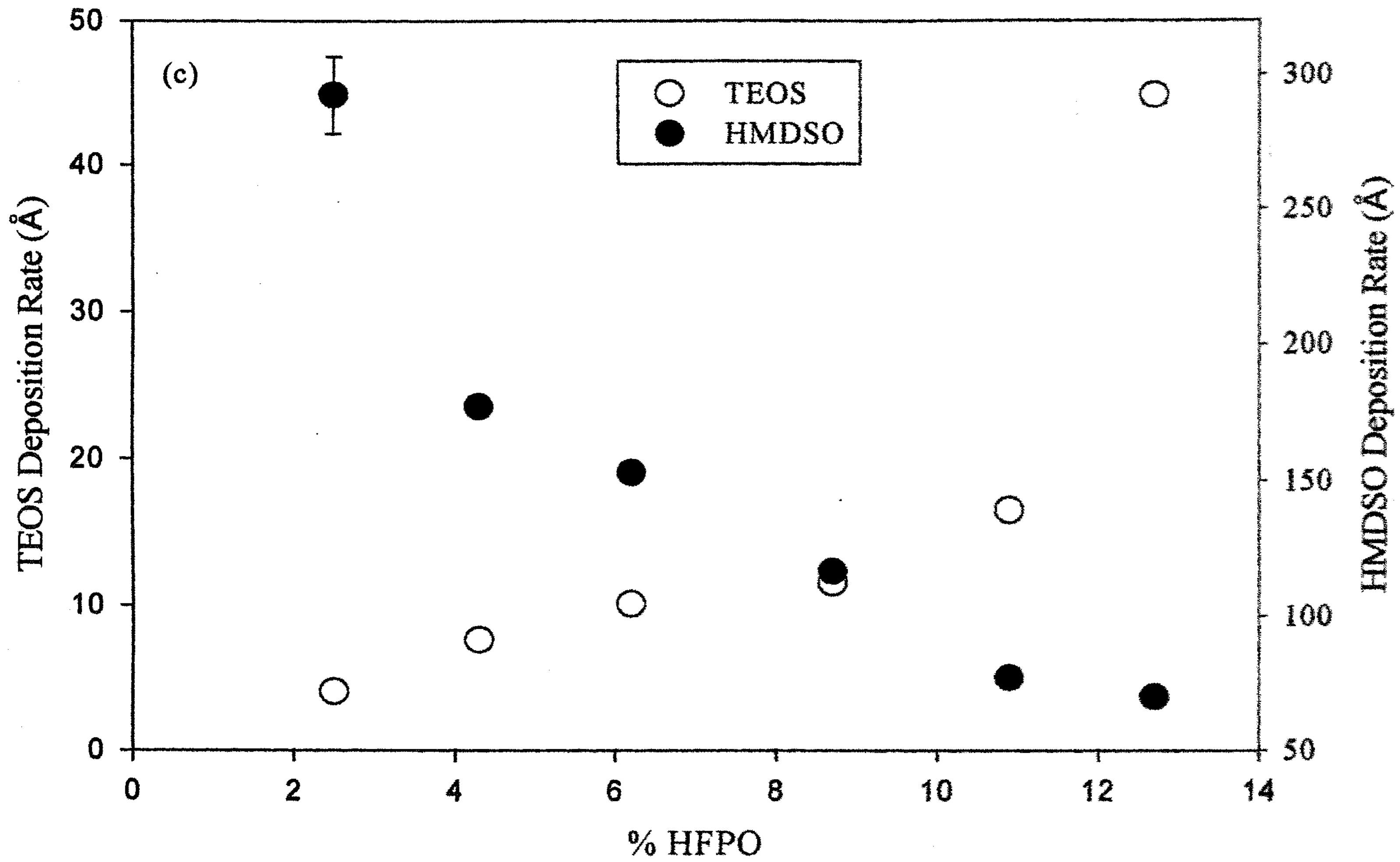

Figure 6.6. (C) Dependence of SiO_2 film deposition rate on HFPO for TOES (○) and HMDSO (●) plasma systems. Error bars indicate standard deviation of the average values. The oxygen content was held constant at ~500-750 mtorr, depending on the system.

concentrations, Fig. 6.6a. This type of dependence has been observed previously,[28,29] and is likely a result of increased etching at high CF_4 concentrations. Although C_2F_6 addition results in an increase in film deposition rate for both Si sources, Fig. 6.6b, the effect is not very dramatic. It is possible that the film deposition rate decreases at higher C_2F_6 concentrations, similar to what is observed with CF_4.[28] The pressure limits of our system, however, prevented additional data acquisition for this system at higher FC flows. HFPO addition, Fig. 6.6c, results in a significant decrease in deposition rate in the HMDSO system, whereas the opposite trend is observed for the TEOS system.

6.2.3. Refractive Index. The ability to vary elemental concentration in the SiO:F,C films also allows tailoring of their electrical properties. Refractive indices for films produced with 0% and ~85% O_2 in the feed for each plasma system are shown in Fig. 6.7. Selected refractive index values and calculated dielectric constants are listed in Table 6.1. The dielectric constants were obtained using Maxwell's relation, $n = (K_e)^{1/2}$.[35] Although Maxwell's relationship is not always valid, it does offer a lower limit to the dielectric constants of our films. For all systems, the addition of O_2 to the feed gas significantly reduced the refractive index, Fig. 6.7, with the greatest decreases occurring in the HMDSO systems. Significant changes in refractive index as a result of varying FC concentration were not observed, Table 6.1. The one exception was the TEOS:O_2:HFPO system, wherein the refractive index increased from 1.417 to 1.482 as a result of increasing the HFPO in the feed by ~10%. This may be related to the order of magnitude increase in film deposition rate with higher HFPO concentration in the feed, Fig. 6.6. For comparison, the accepted literature value for plasma deposited SiO_2 is generally between

Reproduced with permission of the copyright owner. Further reproduction prohibited without permission.

Table 6.1. Refractive Indices and calculated dielectric constant.

Gas System	Variable Parameter[a]	Refractive Index	Dielectric Constant[b]
HMDSO:O_2:CF4	0 % O_2	1.508 ± 0.003	2.274
	81% O_2	1.441 ± 0.030	2.076
	6% CF_4	1.442 ± 0.039	2.079
	34% CF_4	1.453 ± 0.017	2.111
TEOS:O_2:HFPO	0% O_2	1.450 ± 0.018	2.103
	83% O_2	1.424 ± 0.009	2.028
	3% HFPO	1.417 ± 0.010	2.008
	13% HFPO	1.482 ± 0.026	2.196
HMDSO:O_2:C_2F_6	0 % O_2	1.564 ± 0.007	2.446
	83% O_2	1.446 ± 0.014	2.091
	3% C_2F_6	1.429 ± 0.027	2.042
	24% C_2F_6	1.449 ± 0.051	2.100
HMDSO:O_2:HFPO	0 % O_2	1.469 ± 0.003	2.158
	81% O_2	1.472 ± 0.015	2.167
	3% HFPO	1.464 ± 0.012	2.143
	13% HFPO	1.466 ± 0.042	2.149

[a]For the O_2 dependent data, the FC concentrations were held constant at ~130 mtorr for CF_4, ~100 mtorr for C_2F_6, and ~20 mtorr for HFPO. For the FC dependent data, the O_2 pressure was held constant at ~500-750 mtorr, depending on the system.
[b]Dielectric constant calculated using Maxwell's equation relating K_e to n^2. See text for details.

Reproduced with permission of the copyright owner. Further reproduction prohibited without permission.

1.45 and 1.55 at 632.8 nm,[36,37] whereas that for thermally-deposited SiO_2 is generally 1.44-1.46.[37] Thus, films deposited in the $HMDSO:O_2:CF_4/C_2F_6$ and the $TEOS:O_2:HFPO$ systems have refractive indices somewhat lower than that of thermally grown SiO_2, Table 6.1.

6.2.4. Detailed Film Chemistry. To explore the effects of feed gas ratios on film composition more deeply, we have selected to highlight the $TEOS:O_2:C_2F_6$ system. Figure 6.8 shows a series of FTIR spectra for films deposited as a function of O_2 source concentration with a constant 50 mtorr TEOS and 90 mtorr C_2F_6. With no O_2 addition, an amorphous fluorocarbon film is produced, Fig. 6.8a, with broad CF_x and $C=CF_x$ absorption bands at ~1200 cm^{-1} and 1500 cm^{-1}, respectively. Addition of even small amounts of O_2, however, produces significant changes in film composition. With as little as 50 mtorr O_2 in the feed (27%), film composition shifts to a CH_x/SiO_x material. Further increases in O_2 result in a SiO_2 film with only small amounts of carbon and Si-OH incorporation. At the highest O_2 feed concentration, the Si-OH peak disappears completely.

The results seen in the FTIR analysis are echoed in the XPS data for these materials, Figs. 6.9a and 6.9b. XPS atomic % data for C and F as a function of O_2 in the feed demonstrate that films containing large amounts of C and F with F/C ratios of ~1.05 were produced with no O_2 in the feed gas, Fig. 6.9. Addition of 60 mtorr O_2 (~30%) shifts the film composition to primarily a silicon oxide, with a Si:O ratio of 1.9. At O_2 feed concentrations greater than 80%, the Si:O ratio is maintained at ~1:2.

Figure 6.10 shows high resolution XPS C_{1s} and Si_{2p} spectra for films deposited with no O_2 and with 930 mtorr O_2 (~84%). Without O_2 in the feed, the deposited

Reproduced with permission of the copyright owner. Further reproduction prohibited without permission.

Reproduced with permission of the copyright owner. Further reproduction prohibited without permission.

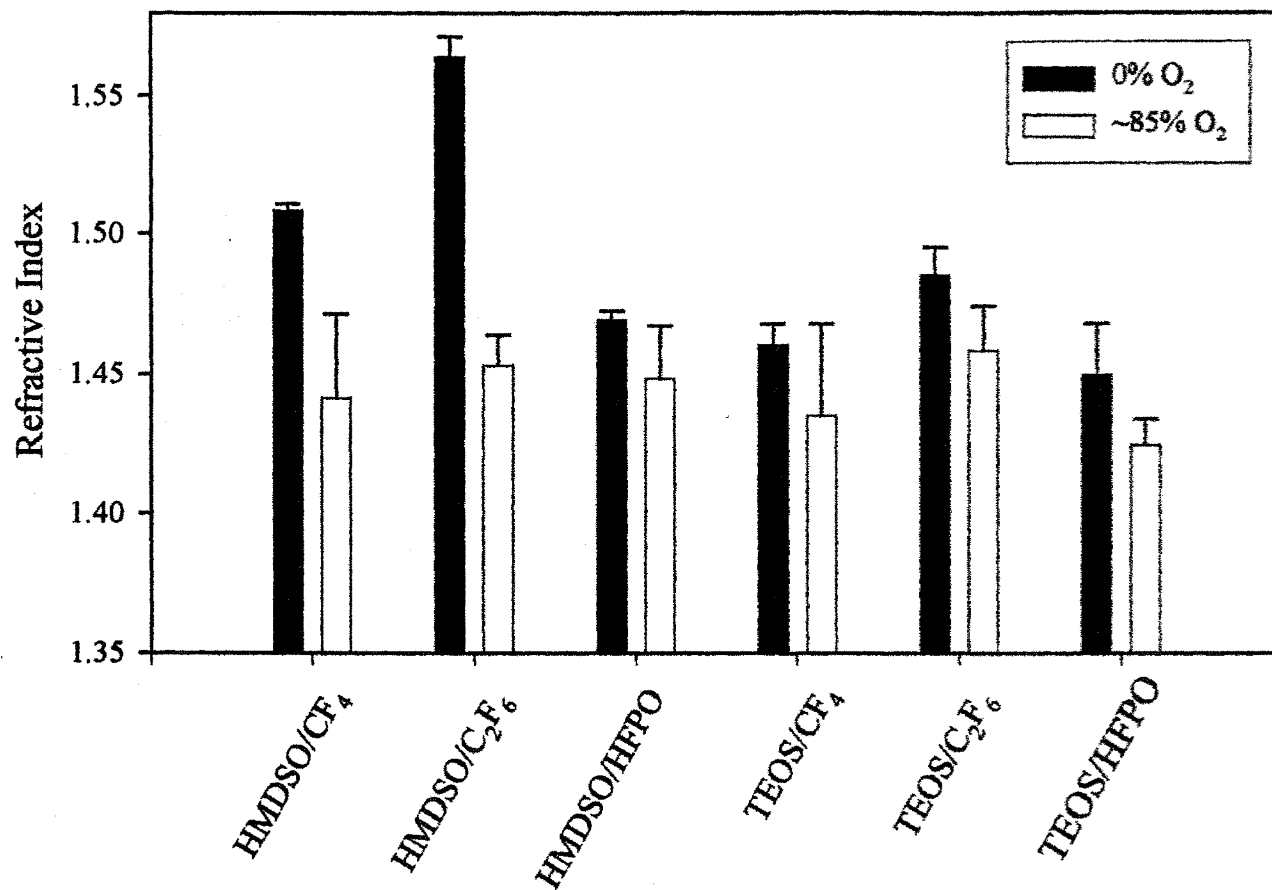

Figure 6.7. Refractive indices for films deposited from HMDSO and TEOS systems for oxygen feed gas concentrations of 0 and ~85% with each of the three FC precursors. The FC concentrations were held constant at ~130 mtorr CF_4, ~100 mtorr C_2F_6, and ~20 mtorr HFPO.

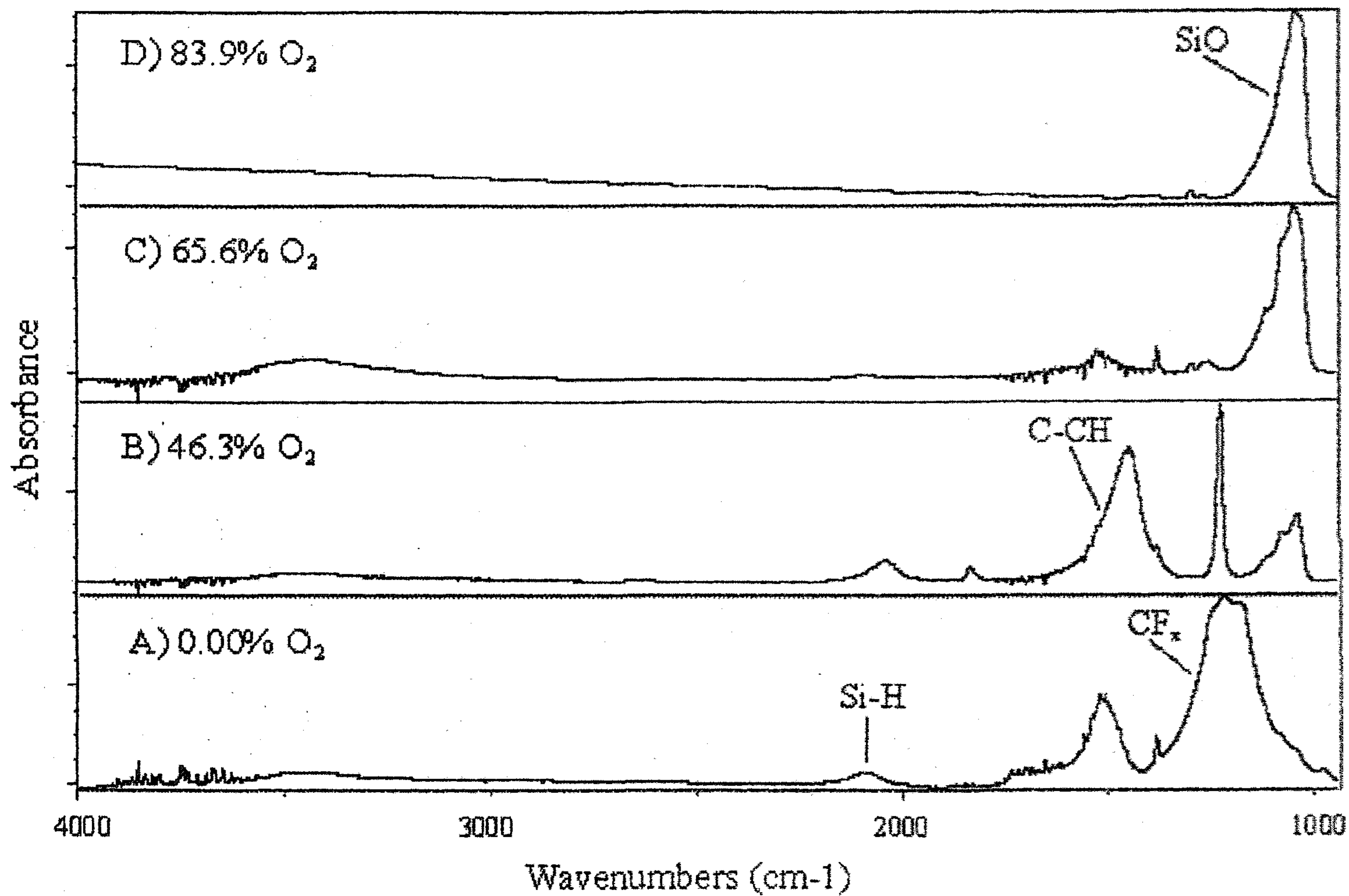

Figure 6.8. FTIR transmission spectra of SiO_2 films deposited on KBr pellets from 50 mtorr TEOS, ~90 mtorr C_2F_6, and a) 0%, b) 50 mtorr (27%), c) 180 mtorr (60%), and d) 930 mtorr (85%) O_2 with $P = 80$ W.

Reproduced with permission of the copyright owner. Further reproduction prohibited without permission.

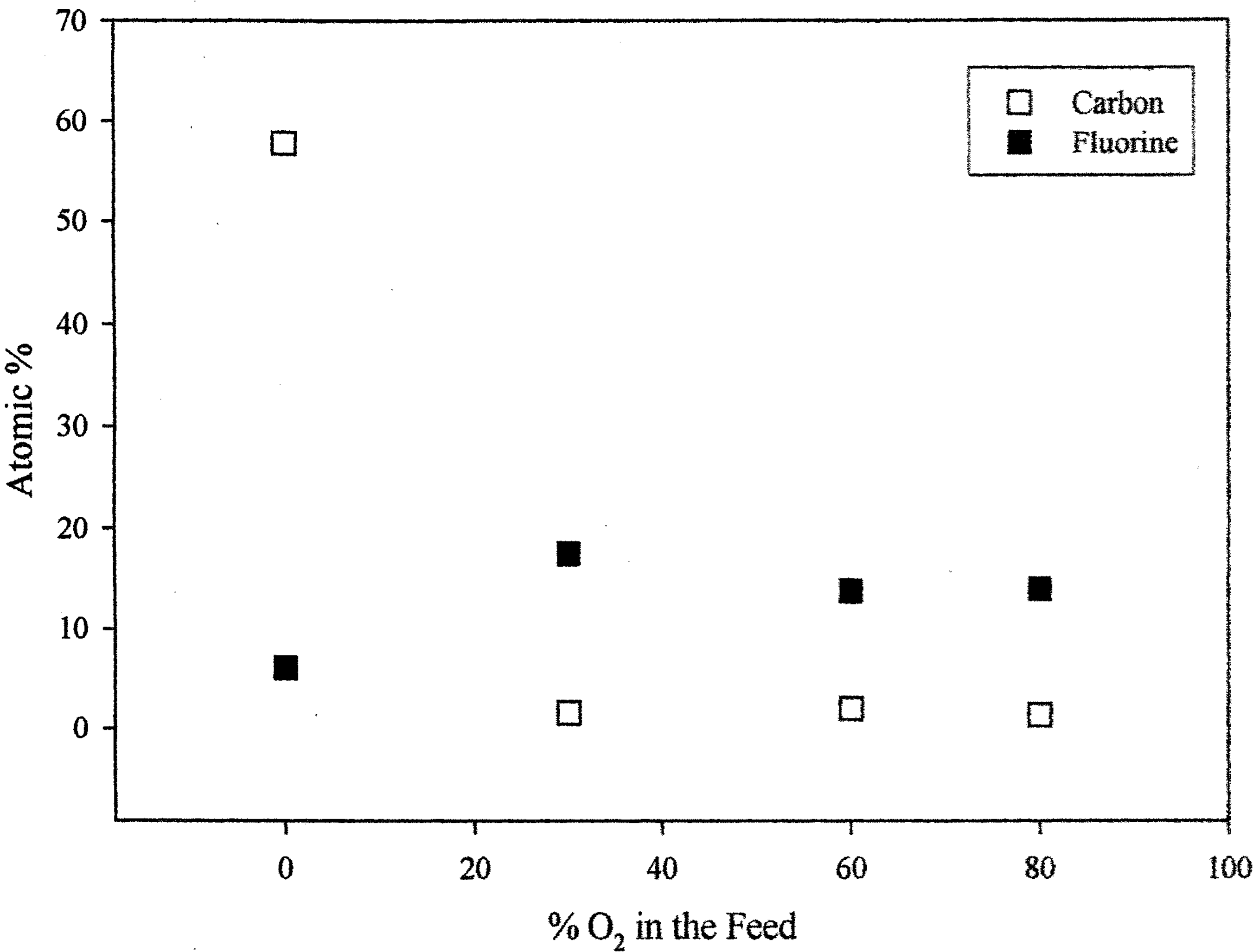

Figure 6.9. (A) XPS elemental composition for films deposited from TEOS:O_2:C_2F_6 plasmas for carbon and fluorine content as a function of % O_2 in the feed gas.

Reproduced with permission of the copyright owner. Further reproduction prohibited without permission.

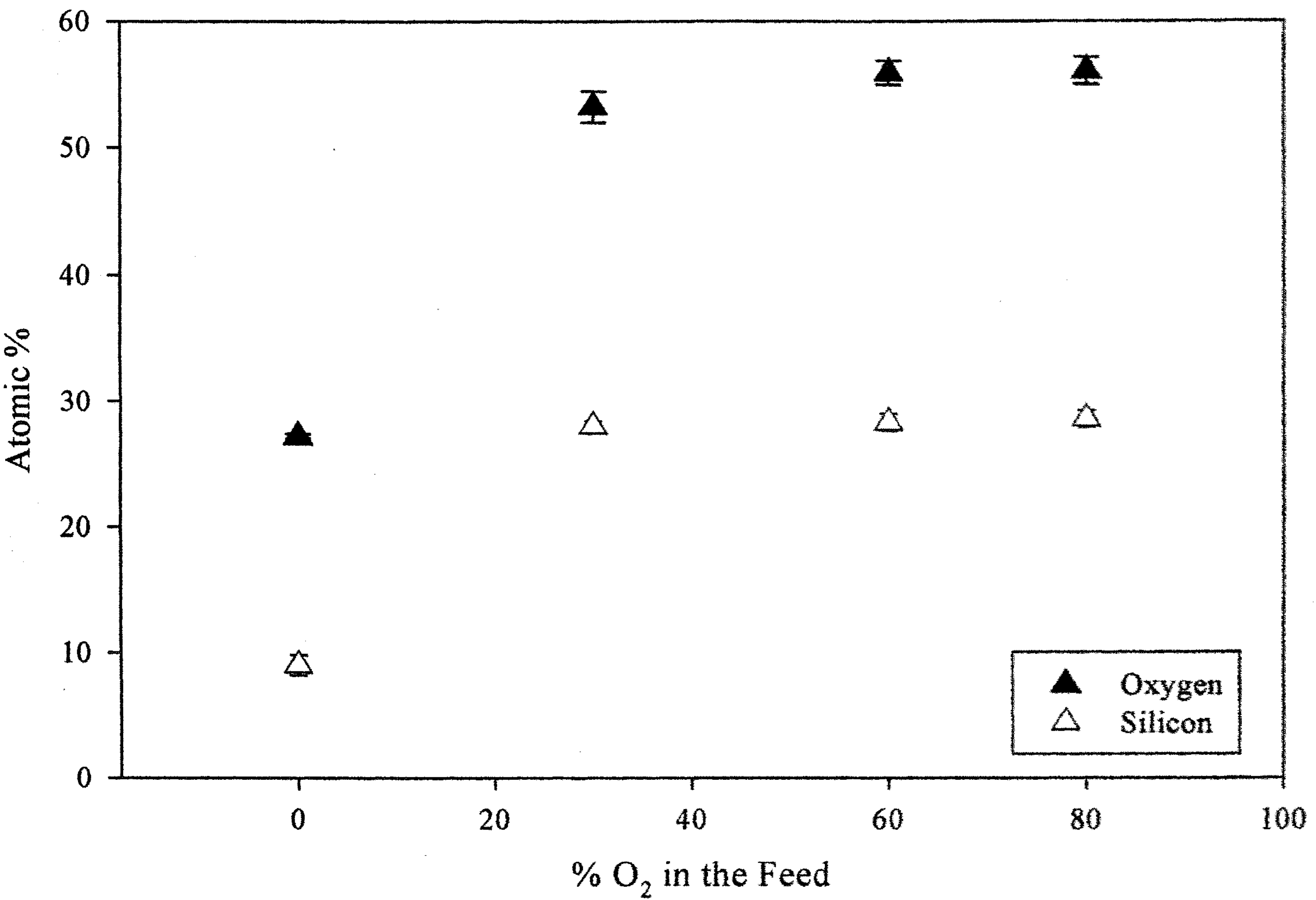

Figure 6.9. (B) XPS elemental composition for films deposited from TEOS:O_2:C_2F_6 plasmas for silicon and oxygen content as a function of % O_2 in the feed gas.

Reproduced with permission of the copyright owner. Further reproduction prohibited without permission.

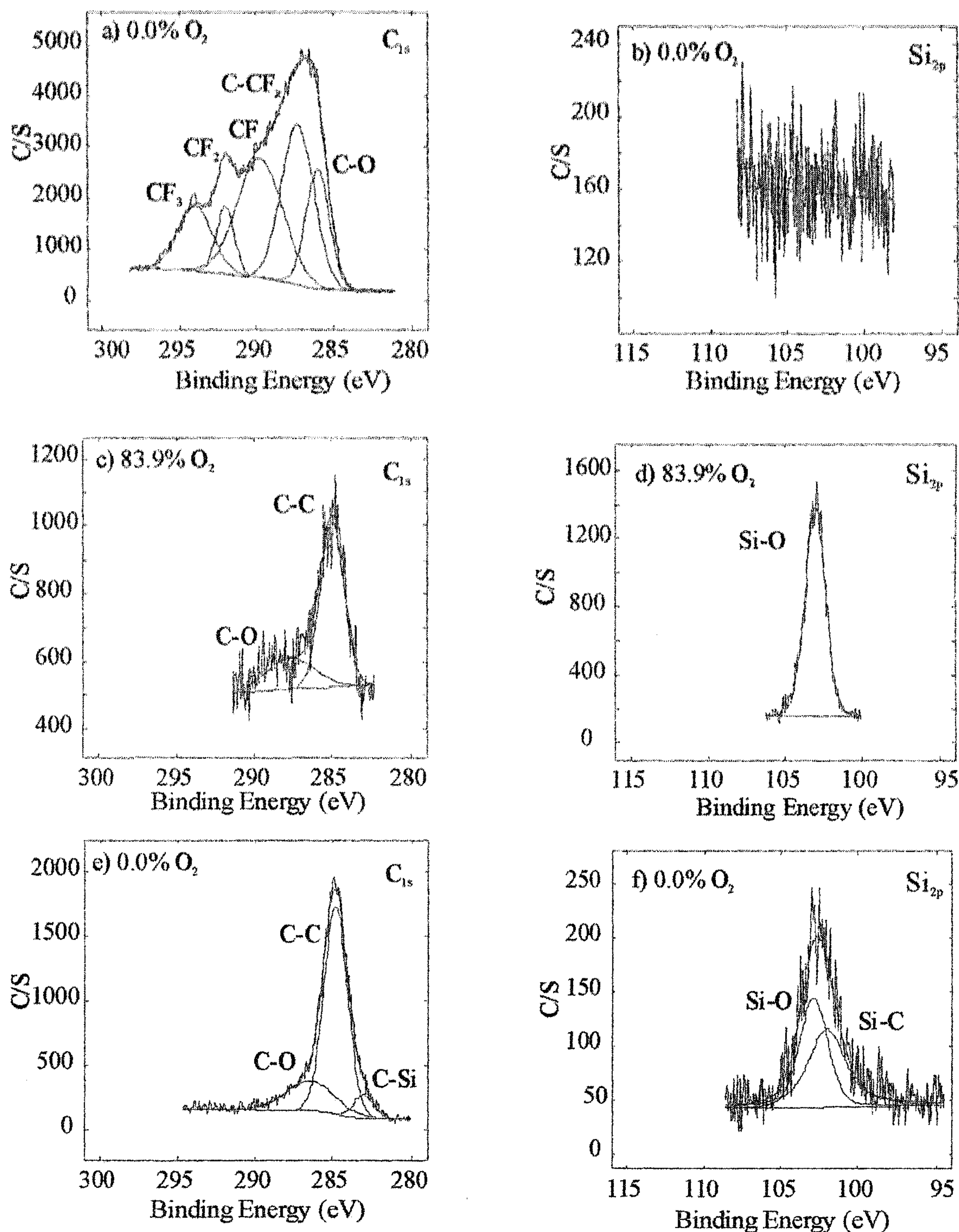

Figure 6.10. C_{1s} and Si_{2p} XPS high resolution spectra of films deposited in TEOS:O_2:C_2F_6 plasmas without O_2 in the feed (a and b, respectively) and with 930 mtorr O_2 (85%) in the feed (c and d, respectively). C_{1s} and Si_{2p} XPS high resolution spectra of films deposited in a HMDSO:C_2F_6 plasma without O_2 in the feed are shown in (e) and (f) respectively.

Reproduced with permission of the copyright owner. Further reproduction prohibited without permission.

materials consist of fluorocarbon moieties (CF_x, C-CF) with small amounts of oxygen in the form of CO bonding. Note that the C_{1s} XPS spectrum in Fig. 6.10a is typical of plasma-deposited amorphous fluorocarbon materials.[28,29] As suggested by the elemental composition analysis, the high resolution Si_{2p} spectrum, Fig. 6.10b, reveals little Si in the film. O_2 addition, however, produces SiO containing materials with C-C and C-O moieties but no CF_x bonding, Figs. 6.10c and 6.10d. For comparison, Figs. 6.10e and 6.10f contain high resolution C_{1s} and Si_{2p} spectra for films deposited from the HMDSO:C_2F_6 system (no O_2). Here, the carbon bonding environment contains no C-F moieties, but rather is predominately composed of C-C and C-O species, with a small contribution from C-Si (BE~283 eV). This demonstrates that F is bonded directly to silicon in these materials. Furthermore, the broad Si_{2p} peak indicates that silicon has multiple bonding environments. Deconvolution of this peak indicates that Si-C and Si-O are present, similar to what is observed using FTIR (Fig. 6.1). Addition of oxygen to this system results in a narrowing of the C-C (BE=284.8 eV) and the Si_{2p} peaks, indicating the elimination of Si-C bonding. The spectra shown in Figs. 6.10e and 6.10f are typical for films deposited using HMDSO as the silicon precursor, regardless of the FC precursor.

6.3. Discussion

Fluorine and carbon doping of SiO_2 films has been shown to decrease the dielectric constant while maintaining film stability under ambient conditions.[7,9,13,17] Because of this, much work has investigated the effects of different silicon, fluorocarbon,

Reproduced with permission of the copyright owner. Further reproduction prohibited without permission.

and oxidant gas precursors in SiO_2:F,C depositing systems.[38-40] In general, these studies have focused on either varying plasma parameters (such as applied power) or gas ratios in a single system, without changing the nature of the source gases. Our investigations contribute to this body of work by providing a comparison of three different FC sources and two different Si sources and varying gas ratios, including amount of oxidant. The observed trends of the six systems studied are discussed below.

The effect of oxidant concentration on plasma deposited SiO_2 films has been well characterized in the literature.[41-43] In all SiO_2 PECVD systems, the oxidant has a dual role, to remove hydrocarbon as well as to add oxygen to the depositing film.[24] This is also true in our systems, Fig. 6.1, wherein we observe a significant change in the O:Si ratio with O_2 addition. For example, in the HMDSO:O_2:CF_4 plasma system (Fig. 6.3b), the O:Si stoichiometry increases linearly from ~1.3 with no O_2 addition to ~2.1 at 800 mtorr O_2 (~80%). Similar changes are observed in all of the HMDSO systems and TEOS systems.

In addition to being a deposition precursor, O_2 also acts to remove carbonacious material (both CH_x and Si-C moieties)[44] from the depositing film, Fig. 6.1. Regardless of the Si precursor, O_2 addition also results in a decrease in film deposition rate, primarily because O_2 is known to increase etching rates in fluorocarbon plasmas.[26,45] This effect is the strongest for the C_2F_6 systems. Interestingly, there is less of an effect with the only FC precursor that contains oxygen, HFPO. This may be because activation of HFPO results in formation of stable molecules,[46] whereas decomposition of CF_4 and C_2F_6 results in formation of gas-phase CF_3 and F atoms. Addition of O_2 to the feed is more likely to

Reproduced with permission of the copyright owner. Further reproduction prohibited without permission.

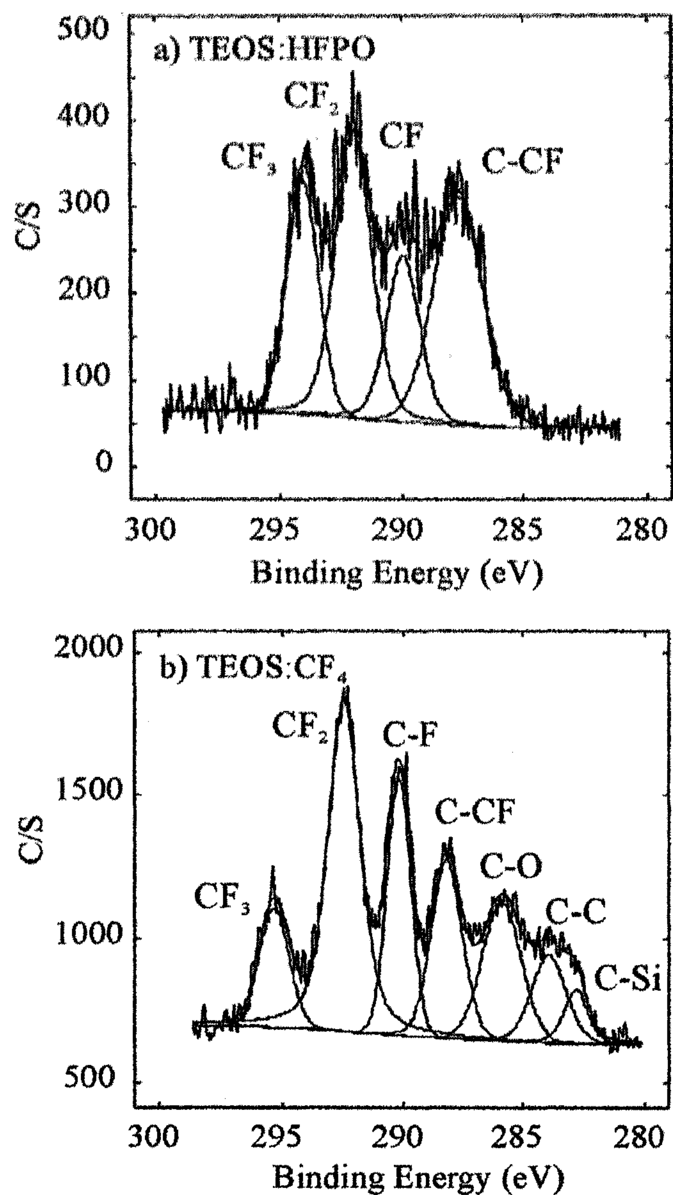

Figure 6.11. C_{1s} XPS high resolution spectra of films deposited from a) a TEOS:HFPO plasma (no O_2) and b) a TEOS:CF_4 plasma (no O_2).

Reproduced with permission of the copyright owner. Further reproduction prohibited without permission.

affect these highly reactive species, rather than the relatively stable CF_2 and fluoroacetyl formed with HFPO. This suggests that although O_2 strongly affects the surface chemistry of the growing material and the gas-phase composition, the FC precursor is also a significant component in determining film chemistry.

As noted above, introduction of fluorine into SiO_2 films is desirable because it lowers the dielectric constant of the material. However, in excess of a few atomic %, it also produces moisture sensitive films. Thus, one goal in choosing multiple FC source gases is to control the amount of F incorporated by the growing SiO_2 material. Despite significant changes in film quality, F atomic % changes only subtly with increasing FC concentration for all three FC source gases. For example, in the HMDSO:O_2:CF_4 system, Fig. 6.4, we measure ~10% F incorporation at all CF_4 concentrations. With the other two FC precursors, significantly less fluorine incorporation is observed, ~4% in the C_2F_6 system and ~3% with HFPO, but these values also do not change significantly with increased FC in the feed. The higher F concentrations obtained in the CF_4 system are likely the result of higher F atom production in the gas phase of the plasma. As noted below, this affects other aspects of the overall plasma chemistry as F atoms are known etchants of silicon-based materials.[45] Moreover, evidence of water (Si-OH) incorporation was observed only in the HFPO system despite the relatively low fluorine concentrations (~3%). This may indicate that in addition to F concentration, the F environment is responsible for regulating the films' moisture sensitivity.

As addition of C and F together can help maintain SiO_2 film stability,[21] an additional hypothesis in this work is that different FC feed gases can result in different fluorine environments in the film. The C_{1s} high resolution XPS spectra in Fig. 6.10

Reproduced with permission of the copyright owner. Further reproduction prohibited without permission.

reveal there is indeed a significant difference in the F/C environment resulting from the two different Si precursors. With HMDSO, no F-C bonding is observed in the deposited material, Fig. 6.10e, suggesting that the fluorine is bonded exclusively to silicon in these materials. Furthermore, changing the FC source in the HMDSO system does not significantly alter the distribution of the C_{1s} bonding environment. With TEOS, however, an amorphous fluorocarbon polymer with very little C-O bonding is produced using C_2F_6 with no oxygen in the feed, Fig. 6.10a. Moreover, different FC source gases appear to direct the carbon-fluorine bonding environment. Figure 6.11 contains high resolution C_{1s} spectra for films deposited in the TEOS:CF_4 and TEOS:HFPO systems (no O_2). The material deposited using HFPO, Fig. 6.11a, is clearly an amorphous fluorocarbon polymer, with no apparent C-O or C-Si bonding. In contrast, the film deposited using CF_4 as the FC precursor has a much more complex C_{1s} spectrum, Fig. 6.11b, with contributions from CF_x as well as C-O and possibly C-Si moieties. The film deposited using C_2F_6 as the FC precursor contains even less C-F bonding and more C-C, C-O, and C-Si bonding, Fig. 6.10a. Interestingly, this decrease in C-F bonding can be correlated to an increase in refractive index for these materials from 1.450 ± 0.007 for the HFPO system to 1.485 ± 0.010 for the C_2F_6 system. Likewise, good film stability, previously associated with Si-CH_3 species, is observed in films containing C-Si bonding, produced primarily using CF_4 and C_2F_6. In contrast, poor film stability is observed with those films containing little C-Si bonding, produced in the HFPO system. From the XPS data, it appears that the Si source determines whether F will be bonded to Si or C in the resulting film. If the F is primarily bonded to carbon, then the FC precursor determines the fine structure of the CF_x environment.

Reproduced with permission of the copyright owner. Further reproduction prohibited without permission.

Similar to the role of O_2 in these systems, FC gases likely have dual roles as both deposition precursor and etchant. Indeed, fluorocarbon precursors with higher F/C ratios create plasma systems with the deposition/etching balance shifted toward etching rather than deposition.[26,45] This can be seen in our systems by examining the deposition rate dependence on added FC in the feed, Fig 6. For the CF_4 system (F/C = 4), a deposition rate maximum is evident at ~130 mtorr CF_4 addition. Above this, a sharp decline in deposition rate occurs, which is likely the result of competitive etching of the growing SiO_2 film by excess CF_4 (F atoms) in the plasma. In contrast, C_2F_6 (F/C = 3) shows no decrease in deposition rate with increasing FC gas concentration. This may be the result of fundamental differences in the plasma decomposition of these two molecules. In the CF_4 systems, CF_3 + F is the most abundant process, whereas formation of two CF_3 molecules is more likely in the C_2F_6.[47] Free fluorine will directly attack Si at the gas-surface interface while CF_3 radicals can participate in polymer growth, which effectively reduces etching.[48]

HFPO is unique among our FC precursors in that it affects the deposition rate in the two silicon systems differently. This can be somewhat understood by considering film composition differences in the two systems. With HMDSO, addition of even small amounts of HFPO leads to films with much higher carbon and much lower silicon content, suggesting the primary precursor shifts from the HMDSO to the HFPO. Previous work in our group has shown that film deposition from 100% HFPO plasmas is extremely slow (only a few Å/min).[30] Thus, the apparent shift in primary precursor results in a significant decrease in the overall film deposition rate. In contrast, films deposited in the TEOS system do not change appreciably in content with higher HFPO

Reproduced with permission of the copyright owner. Further reproduction prohibited without permission.

concentrations, indicating TEOS remains the primary precursor species. As a consequence, addition of HFPO does not significantly alter the deposition rate except at the highest FC concentrations. The change in deposition rate in the TEOS system is <50 Å/min, whereas the decrease observed in the HMDSO system is >200 Å/min.

Although both HMDSO and TEOS have been used extensively in PECVD of SiO_2, there are few reports comparing deposition mechanisms in the two systems, and none for formation of SiO:F,C materials. Sonnenfeld et al. have demonstrated that the decomposition of HMDSO in a dielectric barrier discharge occurs along two primary electron impact pathways: (1) Si-CH_3 bond dissociation and (2) Si-O bond dissociation.[34] From their data, they concluded that pathway (1) dominates the decomposition process, although process (2) does contribute, especially under high power density conditions. Moreover, formation of large, gas-phase oligomers did not occur, suggesting that film growth occurs primarily at the substrate surface. Electron impact dissociation of TEOS results in formation of TEOS-like intermediate species (e.g. Si-O containing molecules) and hydrocarbon radicals.[34,44] It is generally believed that significant additional fragmentation occurs after the initial dissociation of TEOS to create a wide variety of gas-phase Si-O-C and hydrocarbon species, all of which can interact with the surface to create the SiO_2 film. In addition, there are a number of different types of bonds that can be broken in this system, including Si-O, C-O, C-C, Si-C, and C-H bonds. This serves to increase the number of possible dissociation products that can be formed through a single electron impact reaction.

With the addition of a FC gas to the feed, the gas-phase chemistry changes significantly with additional electron-impact dissociation reactions as well as other gas-

Reproduced with permission of the copyright owner. Further reproduction prohibited without permission.

phase reactions between decomposition products. Specifically, an important reaction is gas-phase scavenging of H atoms by F atoms to form HF. This is likely to be more important in the TEOS system, which has a primary decomposition pathway involving C-H bond rupture.[34,44] Although C-H bond dissociation is possible in the HMDSO system, no evidence for this was observed in the gas-phase by Sonnenfeld and coworkers.[34] We find that film composition is highly dependent on the FC source when TEOS is the Si precursor. This is consistent with high fragmentation of TEOS such that the additional gas-phase component changes the nature of gas-phase reactions between fragmentation species. With HMDSO, less dissociation of the precursor through fewer pathways (primarily Si-C, Si-O bond rupture) occurs such that addition of the FC gas does not significantly influence the nature of the decomposition.

In addition to the gas-phase chemistry, physical aspects of the deposition process can also influence the nature of the resulting film. Although our relatively long deposition times likely established a "steady-state" regime, the relatively high deposition rates in the HMDSO systems may be a contributing factor in the deposition mechanism. In contrast, the TEOS systems have significantly lower deposition rates under all conditions, Figs. 6.5 and 6.6. Given that all three fluorocarbon precursors are capable of producing a FC film, the relative amounts of the FC and Si incorporated may vary as a function of the inherent deposition rates for each precursor. Thus, the FC precursors used here could have deposition rates intermediate to the TEOS and HMDSO precursors such that more FC incorporation is seen with the TEOS system. Both chemical and physical processes likely contribute to the overall film composition observed in each PECVD system.

Reproduced with permission of the copyright owner. Further reproduction prohibited without permission.

6.4. Summary

The results presented here demonstrate the effects of oxidant and FC source concentrations on SiO_2:F,C film formation using TEOS and HMDSO as the silicon precursors. Comparison of six different plasma systems demonstrates that without oxidant the silicon precursor determines whether an amorphous fluorocarbon film is produced or if the material is more of a silicon oxycarbide. In the TEOS systems, a variety of amorphous fluorocarbon materials were produced with the different FC sources with no O_2 in the feed. Higher quality SiO_2 materials were produced using either Si source by increasing O_2 concentrations, lower FC source concentrations. The highest quality SiO_2 films were produced with $O_2 > 80\%$ and FC ~ 5%. One measure of the quality is the lower refractive indices of materials deposited under these conditions. In summary, the complex environment of a three component system allows for greater control of film composition, but multiple factors contribute to producing the desired film properties such as low dielectric constant.

Reproduced with permission of the copyright owner. Further reproduction prohibited without permission.

References

1. S. P. Muraka *Solid State Technol.* **39**, 83 (1996).
2. M. K. Bhan, J. Huang, D. Cheang *Thin Solid Films* **308-309**, 507 (1997).
3. R. K. Laxman *Semicond. Int.* **18**, 71 (1995).
4. K. Kim, D. H. Kwon, G. Nallapati, G. S. Lee *J. Vac. Sci. Techno.l A* **16**, 1509 (1998).
5. B.-G. Yu, K.-H. Kim, K. S. Suh, J. T. Baek *Jpn. J. Appl. Phys., Part 2* **35**, L745 (1996).
6. H. Kudo, R. Shinohara, S. Takeishi, N. Awaji, M. Yamada *Jpn. J. Appl. Phys., Part 1* **35**, L745 (1996).
7. J. Lubguban, A. Saitoh, Y. Kurata, T. Inokuma, S. Hasegawa *Thin Solid Films* **337**, 67 (1999).
8. Y.-H. Kim, S.-K. Lee, H. J. Kim *J. Vac. Sci. Technol. A* **18**, 1216 (2000).
9. Y.-H. Kim, M. S. Hwang, H. J. Kim *J. Appl. Phys.* **90**, 3367 (2001).
10. S. P. Kim, S. K. Choi, Y. Park, I. Chung *Appl. Phys. Lett.* **80**, 1728 (2002).
11. S. Mizuno, A. Verma, P. Lee, B. Nguyen *Thin Solid Films* **279**, 82 (1996).
12. M. Yoshimaru, S. Koizumi, K. Shimokawa *J. Vac. Sci. Technol A* **17**, 425 (1999).
13. J. Lubguban, Y. Kurata, T. Inokuma, S. Hasegawa *J. Appl. Phys.* **87**, 3715 (2000).
14. J. Lubguban, Y. Kurata, T. Inokuma, S. Hasegawa *Mat. Res. Soc. Symp. Proc.* **606**, 57 (2000).
15. H. Miyajima, R. Katsumata, Y. Nakasaki, Y. Mishigawa, N. Hayasaka *Jpn. J. Appl. Phys.* **35**, 6217 (1996).

Reproduced with permission of the copyright owner. Further reproduction prohibited without permission.

16. S. Hasegawa, T. Tsukaoka, T. Inokuma, Y. Kurata *J. Non-Cryst. Solids* **240**, 154 (1998).

17. K. Kim, J. Song, D. H. Kwon, J. S. Lee *Appl. Phys. Lett.* **72**, 1247 (1998).

18. S. Hasegawa, A. Saitoh, J. Lubguban, T. Inokuma, Y. Kurata *Jpn. J. Appl. Phys.* **37**, 1247 (1998).

19. K. S. Oh, M. S. Kang, K.-M. Lee, D. S. Kim, C. K. Choi, S. M. Yun, H. Y. Chang, K. H. Kim *Thin Solid Films* **345**, 45 (1999).

20. J. Song, P. K. Ajmera, G. S. Lee *Appl. Phys. Lett.* **69**, 1876 (1996).

21. K.-M. Byun, W.-J. Lee *Metals Mater.* **6**, 155 (2000).

22. T. Usami, K. Shimokawa, M. Yoshimaru *Jpn. J. Appl. Phys.* **33**, 408 (1994).

23. P. Ho, C. F. Melius *J. Phys. Chem.* **99**, 2166 (1995).

24. N. Selamoglu, J. A. Mucha, D. E. Ibbotson, D. L. Flamm *J. Vac. Sci. Technol. B* **7**, 1345 (1989).

25. K. H. A. Bogart, J. P. Cushing, E. R. Fisher *J. Phys. Chem. B* **101**, 10016 (1997).

26. R. d'Agostino, F. Cramarossa, V. Colaprico, R. d'Ettole *J. Appl. Phys.* **54**, 1284 (1983).

27. E. Kay, A. Dilks *Thin Solid Films* **78**, 309 (1981).

28. N. M. Mackie, N. F. Dalleska, D. G. Castner, E. R. Fisher *Chem. Mater.* **9**, 349 (1997).

29. R. d'Agostino, F. Cramarossa, F. Fracassi, F. Illuzzi In *Plasma Deposition, Treatment, and Etching of Polymers*; d'Agostino, R., Ed.; Academic Press: San Diego, CA, 1990, pp. 95-162.

Reproduced with permission of the copyright owner. Further reproduction prohibited without permission.

30. C. I. Butoi, N. M. Mackie, L. J. Gamble, D. G. Castner, J. Barnd, A. M. Miller, E. R. Fisher *Chem. Mater.* **12**, 2014 (2000).

31. G. B. Raupp, T. S. Cale, H. P. W. Hey *J. Vac. Sci. Technol. B* **10**, 37 (1992).

32. K. H. A. Bogart, S. K. Ramirez, L. A. Gonzales, G. R. Bogart, E. R. Fisher *J. Vac. Sci. Technol. A* **16**, 3175 (1998).

33. K. Schmidt-Szalowski, Z. Rzanek-Boroch, J. Sentek, Z. Rymuza, Z. Kusznierewick, M. Misiak *Plasmas Polym.* **5**, 173 (2000).

34. A. Sonnenfeld, T. M. Tun, L. Zajickova, K. V. Kozlov, H.-E. Wagner, J. F. Behnke, R. Hippler *Plasmas Polym.* **6**, 237 (2001).

35. E. Hecht *Optics*, Addison-Wesley: Reading, MA, (1987).

36. D.-H. Kuo, D.-G. Yang *J. Electrochem. Soc.* **147**, 2679 (2000).

37. L. Martinu, D. Poitras *J. Vac. Sci. Technol. A* **18**, 2619 (2000).

38. S. M. Han, E. S. Aydil *J. Vac. Sci. Technol. A* **15**, 2893 (1997).

39. V. Pankov, J. C. Alonso, A. Ortiz *Jpn. J. Appl. Phys.* **37**, 6135 (1998).

40. V. Pankov, J. C. Alonso, A. Ortiz *J. Appl. Phys.* **86**, 275 (1999).

41. K. H. A. Bogart, N. F. Dalleska, G. R. Bogart, E. R. Fisher *J. Vac. Sci. Technol. A* **13**, 476 (1995).

42. D. A. Crosta, J. J. Hackenberg, J. H. Linn *J. Electrochem. Soc.* **143**, 1079 (1996).

43. S. M. Ray, C. K. Maiti, S. K. Lahiri, N. B. Chakrabarti *Adv. Mater. Opt. Electron.* **6**, 73 (1995).

44. F. Fracassi, R. d'Agostino, P. Favia *J. Electrochem. Soc.* **139**, 2636 (1992).

45. H. F. Winters, J. W. Coburn *Surf. Sci. Rep.* **14**, 161 (1992).

Reproduced with permission of the copyright owner. Further reproduction prohibited without permission.

46. M. B. Knickelbein, D. A. Webb, E. R. Grant *Mater. Res. Soc. Symp. Proc.* **38**(Plasma Synth. Etching Electron. Mater.), 23 (1985).

47. K. L. Williams, I. T. Martin, E. R. Fisher *J. Am. Soc. Mass. Spectrom.* **13**, 518 (2002).

48. T. E. F. M. Standaert, M. Schaepkens, N. R. Rueger, P. G. M. Sebel, G. S. Oehrlein, J. M. Cook *J. Vac. Sci. Technol. A* **16**, 239 (1998).

Reproduced with permission of the copyright owner. Further reproduction prohibited without permission.

CHAPTER 7

RESEARCH SUMMARY

This dissertation chapter addresses general considerations for fluorosilane plasma deposition and etching. Additionally, future directions for this work are briefly discussed

Reproduced with permission of the copyright owner. Further reproduction prohibited without permission.

Plasma processing is vitally important to a variety of major industries, including integrated circuits, aerospace, biomedical, and automotive manufacturing.[1] Of these, plasma processing is particularly well suited to very large scale integrated circuit (IC) manufacturing due to the need for extremely small device fabrication.[1-3] As a result, one-third of all fabrication steps involved in IC manufacture use plasma processing.[1] As feature sizes continue to decrease, the focus of research has been directed toward the development of new semiconductor materials with improved properties and improved etch methods to provide complete control of trench features.

The research characterizing 6 fluorinated silicon dioxide systems demonstrates the importance of understanding the chemistry involved in film deposition. Clear differences were seen as a function of feed gas ratios as well as source gas composition. Although the films deposited in these studies did not produce refractive indices as low as other materials such as amorphous FC films deposited by Carmen Butoi in the Fisher laboratories.[4] They do offer decreased refractive indices while maintaining good physical properties. This was not observed for the low k a-FC films. As a result, SiO_2:F,C films are important to the microelectronics industry because it offers a method for seamless integration of a lower k material than is currently used today.

The present SiF_4/H_2 research has sought to characterize the entire plasma system by evaluating the gas phase, the gas-surface interface, and material composition. This three-fold method for studying the SiF_4/H_2 plasma system has elucidated mechanisms involved in a-Si:H,F deposition and F atom etching of silicon. Earlier work in this area has been limited to characterization of gas phase species or

Reproduced with permission of the copyright owner. Further reproduction prohibited without permission.

surface composition, whereas other work characterized gas-surface interactions, but without the full range of species produced in the plasma.[5-10] This work complements the existing body of research by providing insight about surface chemistry during plasma processing and making correlations to gas and film composition.

Although these studies of plasma-deposited a-Si:H,F have been thorough, additional studies may provide additional information. Lee and Deneufville have identified and characterized gas phase production of HSiF in SiF_4:H_2 plasmas.[11] This species is considered an important deposition precursor, yet no surface reactivity studies have been made. Characterization of HSiF using the IRIS technique would lend insight into its true role in the plasma as well as facilitate molecular modeling of the plasma surface interface by increasing the database needed for accurate simulations.

In addition to IRIS experiments, additional film studies could be conducted. Amorphous Si:H,F films have been produced from a variety of source gases including SiF_4/H_2, SiF_2H_2, and $HSiF_3/H_2$, but we have only investigated one plasma source. Because these plasmas are both etching and depositing, any deposition in the current plasma reactor will likely result in side wall etching. Thus, it would be best to conduct any further studies in a steel parallel plate reactor. Use of a steel reactor will also allow for plasma etch rate studies to be conducted for Si, SiO_2, and Si_3N_4 substrates. Although some etch rate measurements have been made, more thorough investigation of plasma etch rates would be useful for correlation with IRIS studies.

As mentioned in Chapter 1, SiF_4 was chosen as a model system to study because of its dual nature. Characterization of SiF_2 in this system has provided the

Reproduced with permission of the copyright owner. Further reproduction prohibited without permission.

initial data for the behavior of etch products. However, SiF_4 is not the primary source gas for plasma etching in industry. Thus, SiF_2 IRIS studies should be extended to etch systems, such as CF_4, C_2F_6, C_3F_8, and SF_6 plasmas. Characterization of SiF2 in these systems will need to be slightly modified since no SiF_2 will exist in the molecular beam but should be observed scattering from the surface.

Studies of SiF_2 can be extended to non-etching systems as well. Film characterizations of six different SiO_2:F,C depositing plasmas were presented in Chapter 6. However, no gas phase or plasma-surface characterizations have been performed on these systems. As with the a-Si:H,F system, mechanistic information can be gained by measuring surface reactivity. Furthermore, there are several small molecules, like SiO, SiF, SiF_2, and SiC, that may be important to film growth and can be studied using the IRIS technique.

As a final characterization, it would be beneficial to ascertain how these fluorine-doped materials (i.e. a-Si:H,F and SiO_2:F,C) compare with traditional, undoped silicon-based materials in functioning electrical components. Amorphous silicon can be tested in solar cells to measure photoconductivity, while dielectric constant measurements for SiO_2 materials can be tested with a simple capacitor setup.

Although the semiconductor industry has recently seen a sharp decrease in the demand for its products, this trend is expected to be temporary as new breakthroughs in technology are made and as these products become relevant to a larger percentage of the world population. With this in mind, the future for plasma processing is quite promising as it remains the best and, in some cases, the only method for many processes in IC fabrication.

Reproduced with permission of the copyright owner. Further reproduction prohibited without permission.

As a result of many years of research to improve transport and isolation of current through transistors, resistors, capacitors, etc. while still reducing feature size, many new materials have been discovered and improved upon. More recently, however, research has been directed toward the improvement of optical relays used to move and redirect light. Although much of the technology for traditional IC fabrication carries over to manufacture of optical relays, there is a need for new designs and new materials. In many cases microscale optics such as lenses and mirrors are required to produce microelectromechanical (MEMs) devices capable of redirecting light in three dimension. The understanding of how the optical properties of plasma deposited materials can be effected by different plasma parameters is vital to generating new materials. For example, recent studies have been conducted that examine the effect of ion bombardment on MgF_2, LaF_3, AlF_3, and LiF film properties.[12-14] It was found that the presence of bombarding ions improved film strength, hardness, and durability, and reduced internal stress. However, ion bombardment also was found to be detrimental to the optical properties of these films by increasing the UV/VIS absorption.[15-17] This and other work like it is part of a growing effort to produce optically superior materials. This is just one example of the many fields to which plasma processing has expanded. Because plasmas are so diverse and easily adaptable to specific needs, it will continue to be heavily used in semiconductor manufacturing as well as many other industries.

Reproduced with permission of the copyright owner. Further reproduction prohibited without permission.

References

1. M. A. Lieberman, A. J. Lichtenberg *Principles of Plasma Discharges and Material Processing*, Wiley and Sons: New York, (1994).
2. A. Grill *Cold Plasma in Materials Fabrication*, IEEE Press: Piscataway, NJ, (1994).
3. R. Gottscho *Phys. World* **6**, 39 (1993).
4. C. I. Butoi, N. M. Mackie, L. J. Gamble, D. G. Castner, J. Barnd, A. M. Miller, E. R. Fisher *Chem. Mater.* **12**, 2014 (2000).
5. G. Bruno, P. Capezzuto, G. Cicala *J. Appl. Phys.* **69**, 7256 (1991).
6. P. Capezzuto, G. Bruno *Pure Appl. Chem.* **60**, 633 (1988).
7. G. Cicala, G. Bruno, P. Capezzuto *J. Vac. Sci. Technol. A* **16**, 2762 (1998).
8. F. Fracassi, R. d'Agostino, P. Favia *J. Electrochem. Soc.* **139**, 2636 (1992).
9. S. M. Han, E. S. Aydil *J. Appl. Phys.* **83**, 2172 (1998).
10. H. F. Winters *J. Vac. Sci. Technol. B* **1**, 927 (1983).
11. H. Lee, J. P. Deneufville *J. Non-Crystalline Solids* **66**, 39 (1984).
12. S. D. Jacobs, A. L. Hrycin, K. A. Cerqua, C. M. Kennemore III, U. J. Gibson *Thin Solid Films* **69**, 144 (1986).
13. C. M. Kennemore III, U. J. Gibson *Thin Solid Films* **23**, 3608 (1984).
14. S. Scaglione, D. Flori, G. Emiliani *Appl. Surf. Sci.* **43**, 224 (1989).
15. L. Dumas, E. Quesnel, J.-Y. Robic, Y. Pauleau *Thin Solid Films* **382**, 61 (2001).
16. U. J. Gibson, C. M. Kennemore III *Thin Solid Films* **124**, 27 (1985).

Reproduced with permission of the copyright owner. Further reproduction prohibited without permission.

17. M. Kennedy, D. Ristau, H. S. Niederwald *Thin Solid Films* **333**, 191 (1998).

Reproduced with permission of the copyright owner. Further reproduction prohibited without permission.